Pitt Polder – BC Hydro ILM Ground Radar Investigations

Final Report

Prepared for:

Katzie Development Corporation
10946 Katzie Road
Pitt Meadows, BC
V3Y 2G6

Project: 14 -15
30 September, 2014

Terrascan Geophysics
4506 West 4th Avenue
Vancouver, British Columbia, Canada V6R 1R3
Tel/Fax: (604) 221-2400
www.terrascan.ca

Terrascan Geophysics
4506 West 4th Avenue
Vancouver, British Columbia, Canada V6R 1R3
Tel/Fax: (604) 221-2400
www.terrascan.ca

Pitt Polder – BC Hydro ILM Ground Radar Investigations

Final Report

Prepared for:

Katzie Development Corporation
Archaeology
10946 Katzie Road
Pitt Meadows, BC
V3Y 2G6

Attention:

Ian Cameron
Tanja Hoffmann

Distribution:
1 copy – Katzie Development Corporation
1 copy – Terrascan Geophysics

September, 2014

TABLE OF CONTENTS

1.0 BACKGROUND - SCOPE OF WORK

As requested, Terrascan has carried out a multi-phase ground penetrating radar (GPR) investigation, as part of broader archaeological impact assessment (AIA), in advance of BC Hydro's Interior to Lower Mainland (ILM) transmission corridor development activities in the Pitt Polder. ILM upgrades include the twinning of an existing transmission corridor that traverses the midsection of the polder. Geophysical investigations focused on the western side of the polder, immediately east of Pitt River and south of the Pitt Polder Wildlife Management Area (Figures 1 and 2).

In general, the aim of AIA investigations, including geophysical reconnaissance, was to identify and delineate the extent of potential archaeological deposits that could be at risk of disturbance in connection with planned construction activities.

A focus on ground radar reconnaissance was motivated, in part, by previous results obtained at a nearby site (DhRp-52 – Figure 1), where GPR was employed to investigate the extent of a stratified peat deposit, incorporating an assemblage of artifacts and associated plant remains, that is potentially suggestive of early horticultural practices. In addition to investigating the potential of similar cultural deposits within the ILM corridor, there was also a general interest to assess the capacity of ground radar to detect and delineate peat deposits more broadly, as part of a strategy for wet-site potential mapping.

The initial phase of ground radar investigations, carried out between 17 October and 19 November, 2012, focused on three ILM tower sites located within recently developed cranberry fields, owned and operated by the Golden Eagle Group (Figure 2). Radar scans were acquired on a pair of orthogonal transects at each site as depicted in Figure 2. In addition, to provide constraints on stratigraphic interpretation, scans were also acquired adjacent to the Pitt River dyke, where prior geotechnical investigations were conducted in February 2012 (Figure 2).

While radar scans acquired near the Pitt River dyke are generally of very good quality and display a pattern of reflectivity consistent with natural fluvial deposits, subsequent results at ILM tower sites 5060, 5062 and 5064 are of poorer quality and suggest substantial ground disturbance associated with agricultural development (including placement of irrigation and drainage infrastructure). In general, no confident interpretation of natural stratigraphy was possible and extensive shovel testing by Golder and KDC archaeologists gave no indication of cultural remains.

A second phase of combined GPR/AIA investigations focused on tower sites 5065 and 5066, located within an apparently undisturbed wooded area, protected under land-use covenant (Figure 2). Ground radar investigations and subsequent AIA shovel testing at tower sites 5065 and 5066 were undertaken between 6–14 March, 2013, prior to soil disturbance associated with site clearance and placement of access roads for staging of subsequent tower construction.

As anticipated, ground radar scans were of better quality than those obtained within agricultural fields to the east, particularly on the north-south transect (GPR-1) at site 5065 where a prominent and potentially significant stratigraphic reflector was detected. Again, however, shovel tests gave no indication of archaeological remains and subsequent auger investigations were ultimately restricted to the interior of crushed-rock access roads and extended staging areas.

Consequently, it has not possible to ascertain the nature of stratigraphic contrast related to the prominent reflector detected at the north end of transect GPR-1 (tower 5065). However, auger investigations in proximity of tower sites 5065 and 5066 confirm the relatively undisturbed nature of near-surface soils/sediments, and related laboratory analysis of representative samples provides useful insight on the connection between radar reflectivity and corresponding stratigraphy.

The following is a factual report of methodology and findings.

2.0 GEOPHYSICAL FIELD INVESTIGATIONS

2.1 Field Methods

2.1.1 Ground Penetrating Radar

Ground penetrating radar (GPR) operates on the basic principle that electromagnetic waves emitted into the ground by a transmitter (Tx) antenna, are partially reflected at subsurface interfaces and subsequently detected by a receiver (Rx) antenna as illustrated in Figure 3a.

Radar scans are acquired by towing transmitter-receiver antennas along an established transect and concurrently recording a series of oscilloscope-like traces having amplitude proportional to reflection strength. The result, as illustrated in Figure 3b, is effectively a cross-sectional depiction of the subsurface with soil electrical contrasts delineated by associated reflectivity.

Notably, while GPR effectively delineates continuous stratigraphic interfaces, localized anomalous zones produce a characteristic (hyperbolic) diffraction pattern. Accurate timing of the reflected signals, together with measurement or estimation of radar velocity, permits corresponding depth to be determined.

Radar reflectivity arises due to subsurface contrasts in soil electrical properties that are largely controlled by soil texture, moisture level and the extent of clay/organic content. Archaeological deposits are mapped by delineating reflective contrasts between associated electrical properties and those of surrounding soils.

Radar range and velocity are also dependent on soil electrical properties. In particular, the propagation velocity of the radar pulse is predominantly controlled by moisture content and related influence of soil texture/composition on the distribution of water within the soil matrix.

The depth extent of radar investigation is limited by the efficiency of coupling between antennas and ground and by progressive attenuation and scattering of the radar pulse within subsurface soils. In general, increased electrical conductivity, associated with higher moisture levels, clay/organic content and mobile ion concentrations, results in degraded coupling and elevated attenuation of the radar pulse. In addition, because effective conductivity generally increases with frequency (particularly for radar frequencies above 100 MHz) and because correspondingly shorter wavelengths are preferentially scattered by soil heterogeneities, radar range decreases at higher frequencies. Consequently, selection of appropriate GPR instrumentation involves a trade-off between range and resolution.

Radar measurements described in the present report were acquired using a GSSI SIR-2000 digital radar system with a combination of 200 MHz and 400 MHz transceivers. Location along transect was constrained by fiducial marks recorded digitally in conjunction with data acquisition for subsequent processing and analysis.

2.1.2 Electrical Resistivity

As depicted in Figure 4, measurement of soil electrical resistivity involves the injection of a commutated DC or low frequency AC current I via source electrodes and simultaneous measurement of the associated potential difference ΔV between a second pair of electrodes. The effective resistance of subsurface material follows from Ohms law $R=\Delta V/I$.

To account for the influence of a specific electrode configuration and spacing, an appropriate geometrical correction factor γ is applied to obtain the corresponding apparent electrical resistivity $\rho_{a=}\gamma R$. A wide range of electrode configurations is employed. For the Wenner configuration depicted in Figure 4, the geometrical factor is $\gamma=2\pi a$, where a denotes the equal separation between adjacent electrodes. In general, investigation depth increases with electrode separation. Depth dependent electrical resistivity variation is obtained by acquiring a series of apparent resistivity measurements with incremental expansion of the electrode array about its midpoint. The result is a vertical electrical sounding (VES).

VES data were acquired by use of an ABEM SAS-300 resistivity transceiver. Computer based data analysis techniques were subsequently applied to obtain corresponding resistivity-depth profiles. In particular, 1-D resistivity inversions were performed via the method described by Zohdy (1989). In effect, the subsurface is modeled as a stack of arbitrary, equi-thickness layers of uniform resistance. Individual layer resistivities are incrementally adjusted via a computer-based optimization procedure to yield optimum agreement between measured resistivities and predicted values computed in accordance with the progressively refined model.

Note that for a uniform soil, apparent resistivity is equivalent to the intrinsic electrical resistivity $\rho=\rho_a$ and, also, that electrical conductivity $\sigma=1/\rho$ is simply the inverse of electrical resistivity.

Direct current (DC) or static electrical resistivity/conductivity of a soil is generally a useful indicator of radar performance, both as related to antenna-ground coupling efficiency and intrinsic attenuation. Notably, however, in connection with attenuation, the effective electrical resistivity/conductivity can be substantially lower/higher at radar frequencies due to viscous effects associated with dielectric polarization of constituent water.

2.2 Phase I – Field Investigations

On the basis of an initial site visit on September 12, 2012, including assessment of potential impact on berry crops by Patrick Brisbin of Golder Associates, it was agreed that an initial phase of combined GPR/AIA investigations should focus on planned tower sites 5060, 5062 and 5064. It was also decided that preliminary GPR investigations should be conducted at the western end of Koerner Road, adjacent to the Pitt River dyke, where prior geotechnical drilling was undertaken in February, 2012. To avoid potential delays associated with mature cranberry crops east of Rannie Road and with access to the wooded parcel under land-use covenant, it was agreed that these areas could be addressed separately, as a second phase of work.

Unfortunately, despite conducive weather and ground conditions throughout September and early October (see following precipitation chart), site access issues delayed progress until mid October. Phase I fieldwork was carried out during the period 17 October to 19 November, 2012. Although, an effort was made to avoid data acquisition during periods of significant precipitation, ground conditions varied substantially. Drainage pumps appeared to be operating continuously and localized standing water was often present.

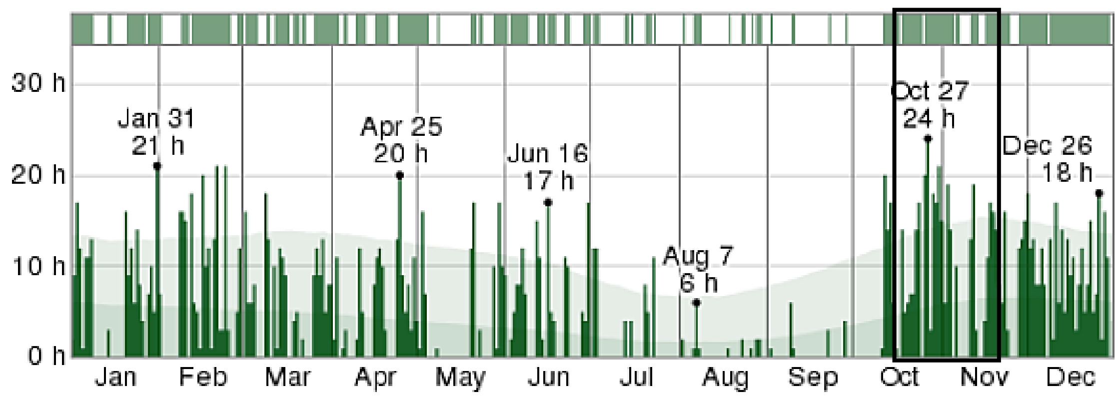

2012 Daily precipitation (hours)
SOURCE: http://weatherspark.com/history/28404/2012/Vancouver-British-Columbia-Canada

2.2.1 Pitt River Dyke

Prior to investigating planned tower sites, a series of ground radar scans were acquired along the western margin of the site and parallel to the Pitt River dyke, where related geotechnical investigations were previously conducted on February 24, 2012. Representative 400 MHz scans are depicted in Figures 5 and 6 for maximum two-way transit times of 80 ns and 120 ns, respectively (transect GPR-1 location indicated in Figure 2).

Results display a pattern of reflectivity that appears to be generally consistent with expected fluvial deposits and with shallow stratigraphy encountered by preliminary geotechnical drilling (location identified in Figure 2). Unfortunately, no intact cores were recovered and no formal logs appear to be available. However, the following observations were recorded by Amy Homan (2012, personal communication):

- *0 – 20/30 cm - clay fill mix*
- *20/30 cm -1.5 m - fine gray sand*
- *1.5 m - 1.8 m – coarse reddish/gray sand, becoming dark gray with small fragmented shell*
- *2.4 m - 2.8 m - organics within gray sandy silt*

- *3 m - 4.5 m - grass and roots, along with pebbles and gravels mixed with gray silt (slight peaty smell)*.

Notably, observed sediments and organic content are generally compatible with the following description of local surficial geology (Armstrong and Hicock, 1980):

<u>Fraser River Sediments (Units Fb/d)</u> :
Overbank sandy to silt loam up to 2 m thick overlying 15 m or more of deltaic and distributary channel fill.. sandy to silt loam.. interbedded fine to medium sand and minor silt beds; may also contain organic and fossiliferous material.

Although GPR scans suggest additional stratification (particularly in the interval 0.3 – 1.5 m) and considerable variability along transect, results are largely consistent with the foregoing description of local sediments. Consequently, while precise correlation and calibration of GPR results was not possible, radar scans acquired along the dyke road established that ground conditions were generally favourable for GPR and indicated a maximum range of approximately 2.5 metres at 400 MHz.

Similar results were obtained on a second transect along Koerner Road, immediately east of the dyke. Multiple antenna frequencies and a range of record lengths were employed to investigate related influence on effective range and resolution. Finally, a number of vertical electrical soundings were acquired to assess the bulk electrical conductivity of local soils.

In general, results are comparable with previous results at DhRp-52 as indicated by comparison of Figure 7 with Figure 5 and respective electrical soundings in Figure 8. Although similar results were expected, given proximity and related geomorphic context[1], confirmation reinforced expectation that subsequent investigation of tower sites would yield effective delineation of potential cultural deposits.

2.2.2 Tower Sites 5060, 5062 and 5064

In contrast with ground radar scans acquired near the Pitt River dyke, results at tower sites 5060, 5062 and 5064, located within adjacent agricultural fields (Figure 2), are generally of lower quality and display a relatively unnatural character. Representative S-N and W-E scans (400 MHz) at tower site 5064 are presented in Figures 9 and 10, respectively. Pronounced system-generated noise, appearing

[1] It is noted that DhRp-52 is located at marginally higher elevation, at the transition between mid-late Holocene fluvial overbank sediments (Unit Fb - Armstrong and Hicock, 1980) and coarser-grained, Pleistocene proglacial deltaic deposits (Unit Se). Radiocarbon dating indicates that the wet-site component at DhRp-52 resides in within Holocene (Fb/Sab) deposits.

as consistent horizontal banding, is attributed to saturated ground conditions and related antenna-ground coupling effects. Notably, "ringing" is also observed in connection with strong reflection events.[2]

In addition to degraded signal quality, it is further observed that recorded reflectivity displays a relatively irregular and discontinuous nature that may be due in part to soil disturbance associated with agricultural development. Notably, radar scans in Figures 9 and 10, give clear indication of irrigation and drainage infrastructure and suggest that near-surface reflectivity could in some locations be related to placement of these structures or to prior clearance of pre-existing vegetation (including stumps/roots) and/or subsequent regrading of near-surface soils/sediments.

Moreover, there is a general lack of coherent reflectivity at two-way transit times exceeding roughly 60 ns (effective range of approximately1.5 m at $v \approx 0.05$ m/ns) and, again, this is potentially attributable to inefficient antenna-ground coupling and/or increased attenuation associated with saturated ground conditions and elevated electrical conductivity.

Figure 11 compares a vertical electrical sounding acquired at tower site 5064 with previous results parallel to the dyke. As anticipated, near-surface soils/sediments at tower site 5064 are considerably more conductive, having near-surface electrical resistivity roughly an order of magnitude lower than that measured near the dyke. Although a static electrical conductivity of roughly 5-10 mS/m is not exceptionally high for saturated fine-grained sediments, related effect on antenna-ground coupling together with elevated intrinsic attenuation (and including dissipation associated with radar-frequency polarization of constituent soil water) are collectively responsible for limiting the range of investigation. It should also be noted, however, that the absence of reflectivity can also mean an absence of sufficient stratigraphic contrast (in terms of associated electrical properties) to generate a significant reflection and, moreover, that sufficiency of contrast becomes a taller order as range increases.

As noted in Section 2.1.1, increased range can generally be achieved at lower frequency at the expense of resolution. Consequently, to investigate the potential for extended range at tower 5064, scans were repeated at 200 MHz. For example, Figure 12 displays a S-N scan approximately coincident with the 400 MHz scan in Figure 9. Significantly, the extent of subsurface penetration is

[2] Notably, although horizontal banding and other system-generated noise has been addressed through post-acquisition filtering in connection with data processing and analysis, radar scans presented as part of the present report are displayed in raw form to illustrate the variable influence of local ground conditions on data character and quality.

marginally improved (<2.0 m) with suggestion of a deeper sub-horizontal interface (~1.5 – 2.0 m). In addition, broad hyperbolic signatures attributed to overhead transmission lines are clearly visible (despite antenna shielding) and reinforce expectation that inefficient antenna-ground coupling is a significant contributor to restricted radar range.[3]

The apex of identified signatures (due to overhead lines) establishes proximity of the S-N transect in relation to the pre-existing transmission corridor and, notably, there appears to be an associated contrast in the general character of subsurface reflectivity (relatively natural character within the corridor). A similar contrast is observed for the corresponding 400 MHz scan, in Figure 9, providing further suggestion that anomalous reflectivity beyond the existing transmission corridor might be related to clearance of pre-existing vegetation (including stumps/roots) and subsequent removal and/or regrading of near-surface soils/sediments.

In general, similar results were obtained at tower sites 5062 and 5060, as presented in Figures 13-16. Although the general character of reflectivity is relatively discontinuous and irregular (compared with scans acquired adjacent to the Pitt River dyke), it remains plausible that reflectivity is attributable to natural stratigraphic features. In particular, it is noted that tower site 5062 appears to coincide roughly with a prior distributary/drainage channel (e.g. southern arm of Quarry Slough) as currently observed within Pitt Polder Wildlife Management Area to the north (Figure 2). Unfortunately, however, confident interpretation is restricted by foregoing limitations and would require additional direct constraints.

Although it was initially planned that coincident geotechnical investigations would provide constraints for assessment and interpretation of ground radar scans, these investigations were delayed and effective coordination between geophysical and archaeological components of the impact assessment study was limited by site access and related project logistics. Ultimately, archaeological investigations at tower sites 5060, 5062 and 5064, were completed in advance of, or concurrent with geophysical work and, consequently, do not provide direct constraints on GPR scans. Results of grid-based shovel testing as summarized in Wilkerson (2012), however, provide a general indication of sediments and stratification encountered at each of the three tower sites.

Shovel tests were advanced to a minimum of 0.5 m below grade and encountered a generally consistent sequence of sediments, with thickness/depth of individual

[3] Note that a similar range of investigation was obtained on radar scan GPR-2, along Koerner Road east of the dyke, where electrical sounding VES-2 indicated resistive near-surface conditions comparable with VES-1, but rapidly more conductive with depth (comparable with tower site 5064 below 0.25 m).

strata varying significantly from site to site. The reported sediment sequence is generally as follows:

- *0 cm – 12/27 cm - mottled orange/gray sandy/silty clay*
- *12/27 cm – 15/31 cm - grey-blue silty clay*
- *15/31 cm – 15/37 cm - dark brown peaty loam*
- *15/37 cm – 36/70 cm - gray brown silty clay*
- *36/70 cm - 100 cm - brown silty clay with plant material*.

Notably, the foregoing sequence describes largely finer-grained sediments than encountered in near proximity to the Pitt River dyke, suggesting a lower energy depositional environment (as reasonably expected at significant distance from Pitt River[4]) and consistent with more conductive conditions as indicated by vertical electrical soundings.

Similarly, and consistent with assessment of ground radar scans, shovel tests often encountered drainage and irrigation infrastructure at depths between 0.2 and 0.4 m and at tower site 5054 a drainage conduit was confirmed at a depth of approximately 0.9 m. Moreover, it was observed that “many layers were noted as disturbed, or ‘appears disturbed’, with some mixing, most likely due to drainage and sprinkler pipe installation”.

Finally, while a thin “peat-like” loam layer (thicker at tower site 5062 - <0.2 m) was detected at depths of between 0.15 and 0.31 m below grade, no fibrous peat was encountered (Wilkerson, personal communication), nor were any cultural materials identified.

Unfortunately, in the absence of stratigraphic sections and/or additional direct constraints on GPR scans, it is difficult to establish confident correlation between radar reflectivity and specific stratigraphic contacts. Moreover, it is possible that radar reflectivity is related to recent soil disturbance associated with agricultural development (including placement of irrigation and drainage infrastructure) to a greater extent than it is to more subtle stratigraphic contrasts.

Finally, while radar reflectivity suggests potential stratigraphic contacts at depths beyond the extent of shovel tests, the maximum range of investigation is approximately 2.0 m and, again, it is difficult to attach any archaeological significance to this reflectivity in the absence of direct constraints.

[4] Note, according to Ashley (1977), Pitt River “floodplain geomorphology reveals no evidence of extensive river channel migration from its present site on the west side of Pitt Valley”, adding that “the location and shape of the (major s-shaped) bend appears to be mainly due to bedrock control”. It is also noted that near-surface conditions in close proximity of the dyke may have been altered by construction.

2.3 Phase II – Field Investigations

In view of foregoing Phase I results, it was determined that a second phase of combined GPR/AIA investigations should focus on tower sites 5065 and 5066, located within an apparently undisturbed wooded area that is protected under land-use covenant (Figure 2). Moreover, given uncertainty regarding to the extent to which results obtained at tower sites 5060, 5062 and 5064 are reflective of agricultural development, it was emphasized that Phase II investigations should be undertaken prior to any ground disturbance related to planned ILM construction activities. Finally, it was agreed to ensure closer coordination of ground radar investigations and subsequent archaeological testing (i.e. targeted placement of shovel/auger tests on GPR transects) to yield more effective constraints on the interpretation of radar reflectivity.

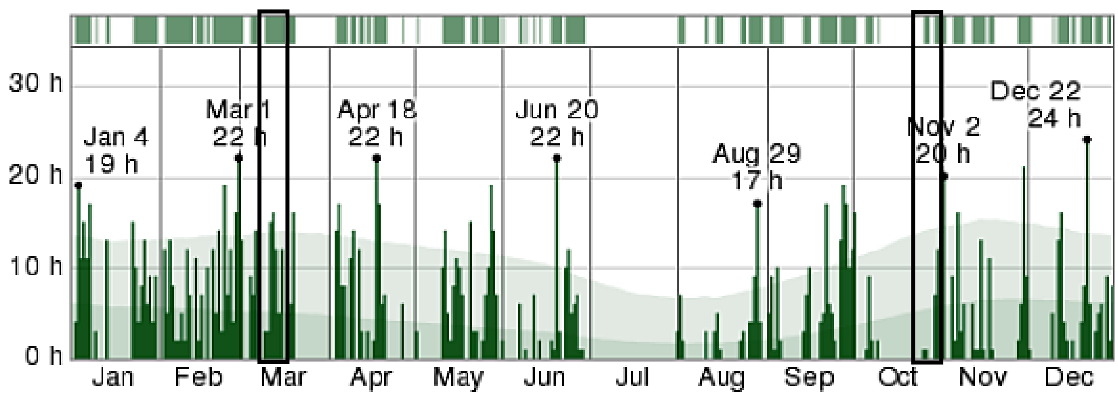

2013 Daily precipitation (hours)
SOURCE: http://weatherspark.com/history/28404/2013/Vancouver-British-Columbia-Canada

Phase II fieldwork was conducted during the period 6 – 14 March, 2013, under relatively conducive conditions (compared with Phase I). However, substantial prior precipitation left saturated ground conditions and localized standing water at tower site 5066.

.

2.2.1 Tower Sites 5065 and 5066

As anticipated, radar scans acquired on orthogonal transects at tower site 5065 (Figures 17 and 18) are of considerably better quality than those obtained in berry fields to the east. Antenna-ground coupling is clearly much improved (relatively limited system-generated noise is observed) and coherent reflectivity is observed at two-way transit times exceeding 80 ns, implying an investigation range of approximately 2.0 m (v ~ 0.05 – 0.06 m/ns at 400 MHz center frequency). Again, however, the character of reflectivity is in clear contrast with results obtained near the Pitt River dyke and suggests a relatively low-energy, overbank depositional environment.

Although radar scans, once again, display a relatively irregular and intermittent character (i.e. reflectivity is coherent on a variable and limited length-scale) with significant associated scattering, overall features appear to confirm a largely undisturbed, natural stratigraphy. Over the majority of investigated transects, both GPR-1 (N-S, Figure 17) and GPR-2 (E-W, Figure 18), reflectivity is mainly comprised of semi-continuous and subhorizontal horizons within approximately 1.0 m below grade (assuming an estimated radar velocity of 0.05 m/ns). Significantly, however, a prominent and collectively continuous band of reflectivity was recorded at a two-way transit time interval of approximately 40 – 60 ns (approximately 1.0-1.5 m) at the north end of transect GPR-1 and extends to roughly 25N before shallowing to approximately 0.5 – 1.0 m (20 – 40 ns) and largely terminating at about 17N.[5]

The pattern of reflectivity changes abruptly south of 17N. In general, reflectivity south of 17N is relatively weak, sub-horizontal and less coherent, apparently in large part due to near-surface scattering. Although the pattern of near-surface reflectivity varies substantially, there is a generally consistent zone of more or less coherent reflectivity in the range 20 40 ns (0.5 – 1.0 m). South of planned tower center 5065 (0N/S), the amplitude of reflectivity increases significantly with clear indication of near-surface scattering. Scattering is tentatively attributed to root structures present within near-surface soils and, notably, this scattering diminishes south of about 10 – 15S, roughly the boundary of the pre-existing transmission right-of-way.

Farther south, between approximately 15S and 20S, the previous pattern of banded reflectivity (identified at the northern end of GPR-1) appears to re-emerge and trend gradually toward surface near the transect’s southern end. Notably, the observed change in character and attitude of the reflector may be associated with

[5] Note that although no topographic correction has been applied, relief is generally limited over radar transects and there is no substantial grade over the northern section of GPR-1 where observed prominent reflectivity is observed to shallow. Elevation constraints are limited to transect endpoints and tower 5065 center, as follows: TWR-5065 CNTR – 1.514 m, GPR-1 North – 1.747 m, GPR-1 South – 1.282, GPR-2 East – 1.369 m, GPR-2 West – 1.508 m. Foregoing elevation data are referenced to local mean sea level (Geoid Model CVD28GVRD) via BC-GCM No. 179606 (1.967 m) located at the intersection of Koerner/Middleton and Rannie Roads.

locally lower ground and relatively moist conditions, approaching a narrow drainage channel (of natural origin?).

Similar patterns of reflectivity were recorded on the orthogonal E-W transect (GPR-2) at tower site 5065. Specifically, at the eastern end of transect GPR-2 (Figure 18), a zone of high-amplitude reflectivity was recorded within two-way transit time range of 20 – 60 ns, corresponding to a depth interval of approximately 0.5 – 1.5 m. Although the lateral extent of the feature is limited, the character of reflectivity is comparable to that comprising the zone of prominent reflectivity identified at the northern end of GPR-1. Again, there is some indication that noted reflectivity shallows to the west and terminates at roughly 15E, where reflectivity becomes relatively limited in amplitude and largely flat-lying. Subsequently, west of 10E, amplitude increases once again and the pattern of reflectivity is similar to that observed south to tower center 5065 on GPR-1.

Again, there is generally a consistent zone of variably coherent, sub-horizontal reflectivity spanning a roughly consistent interval of about 20 ns (approximately 0.5 m), with associated onset time varying gradually, but significantly along the scan. In particular, near the intersection with N-S transect GPR-1 (0 E/W at approximately 2 m south of tower 5065 center), the identified reflectivity zone appears to shallow, with a corresponding onset time as early as 10 ns (approximately 0.25 m). Moreover, as for GPR-1, there is prevalent near-surface scattering in proximity of the tower center and to a greater extent farther west (over the range 20W – 35W) and, again, this scattering appears to be attributable to shallow root structures in near-surface soils. As might be expected, there is also associated indication of significant variation in antenna-ground coupling along transect.

For additional insight into the influence of ground conditions on limiting radar performance, vertical electrical soundings were acquired on both N-S (GPR-1) and E-W (GPR-2) transects at tower site 5065. Results displayed in Figure 19 reveal a significant contrast in static electrical resistivity/conductivity that appears to be consistent with local ground conditions and observed change radar reflectivity. In particular, sounding VES-1 (centered at 30N on N-S transect GPR-1) indicates relatively conductive near-surface conditions, becoming gradually more resistive to a depth of roughly 1.0 m, before reversing trend to higher conductivity at greater depth. In contrast, VES-2 (centered at 0E/W on E-W transect GPR-2) reveals relatively resistive near-surface conditions and a comparatively shallow transition to more conductive sediments, beginning at about 0.4-0.5 m.

Notably, foregoing observations appear to be consistent with relatively moist moss-covered ground conditions within the interior of the wooded area (VES-1), compared with drier conditions nearer the open right-of-way (VES-2). More significantly, the deeper transition to more conductive conditions indicated by VES-1 may also be consistent with deeper reflectivity identified at the northern end of GPR-1.[6]

In general, comparison of GPR scans and associated electrical soundings at tower site 5065 with corresponding results at tower site 5064 and Pitt River dyke appears to confirm that progressive attenuation imposes a more fundamental and predictable restriction on radar range than inefficient antenna-ground coupling. In some instances, however, system-generated noise related to coupling between antenna and ground can largely prevent the acquisition of reliable data and this was, unfortunately, the case at tower site 5066.

In particular, the presence of extensive standing water, combined with a highly irregular and variable-thickness layer of sphagnum moss (in some locations approaching 0.5 m) prevented effective data acquisition. Although multiple radar scans were acquired by deploying the antenna in a plastic sled, resulting data were dominated by sustained and fluctuating system noise attributed to variable impedance mismatch between antenna and saturated ground cover. Despite efforts to improve signal-to-noise ratio through real-time and post-acquisition filtering, results could not be confidently interpreted.

Given initial delays with access and pending closure of the area by the Ministry of Environment (spring nesting period), no further geophysical investigations were pursued at tower site 5066. Focus was, instead, directed toward preliminary evaluation of acquired data (principally at tower site 5065) and identification of sites for subsequent AIA investigations. A total of 13 sites were identified for targeted shovel testing on radar transects at tower site 5065. Shovel test locations are indicated in Figure 17 and 18. An additional four sites were targeted at tower site 5066.

Shovel testing was undertaken by KDC Archaeology on March 13, 2013. Again, as for prior AIA investigations at tower sites 5060, 5062 and 5064, shovel tests were advance to a minimum depth of 0.5 m with no cultural remains identified. Although no written report of findings was prepared, Terrascan was advised that no significant stratigraphic contacts or peat deposits were noted (Tyler Hicks, 2013, personal communication).

[6] Comparison of electrical soundings at tower site 5065 with corresponding results at tower site 5064 and near Pitt River dyke appears to confirm that progressive attenuation imposes a more fundamental restriction on radar range than inefficient antenna-ground coupling, despite significant signal degradation due to coupling and impedance mismatch effects.

In view of well-defined near-surface (<0.5-1.0 m) reflectivity, particularly in the areas 25N-15N, 15S-25S, 25E-15E and 5W-15W, the lack of notable stratigraphic contacts was unexpected and suggested that texture-related moisture variation or other inevident sources of electrical contrast could be responsible for recorded reflectivity. Notably, deeper reflectivity identified at the northern end of transect GPR-1 is beyond the depth of shovel testing and, consequently, there was no assessment of related subsurface conditions prior to extended auger investigations reported in the following section.

3.0 AUGER INVESTIGATIONS & LABORATORY TESTING

In general, combined geophysical and AIA testing described in foregoing sections yielded mixed and inconclusive results.

Given:

1) uncertainty regarding the extent of disturbance associated with agricultural development,
2) a lack of direct and discernable constraints on the interpretation of recorded reflectivity and
3) no evidence of cultural deposits,

auger investigations at tower site 5065 were viewed as an opportunity to derive a clearer understanding of the correlation between observed reflectivity, associated stratigraphy and related soil/sediment electrical properties.

Although prior shovel testing suggested that auger investigations were unlikely to encounter cultural deposits, previous testing was restricted to depths between 0.5 and 1.0 m below surface. In addition, there was a general interest to evaluate the potential of ground radar reconnaissance for detection and imaging of peat deposits, more widely, as part of a strategy for wet-site potential mapping within the broader polder.

Although auger testing was initially planned at tower sites 5065/5066 as an integral part of Phase II field investigations, testing was initially delayed by a seasonal wildlife closure (BC Ministry of Environment) and subsequently restricted by a redesign of site access. Instead of accessing tower site 5065 south from Koerner Road, an alignment that would have roughly coincided with transect GPR-1, the revised design relocated the access west from an existing service road at the western margin of adjacent agricultural fields (see Figure 20).

Moreover, despite GPR and shovel testing already carried out along transects GPR-1 and GPR-2, KDC Archaeology was subsequently informed that (due to environmental impact considerations) auger testing would not be permitted beyond the extent of planned access roads and extended staging pads ("impact areas") as delineated in Figure 20. As a consequence, direct constraints on the interpretation of radar reflectivity have been substantially restricted (see auger test site locations in Figures 17, 18 and 20). In particular, aims to ascertain the nature of stratigraphic contrasts associated with prominent reflectivity at the northern end of transect GPR-1 have been largely prevented.

Finally, planned site GPR1-AH1 was determined to be too close to the edge of the access road for the drill rig to operate safely (relocated approximately 1 m south at ~19N) and the pad did not extend as far south as planned site GPR1-AH4 (relocated to approximately 11S and marginally west of the transect). Thus, ultimately, auger site GPR1-AH1 provides the only constraint on origin of deeper reflectivity observed at the northern end of transect GPR-1.

Despite foregoing limitations, however, best efforts were made to extract as much understanding as possible, regarding the connection between recorded reflectivity and associated soil/sediment stratigraphy.

Auger investigations were conducted during the period October 28-31, 2014 under generally clear skies[7]. In fact, reference to the charts of Vancouver precipitation for 2012 (Section 2.2, p. 5) and 2013 (Section 2.3 p. 10), reveal that prevailing conditions were dramatically different year to year and serve as a reminder that sampled near-surface soil conditions in October 2013 may not be entirely reflective of conditions prevailing during acquisition of ground radar scans in March 2013.

A total of 15 auger holes were completed at tower sites 5065 and 5066 using standard sonic drilling and core recovery methods. In general, auger holes were advanced and sample cores recovered in 1.52 m sections. Individual core sections were subsequently examined on-site for identification of potential cultural remains, recovery of suitable organic samples for carbon dating and recording of depth-dependent soil/sediment characteristics.

[7] Reported auger investigations were part of an ongoing effort to characterize the post-glacial evolution of the Fraser River floodplain with particular focus on late-Pleistocene/Holocene geomorphology and environment of the broader Pitt Polder (Locher and Clague, 2007). Auger investigations were previously conducted at sites within agricultural fields (including tower sites 5060, 5062 and 5064) during June and July, 2013 (Locher.

Initially, it was understood that soil samples would not be permitted to leave the site and, consequently, preparations were made for on-site measurement of soil/sediment electrical properties in connection with the inspection and logging of recovered cores. Ultimately, however, authorization to acquire representative samples for off-site laboratory analysis was received immediately prior to initiation of sonic drilling. Related sampling and analysis focused on tower site 5065 and specifically on the upper soil/sediment section (< 3 m) from auger holes GPR-1-AH1, GPR-1-AH2, GPR-2-AH1 and GPR-2-AH2 (see Figures 17, 18 and 20).

Identification and sampling of soil/sediment units was based on visual assessment of solid-fraction composition, structure, texture, and colour. Upper soil/sediment sections (approximately 3 m) recovered from the entire suite of auger holes identified in Figure 20 are pictured in Figures 21-27. Notably, all cores display a well-developed near-surface soil profile with characteristics typical of wetland soil development[8].

Adjusted depth, as indicated, accounts for variable-thickness of crushed rock fill by identifying the transition from fill to soil and presuming that the recovered soil section comprises the full extent of the initial core. Deeper core sections are assumed to span the standard 1.52 m, with linear adjustment applied to compensate for assumed compaction. For example, with reference to Table 2 and Figure 21, the upper soil section (Core 1 – Figure 21) has a length of approximately 0.4 m and is assumed to constitute the full extent of Core 1. Core 2, in contrast, has a length of approximately 1.35 m and is assumed to be linearly compacted to the extent that it is representative of the standard 1.52 m core length. Thus, the adjusted net depth to the contact between units 7 (Sample 5) and 8 (Sample 6) located at approximately 0.32 m in Core 2 is $0.40+(0.32/1.35)\times1.52=0.76$ m.[9]

Nine representative soil units were identified (Figure 28) as an initial basis for investigating the connection between soil contrasts and radar reflectivity. The following sections describe laboratory methods for measurement of associated soil electrical properties and related findings.

[8] Notably, organics-rich topsoil horizons (units 1, 2 and 3 in Figure 28) were often absent from cores recovered at tower sites 5060, 5062 and 5064 (Peter Locher, 2013, personal communication), suggesting potential removal and/or redistribution of near-surface soils in connection with agricultural development (Locher, 2014).

[9] Note that this approach is in contrast with that taken by Golder Associates for reporting of auger logs, wherein the soil section of the upper core is also assumed to be representative of the standard 1.52 m core length. Thus, Golder geotechnical logs would record a corresponding net depth to same contact of $1.52+(0.32/1.35)\times1.52=1.88$ m.

3.1 Laboratory Methods

3.1.1 Electrical Resistivity / Conductivity

The electrical conductivity σ and, its inverse, electrical resistivity ρ are measures of a material's capacity to support and sustain a free-charge conduction current in response to an applied potential gradient (electric field). Static and/or low-frequency conduction in soils is principally ionic, involving the net migration of electrolyte ions through interconnected pore spaces within the soil matrix. Principal factors controlling electrical conductivity/resistivity include soil moisture level, porosity/permeability, ionic/organic content and texture. In general, fine-textured soils (clays-silts) are conductive compared with coarse-textured soils (sands-gravels).

Owing to enormous relative surface area and related intrinsic charge characteristics, the clay-sized fraction (<2.0 μm) and, particularly, the colloidal (1.0 nm – 1.0 μm) content of soils, including both inorganic and organic components, has a major influence on the electrical properties of common soils. In addition to controlling the moisture distribution and retention capacity of soils, the colloidal component also functions as a dynamic reservoir of ionic charge carriers. In response to time-variable moisture/temperature conditions, related chemical weathering, organic decomposition, leaching and associated fluctuation of soil pH, nominally exchangeable ions are correspondingly adsorbed and/or liberated at and surrounding colloid surfaces, resulting in substantial and significant variability in bulk electrical characteristics of the soil.

In general, laboratory measurement of electrical resistivity employs the same methodology and instrumentation as described in Section 2.1.2 for in situ field investigations. Rather than inserting electrodes into the soil, however, soil samples are placed into a "soil box" sample fixture as depicted in Figure 29. As for in situ measurements, a commutated DC or low frequency AC current I is established through the sample, via end-plate source electrodes, with simultaneous measurement of the associated potential difference ΔV between a pair of an interior electrodes. The effective resistance of subsurface material follows from Ohms law as $R=\Delta V/I$.

Fixture geometry, including cross-sectional area, length and electrode separation, is designed such that four-electrode measurements of electrical resistance R in Ohm provide direct indication of intrinsic soil electrical resistivity ρ in units of Ohm-cm. The corresponding design constraint is $\gamma_c = A/s_v = 1.0$, where A denotes the area (cm^2) of end-plate electrodes and s_v (cm) is the separation between interior potential electrodes. Resulting resistivity (conductivity) follows as $\rho = 1/\sigma = \gamma_C R = R$ (see following table for related conversion unit conversions).

Table 1

Electrical Unit Conversions

Electrical Resistivity (Ω-m)	Electrical Resistivity (Ω-cm)	Electrical Conductivity (mS/m)
0.01	1	100,000
0.1	10	10,000
1	100	1,000
10	1,000	100
100	10,000	10
1,000	100,000	1

Although dielectric polarization of constituent water has considerable influence on the effective electrical conductivity/resistivity at radar frequencies, static or low-frequency measurements are a good predictor of antenna coupling efficiency (for surface soils) and provide a rough indication of relative attenuation rates within deeper soils/sediments. Although radar-frequency electrical permittivity measurements are a better indicator of potential reflectivity, the extent of contrast in static or low-frequency electrical conductivity/resistivity for identified soil-sediment units is also considered.

Measurements were acquired using an ABEM SAS-300C transceiver, at source current levels between 1 and 5 mA. To every extent possible, cohesive samples were placed in the soil box in such a way as to preserve structure and orientation of the soil/sediment as recovered. Samples having a non-cohesive, granular structure were uniformly compacted to an extent approximating as-sampled condition.

3.1.2 Electrical Permittivity (Dielectric Constant)

The real-valued, or “in-phase”, electrical permittivity ε' is a measure of a material’s capacity to become electrically polarized on application of an electric field. A range of bound and free-charge polarization mechanisms contribute to varying degrees as a function of frequency. Moreover, it should be appreciated that the electrical permittivity is more generally a complex-valued quantity $\varepsilon^*=\varepsilon'-i\varepsilon''$, including a quadrature component ε'' related to energy dissipation associated with cyclical polarization and depolarization in an alternating electric field.

Further, ε' and ε'', as measured, are effective parameters[10] reflecting the influence of conduction as well as polarization and are generally reported as unit-less relative quantities, $\varepsilon_r'=\varepsilon'/\varepsilon_0$ and $\varepsilon_r''=\varepsilon''/\varepsilon_0$, normalized by the electrical permittivity of free space $\varepsilon_0 = 8.85\times10^{-12}$ Fm^{-1}. Although the term "dielectric constant" refers in a strict sense to the static, real-valued relative permittivity $\kappa=\varepsilon_r'(0)$, the term is commonly used more loosely as a synonym for the frequency-dependent permittivity (i.e. $\kappa(f)=\varepsilon_r'(f)$). Here, as described above, we shall use the symbols ε' and ε'', respectively, to represent the real and quadrature components of the relative effective electrical permittivity and the term "dielectric constant" to refer to the real-valued part at zero frequency.

In general, because the electrical permittivity or dielectric constant of water ($\kappa \approx 80$) is more than an order of magnitude greater than the average for dry soil matrix constituents ($\kappa \approx 3-6$), soil moisture content is the primary factor controlling bulk soil electrical permittivity. Frequency dependence and associated attenuation, however, are substantially influenced by ionic conductivity as well as a wide range of interfacial polarization processes related to the spatial distribution and mobility of free and exchangeable ions within the pore structure of the soil or sediment. Again, as for electrical conductivity, texture has a significant influence, both in relation to moisture capacity and retention, as well as space-charge polarization, particularly in connection with colloidal clay and organic content.

Laboratory measurements of frequency-dependent, complex permittivity were acquired using a HP85070A dielectric probe, configured with an HP8752A vector network analyzer as illustrated in Figure 30. The dielectric probe is effectively a terminated or open-ended coaxial transmission line. Measurements are made by bringing the probe face into firm contact with the sample and measuring the fringe-field reflection coefficient at the probe/sample interface. A sequence of automated measurements is acquired at discrete frequencies spanning the range 20 MHz – 3 GHz.

Samples were placed in 60mm x 15mm polystyrene culture dishes for analysis. In general, cohesive samples were tested in undisturbed, as-sampled condition, with care taken to maintain sample orientation. In the case of non-cohesive (granular) soils, samples were uniformly compacted to an extent approximating as-sampled condition.

---

[10] In-phase and quadrature relative permittivity as reported herein are given by $(\varepsilon'+\sigma''/2\pi f)/\varepsilon_0$ and $(\varepsilon''+\sigma'/2\pi f)/\varepsilon_0$, respectively, with associated complex intrinsic permittivity and conductivity defined as $\varepsilon^*=\varepsilon'-i\varepsilon''$ and $\sigma^*=\sigma'+i\sigma''$ and $\varepsilon_0 = 8.85\times10^{-12}$ Fm^{-1} denoting the electrical permittivity of free space (see Cross (2000) Section 3.0 for details).

3.2 Laboratory Results

Frequency-dependent electrical permittivity spectra, measured under as-sampled moisture condition, are displayed in Figures 31-34. In addition to spectra for soil/sediment samples, reference spectra for three polar liquids (water (H2O), isopropanol (ISO) and methanol (MTH)) are included as internal calibration standards to confirm consistent and accurate measurements.

Results are largely in line with expectation and suggest a generally consistent pattern of correlation between identified soil units and associated electrical permittivity. The general similarity between in-phase permittivity spectra (ε') for soils and the H2O reference confirms the dominant influence of constituent water on the bulk permittivity of soils/sediments, with the extent of relative permittivity directly related to associated moisture content. In general, the higher the moisture level, the higher the permittivity.

Significantly, however, the capacity of soils and sediments to accommodate and retain moisture is strongly dependent on a range of properties, including the composition of solid phase constituents (organic and inorganic), texture and structure (largely the same characteristics on which representative soil units in Figure 28 were identified). Consequently, while in-phase permittivity is generally higher with increasing moisture level for any given soil, there is considerable and systematic variability under prevailing moisture conditions that is predictable to a significant degree on the basis of soil characteristics, particularly with benefit of calibration.

The same is true for the electrical resistivity/conductivity of soils/sediments. Once again, moisture level is the primary controlling factor for any given soil, but the relative influence from soil to soil is substantial and strongly dependent on a similar range of soil properties, including the ion exchange capacity and associated influence of time-variable soil chemistry, both short and long-term.

Measurements of static (DC) electrical resistivity (see Table 1 for corresponding electrical conductivity), are presented in following Tables 2 – 5 together with associated permittivity data.[11] Associated soil units (as identified in Figure 28) are also indicated as per Figures 31-34.

[11] Tabulated relative permittivity values (Tables 2-5) were extracted from associated spectra presented in Figures 31-34 and representative of measurements in proximity of 400 MHz, the nominal center frequency of GPR scans acquired tower site 5065. Notably, acquired data suggest that the effective center frequency is substantially lower and variable, depending on local electrical characteristics of surface soils/vegetation and related antenna loading/coupling effects. Figures 31-34 indicate that related influence on real permittivity values is minimal and a somewhat greater deviation for quadrature permittivity is not considered significant for purposes of the present study.

Table 2

GPR-1-AH1 (BH13-54-5065)					
Sample	**Adjusted Depth (m)**	**Resistivity (Ω-m)**	**In-Phase Permittivity**	**Quadrature Permittivity**	**Soil Unit**
1	0.00	62.9	45.25	3.01	1
2	0.12	185.4	46.91	2.28	3
3	0.22	209.0	52.95	2.35	3
4	0.32	177.1	53.42	2.31	4
5	0.46	49.3	35.51	3.89	7
6	0.76	55.0	32.60	3.13	8
7	1.92	97.8	32.20	2.87	8

Table 3

GPR-1-AH2 (BH13-53-5065)					
Sample	**Adjusted Depth (m)**	**Resistivity (Ω-m)**	**In-Phase Permittivity**	**Quadrature Permittivity**	**Soil Unit**
1	0.00	51.2	43.10	3.89	1
2	0.08	62.7	41.10	2.74	2
3	0.19	84.2	39.33	2.15	3
4	0.24	78.8	39.13	2.18	3
5	0.32	135.8	37.58	1.97	4
6	0.37	149.2	39.84	3.09	5
7	0.44	62.3	34.74	4.82	6
8	0.75	85.4	36.32	4.75	6
9	0.87	50.7	33.93	4.55	7
10	1.70	118.8	31.34	3.00	8
11	2.81	71.9	31.41	3.23	8

Table 4

GPR-2-AH1 (BH13-46-5065)					
Sample	Adjusted Depth (m)	Resistivity (Ω-m)	In-Phase Permittivity	Quadrature Permittivity	Soil Unit
1	0.00	63.8	47.94	3.39	1
2	0.10	122.6	51.76	3.13	3
3	0.23	216.0	51.34	2.71	2
4	0.30	170.2	53.69	2.69	3
5	0.47	146.6	49.02	2.77	3
6	0.50	137.5	39.82	2.97	4
7	0.88	46.2	34.67	3.81	7
8	1.14	66.9	34.36	3.58	8
9	1.33	112.1	31.97	2.10	9
10	2.48	75.4	29.50	2.95	8

Table 5

GPR-2-AH2 (BH13-47-5065)					
Sample	Adjusted Depth (m)	Resistivity (Ω-m)	In-Phase Permittivity	Quadrature Permittivity	Soil Unit
1	0.00	55.5	52.63	3.94	1
2	0.05	251.0	43.93	1.84	3
3	0.13	935.0	37.37	2.89	4
4	0.28	151.9	38.66	3.85	5
5	0.34	95.8	38.00	4.62	6
6	0.57	58.0	31.13	4.29	7
7	0.94	43.8	33.42	3.81	9
8	2.62	49.9	36.64	3.26	8

As for permittivity measurements, results again suggest a generally consistent pattern of correlation between identified soil units and associated electrical resistivity. Moreover, on plotting the relation between measured electrical resistivity and in-phase permittivity, as displayed in Figure 35, we find that representative soil units identified on the basis of qualitative field assessment are largely substantiated by quantitative analysis of associated electrical properties.

In particular, despite a number of interesting exceptions, it is observed that samples associated with given soil units group within separate and reasonably well-defined fields as delineated in Figure 35. Notable exceptions are as follows:

1. Unit 2 soils, identified as transitional between Units 1 and 3 (darker colour, despite apparently lesser organic content). Electrical measurements suggest that transition between surface organic layer and underlying topsoil horizon is better differentiated than appreciated.
2. A pair of identified Unit 3 soils (GPR-1-AH2 Samples 3 and 4) are far removed from Unit 3 field and plot intermediate between Unit 1 and Unit 6 fields.
3. Unit 4 soils appear to group well with Unit 5 soils with an exception again suggesting transition between Units 3 and 4 is better differentiated than appreciated.
4. Although Units 6, 7 and 8 are relatively similar in electrical properties, associated electrical characteristics remain distinct, within partially overlapping fields and support identified soil units.

Acknowledging foregoing limitations and with related appropriate adjustments, the appearance is that laboratory measurements have largely confirmed the validity of identified representative soil units as a reasonable preliminary basis for assessing the origin of observed radar reflectivity. What's also clear, however, is that even for soils with apparently similar physical characteristics, associated electrical properties can differ substantially and that significant variability in a given electrical parameter is not necessarily reflected in another.

Notably, for example, while prevailing moisture level has a predominant influence on the electrical properties of soils and sediments, Figure 35 reveals that in-phase permittivity and resistivity are not generally well correlated as might be expected. Rather, the appearance (base on a limited number of samples) is that the extent and nature of correlation between the two parameters varies considerably from soil unit to soil unit. Of course, it's important to appreciate that we are comparing radar-frequency permittivity with DC resistivity measurements, but what's more important is that the influence of soil moisture, as related to free-charge conduction and associated dispersion (frequency dependence) is reflected in the quadrature permittivity (ε''), rather than the in-phase component (ε').

In particular, with reference to Figures 31-34, it is moisture-dependent free-charge conduction and associated interfacial polarization that are responsible for the pronounced increase in quadrature permittivity at lower frequencies, while a lesser increase at the opposite end of the spectra is associated with high-frequency rotational polarization of constituent water. Significantly, at moderate frequencies in the range of 400 MHz (nominal center frequency for radar scans at tower site

5065), quadrature permittivity is roughly at minimum levels for tested soils/sediments.

Figure 36 displays the relationship between static electrical resistivity and quadrature permittivity for frequencies of approximately 400 MHz and 50 MHz. Predictably, the expected inverse correlation is more evident at lower frequency, but results generally confirm the significance of static electrical resistivity as a practical indicator of radar-frequency electrical properties. In particular, as described in Section 3.1.1, static or low-frequency electrical resistivity/conductivity is a useful predictor of antenna coupling efficiency (for surface soils) and provides a rough indication of relative attenuation rates within deeper soils/sediments.

With the benefit of radar-frequency electrical permittivity measurements, however, a more general and reliable predictor of frequency-dependent radar performance in soils and sediments is the so-called loss tangent, defined as the ratio of quadrature to in-phase permittivity, $tan\delta = \varepsilon''/\varepsilon'$. With reference to Figures 31-34, corresponding loss tangent spectra are displayed in Figures 37-38. Clearly, the normalizing influence of in-phase permittivity yields spectra that are better differentiated in proximity of 400 MHz than are associated quadrature permittivity spectra.

Again, as noted in Section 3.1.2, in-phase ε' and quadrature ε'' permittivity parameters (as reported here), are composite, effective parameters reflecting a wide range of physical and chemical processes, affecting both free and bound electric charge distributions within soils/sediments in response to application of time-variable electric fields of given frequency. In effect, the loss tangent represents the ratio of energy dissipated to energy stored through these processes and is obviously inversely correlated with both static electrical resistivity and in-phase permittivity as illustrated in Figure 39.[12]

In general, foregoing results confirm expectation that compact silt/clay-dominated units (Units 6, 7 and 8), developed at or below a seasonally fluctuating watertable, are characterized by relatively elevated loss tangents ($\varepsilon''/\varepsilon'$)[13], compared with granular silt loams, forming predominantly above the fluctuating watertable. Moreover, it is notable that loss tangents are generally higher at sites GPR-1-AH2

[12] Notably, loss tangent spectra in Figures 37-38 indicate that energy dissipation (~400 Mhz) in relatively resistive, near-surface loams (Units 3 and 4) is attributable in substantial part to viscous drag resisting rotational polarization of constituent water. Note that in all cases, loss tangent spectra approach that for water at high frequencies.

[13] While this is generally the case for lower frequencies, the relative extent of quadrature permittivity (ε'') reverses above approximately 500 MHz, presumably due to increasing influence of free/adsorbed water and related relaxation of associated orientational polarization.

and GPR-2-AH2, where a distinct, iron oxide-rich illuviation layer (Unit 5) is observed to mark the transition between foregoing regimes.

4.0 INTEGRATED ANALYSIS OF FIELD & LABORATORY INVESTIGATIONS

As described in Section 1 and 2, combined geophysical field investigations and AIA testing gave no indication of cultural remains and, otherwise, yielded mixed and inconclusive results. Consequently, auger investigations at tower site 5065 were viewed as an opportunity to derive a clearer understanding of the correlation between observed reflectivity, associated stratigraphy and related soil/sediment electrical properties. There is also a general interest to evaluate the potential of ground radar reconnaissance for detection and imaging of peat deposits, more widely, as part of a strategy for wet-site potential mapping within the broader polder.

Results described in foregoing Section 3 confirm that representative soil units identified through auger investigations at tower site 5065 are well differentiated on the basis of measured electrical properties and are reasonably expected to form a practical basis for addressing foregoing objectives.

Significantly, as described in Section 2.1.1, radar reflectivity is primarily related to the extent of contrast between the electrical properties at the interface between distinct soil/sediment units, rather than the absolute value of electrical parameters for any given unit. However, prior to turning our attention to radar reflectivity, we briefly consider the range of laboratory measurements reported in the previous section as related to corresponding field measurements and estimated radar velocity.

First, while there appears to be a consistent pattern of correlation between soil units and DC electrical resistivity, lab-measured resistivity levels (Tables 2 – 5) are generally lower than corresponding in situ measurements (presented in Figure 19) and display substantially greater variability as a function of depth. The latter observation is not surprising and is presumably attributable to underlying assumptions and related spatial averaging inherent in the VES inversion process[14].

Consistently lower lab-measured resistivities, however, imply correspondingly higher moisture levels in sampled soils and this is confirmed to some extent by comparison between estimated radar velocities and lab-measured electrical

[14] Note, by assuming a stack of horizontal layers having uniform electrical resistivity, the one-dimensional inversion procedure described in Section 2.1.2 effectively ignores natural lateral variability in stratification and associated electrical resistivity. The result is an inherently averaged model representing the predominant stratification and associated depth-dependent electrical resistivity of the subsurface.

permittivity values. In particular, on assuming the dielectric approximation $v \approx c/(\varepsilon')^{1/2}$, and with c=0.3 m/ns denoting the velocity of electromagnetic radiation in free space, estimated radar velocities between 0.045 and 0.055 m/ns imply a relative permittivity range of roughly ε'=30 – 45.[15] In contrast, the range of lab-measured permittivity is roughly ε'=30 – 54 (Figures 31-34 / Tables 2 – 5). Although the difference is presumably (again like VES measurements) attributable, in part, to spatial averaging inherent in velocity estimation[16], higher permittivity values are consistent with lower resistivity and, in general, with higher moisture content.

Again, however, radar reflectivity is primarily related to the extent of contrast between the electrical properties at a given stratigraphic contact, rather than the absolute values for individual soil units. Consequently, while variation in overall moisture level can have a significant modulating influence on the general extent of reflectivity, the effect on relative reflectivity is limited and, thus, foregoing deviation between in situ and lab-measured electrical parameters is not considered significant in relation to following analysis.

As described in Section 2.1.1, ground radar operates on the basic principle that a radar pulse emitted into the ground by a transmitter (Tx) antenna, is partially reflected at subsurface interfaces and subsequently detected by a co-located receiver (Rx) antenna as illustrated in Figure 3. In particular, the degree to which the propagating radar pulse is reflected is determined by the extent of electrical contrast at a given interface between dissimilar soil/sediment units as quantified by a so-called reflection coefficient R. The greater the electrical contrast, the larger the reflection coefficient and the higher the amplitude of the resulting signal registered at the receiver.

What's essential, however, is that the radar pulse continues to propagate into the subsurface, with the remainder of energy proportional to T=1-R, where T is the associated transmission coefficient. Energy carried by the transmitted radar pulse continues to be partitioned at successive stratigraphic contacts in accordance with associated reflection/transmission coefficients until at some

[15] Although a low-loss, dielectric assumption is routinely employed in connection with computer-based velocity analysis, it is rarely valid in a strict sense, particularly for fine-grained soils having substantial moisture content, and generally over-estimates associated permittivity for quasi-conductive media.

[16] Note that diffraction-based velocity estimation yields an average (RMS) velocity to the effective depth of a given signature and requires analysis of multiple signatures to establish depth-dependent velocity. For present purposes, approximate depth scales are based on a uniform representative velocity of 0.05 m/ns for tower site 5065 (consistent with that for tower sites 5060, 5062 and 5064).

point (dependent on radar system performance characteristics) energy returned via the reflected pulse is insufficient to be detected by the receiver.[12]

In general, the normal-incidence reflection coefficient for nonmagnetic, quasi-conductive media ($0.01 \leq tan\delta = \varepsilon''/\varepsilon' \leq 100$), including the majority of moist fine-grained soils, is $R_n=(Z_n-Z_{n-1})/(Z_n+Z_{n-1})$, where $Z_n=[(1/\varepsilon')/(1-\mathrm{i}\,tan\delta)]^{1/2}$ denotes the complex intrinsic impedance of the nth soil/sediment unit.

As illustrated in Figure 40, the radar signal acquired at a given location is effectively the depth/time-dependent reflection coefficient (reflectivity) sequence r(t) convolved with the radar pulse or wavelet w(t), where convolution denoted by $*$ amounts to replacing discrete reflectivity values with an appropriately scaled version of the radar wavelet.

Results of laboratory testing described in Section 3.2 are summarized in Figures 41 and 42, depicting depth-dependent variation of electrical resistivity (ρ —), permittivity (ε' – – / ε'' —) and loss tangent ($tan\delta = \varepsilon''/\varepsilon'$ —). In each case, associated reflection coefficients were computed and subsequently convolved with a representative wavelet[13] to yield a corresponding synthetic radar signal (—).[14] Finally, resulting synthetic signals are overlaid on associated radar scans in Figures 43 and 44 and, despite significant assumptions and approximations, synthetic signals appear to be very well correlated with acquired data.

Again, as observed in connection with the analysis of lab-measured electrical parameters, results suggest that field-identified soil/sediment units are generally representative, particularly for near-surface soils. Notably, however, comparison with corresponding stratigraphic sections in Figure 45 indicates that apparently continuous reflectivity is not in all instances associated with a consistent soil contrast. In particular, it is noted that more or less prominent reflectivity evident at

[12] Notably, only a portion of the energy carried away from a given interface is effectively incident at the subsequent interface, with the balance progressively dissipated through a range of intrinsic attenuation mechanisms, and to an extent quantified by the effective loss tangent ($tan\ \delta$) for the particular soil/sediment.

[13] The radar pulse is modelled by a pseudo-causal (time/phase-shifted) Ricker wavelet with a 400 MHz dominant frequency. As previously noted (see Footnote 11), acquired data suggest that the actual dominant frequency is substantially lower (perhaps as low as 300 MHz). However, in view of the gradual transitional characteristics of the Ricker wavelet, it is anticipated that assumption of a nominal 400 MHz dominant frequency yields better timing accuracy for present purposes.

[14] Note that present modelling of radar signals does not account for spherical spreading, progressive attenuation or related dispersion. Reflection phase is approximated as $\phi=(\mathrm{Re}[R_n]/|\mathrm{Re}[R_n]|)\times 180$ degrees, uniform antenna-ground coupling is assumed and multiple reflections are ignored.

a two-way transit time of approximately 15 – 25 ns (~ 0.5 m) is associated with a range of soil contacts, rather than a consistent or continuous stratigraphic horizon.

To some extent, this observation is attributable to limitations in associating specific samples with identified soil units as revealed by subsequent analysis of lab-measured soil electrical parameters (see noted exceptions above – pg. 23 – with reference to Figure 35). However, it is also noted that the character of subject reflectivity varies substantially along GPR transects and it is perfectly reasonable to presume that this variability is related to stratigraphic variation associated with minor topographic relief, moisture level, vegetation and related influence on sediment deposition and soil formation. Moreover, despite a lack of direct constraints on local groundwater level, it is evident from soil profiles (Figures 21-26 and 45) that substantial lateral variability exists and that discontinuous reflectivity at approximately 15-25 ns (~ 0.5 m) coincides roughly within the long-term range of local water table fluctuation.[15]

Figures 43-45 also reveal that the level of soil sampling was insufficient to resolve smaller-scale and less apparent stratification associated with significant radar reflectivity. In particular, the appearance is that variably laminated silt/sand sequences within Units 7/8 have in some instances given rise to a composite pattern of reflectivity due to multiple reflection and interference and could potentially explain the zone of prominent reflectivity identified at the north end of transect GPR-1 (see Figure 43 and Section 2.2.1 for related discussion).

In general, for laminated stratification comprising layers that are thin in comparison with the dominant radar wavelength[16], there is potential for multiple reflection and interference to yield a pattern of apparent reflectivity (interference pattern) that is generally stronger than it would be for an isolated interface at equivalent depth, and for which the apparent thickness and spacing between interference bands is on the order of the radar pulse-width.

Notably, characteristics of prominent reflectivity at the northern end of transect GPR-1 (Figure 43) appear to be largely consistent with foregoing expectations and with laminated sediments encountered at auger site GPR-1-AH1. Moreover, a similar pattern of reflectivity appears to be associated with comparable stratification at the eastern end of radar scan GPR-2 (Figure 44 - auger site GPR-

[15] Notably, the local water table was not encountered by AIA excavations (to maximum 1.0 m) at any of the sites described herein. In general, beyond seasonal precipitation and tidal effects, the water table beneath Pitt Polder is strongly influenced by dyking, an extensive network of drainage/irrigation channels and associated pumping.

[16] Note radar scans acquired at tower site 5065 suggest a dominant radar wavelength of approximately 15 cm compared with thin-bed thickness generally less than 1 cm.

2-AH1). Significantly, however, the observed band of apparent reflectivity is generally limited to an equivalent thickness of roughly 0.5 – 0.6 m (assuming an estimated radar velocity of 0.05 m/ns) and, consequently, appears to be associated with only the upper section of a more extensive sequence of interbedded deposits. Moreover, the noted pattern of reflectivity is in some locations absent in connection with similar laminated sediments (e.g. GPR-1-AH2).

In particular, after shallowing in proximity of auger site GPR-1-AH1, the distinct band of reflectivity observed at the northern end of GPR-1 diminishes abruptly and is no longer discernable south of approximately 17N. Strongly laminated sediments at GPR-1-AH2 (~12N) yield only minor reflectivity consistent with modelling based on bulk electrical properties. Shallower, sub-horizontal reflectivity persists in the interval 15 – 25 ns (~0.5 – 1.0 m), but again with relatively limited amplitude compared with a stronger signature at auger site GPR-1-AH1.

Given the evident disparity between associated soil profiles (Figures 21 and 22), it is not difficult to appreciate that related radar reflectivity is considerably different at the two sites. And, notably, a similar contrast is observed between stratigraphic sections sampled at auger sites GPR-2-AH1 and GPR-2-AH2 (Figures 25 and 26). What is more significant, however, is the relative similarity of stratigraphic sections at GPR-1-AH1 and GPR-2-AH1 in association with generally stronger and more extensive reflectivity.[17] In particular, corresponding radar scans at both locations display banded reflectivity that is tentatively attributed to multiple reflection and interference effects associated with the upper section of variably laminated sediments (Units 7/8).

Significantly, although further quantitative analysis of sediments is required, the appearance is that the anomalous reflectivity pattern may be enhanced due to substantially higher organic/clay content and related moisture level within the upper section of laminated sediments at these sites.

In general, foregoing analysis demonstrates the benefit of combining geophysical reconnaissance with direct soil sampling and laboratory measurements to yield efficient, well-constrained characterization of subsurface conditions with minimal disturbance. Despite significant limitations and uncertainty related to natural stratigraphic complexity, localized constraints on the nature and electrical

[17] Conversely, note also the relative similarity of stratigraphic sections at GPR-1-AH2 and GPR-2-AH2 in association with generally more limited reflectivity.

properties of stratified soils/sediments provides a basis for more confident and reliable assessment of broader stratigraphic trends and features.

5.0 ASSESSING RESULTS IN ARCHAEOLOGICAL CONTEXT

To assess potential archaeological implications it is necessary to frame foregoing findings in the context of Holocene geomorphology and radiocarbon chronology.

It is well established (Clague et al., 1982; 1983) that following retreat of the Cordilleran ice sheet (approximately 11,000 BP), the lowland presently comprising Pitt Polder was a effectively a fjord open to the Strait of Georgia (Figure 46). By roughly 10,000 BP, rapid redeposition of glacial sediments by the Fraser River subsequently formed a prograding delta front across and northward into the fjord as well as to the southwest (between Burrard and Surrey uplands) into the Strait of Georgia at what is presently New Westminster. Sea level was simultaneously falling due to isostatic uplift of the coastal landmass and continued to fall to a Holocene low of roughly 12 m below present level before a balance between isostatic and eustatic adjustments was reached approximately 8500 BP.

Radiocarbon dating of peat deposits situated roughly 11–12 m below present sea level (Mathews et al., 1970; Clague et al, 1983) suggests that this balance persisted for about a millennium and that associated estuarine depositional environments were comparable to present-day wetlands on the Fraser River floodplain, including Pitt Polder.

As indicated in Figure 46, however, sea level subsequently rose at a relatively rapid rate during the following two millennia (due predominantly to continued eustatic forcing with diminished isostatic adjustment), approaching present day level by about 5500 - 5000 BP. Associated marine transgression, tidal flooding and fluvial aggradation continued to advance deltaic deposits northward into the former Pitt fjord, with the delta front located well north of the present project site by 5000 BP.[18] Accompanying vertical accretion amounted to roughly10 metres of silt and sand deposits, prior to sea level restabilizing at approximately 2 m below present-day level (Mathews et al., 1970; Clague et al, 1983; Williams and Roberts, 1988).

[18] Ashley (1977) notes that “by 4,645 ± 95 BP the leading edge of the Pitt delta stood at least 20 km north of Fraser River near the present outlet of Pitt Lake”. Moreover, while details of the Pitt River’s evolution do not appear to be well established, Ashley asserts that “there is no geomorphic evidence on the floodplain to suggest that the channel has migrated extensively during its development”.

With relatively limited and gradual sea-level rise Since 5000 BP, stable wetland and estuarine depositional environments developed on the Fraser River floodplain and have largely persisted to present day. The Pitt delta has continued to advance (presently extending well into the southern reaches of Pitt Lake) and vertical accretion has continued on the broader polder floodplain, comprising up to 2 m of stratified overbank deposits (Armstrong and Hicock, 1980). Soils have subsequently developed on these sediments and significant localized peat deposits have also accumulated, including within the subject project area as identified in Figure 47 (Unit SAb).

Preliminary results of radiocarbon dating on samples from cores recovered at tower site 5065 (Table 6 - Peter Locher, 2014, personal communication) confirm that the upper 2.0 – 3.0 m of soil/sediment sections span the late Holocene transition to stable present-day sea level, including roughly the full range of dated occupation at DhRp-52 (5700 – 3200 cal BP).[19]

Table 6

Calibrated Radiocarbon Dates – Tower 5065

UCIAMS - University of California Irvine AMS

UCIAMS #	Adjusted Depth (m)	Sample Material	Conventional ^{14}C Age (BP)	Calibrated ^{14}C Age (cal BP)
135532	0.55 (GPR-2-AH1)	wood	2,600	2,735 – 2,755
135533	1.02 (GPR-1-AH3)	wood	4,060	4,515 – 4,580
135534	3.04 (GPR-1-AH3)	wood	4,945	5,640 – 5,715
140039	3.76 (GPR-1-AH3)	wood	5,350	6,100 – 6,160
135535	4.10 (GPR-1-AH3)	wood	5,820	6,600 – 6,670
135536	16.85 (GPR-1-AH3)	wood	8,275	9,195 – 9,325
135537	17.46 (GPR-1-AH3)	wood	8,670	9,550 – 9,675
135538	21.38 (GPR-1-AH3)	wood	9,080	10,210 – 10,250
135539	29.68 (GPR-1-AH3)	wood	44,000	45,080 – 49,940

As identified in Figure 48, DhRp-52 is situated on Sumas Drift (Unit Se) deposits at an elevation sufficiently above the broader Fraser River floodplain to have remained habitable throughout the Holocene deglaciation and associated sea-level adjustment (Diaz and Hoffmann, 2010).[20] However, marginal estuarine and

[19] The wet-site component of DhRp-52 appears to have been a later phase focus of cultural activity, with associated dates ranging from approximately 3800 – 3200 cal BP. See Connaughton and Diaz (2010) for details of radiocarbon chronology at DhRp-52.

[20] Significantly, mapping in Figure 48 also places DhRp-52 at roughly the contact between mid-late Holocene fluvial overbank sediments (Unit Fb) and coarser-grained, Pleistocene proglacial deltaic deposits (Unit Se). In fact, the suggestion on basis of stratigraphy and radiocarbon dating is that DhRp-52 actually straddles this contact, with the wet-site component of the DhRp-52 residing within mid to late Holocene sediments (Units Fb/SAb) deposited at the western margin of a relict proglacial ridge (Unit Se).

wetland habitats at lower elevations offered a rich diversity of aquatic and terrestrial resources that were certainly exploited by residents of DhRp-52 and/or other local habitation sites.

Although few have been extensively investigated, numerous archaeological sites have been recorded within the upper Pitt Polder, largely along tributary and distributary channels of the Pitt River. In general, the primary focus of prehistoric activity at these sites was on seasonal procurement and processing of food resources and other raw materials. A wide range of wetland plant resources was gathered, including berries, roots and tubers. Among these, according to ethnographic sources, was the wild potato, or wapato, a highly valued food source harvested from a variety of shallow-water, wetland environments (Crowe-Swords, 1974; Spurgeon, 2001).

In particular, it was the discovery of dense concentrations of wapato, preserved in water-saturated peat deposits at DhRp-52 that ultimately motivated the present study. Significantly, wapato concentrations were associated with a submerged rock pavement feature and pointed wooden implements, tentatively interpreted as partial remains of digging sticks employed in the harvesting of wapato tubers (Hoffman and Huddlestan, 2010). The implication that residents of DhRp-52 were potentially engaged in deliberate and organized plant management amounts to an unprecedented development in Northwest Coast archaeology and there is significant interest to assess the extent of evidence for similar practices in similar contexts at other sites in the broader Pitt Polder wetlands.

According to Styan (1981) later Holocene peat deposits began developing across the Fraser River floodplain about 4500 BP, with specific characteristics depending on the local depositional setting. In particular, peat deposits near Pitt Meadows initially accumulated within freshwater marsh enviroments in shallow depressions and inactive distributary channels. Consistent with the description of peat deposits (Unit SAb) in Figure 47 (Armstrong and Hicock, 1980), Styan observes that these deposits generally developed on stratified and inter-laminated sequences of silty sand, silt and silty clay (overbank deposits), becoming predominantly finer-grained upward as a reflection of stabilizing sea level.

Peat deposits accumulated in flooded depressions and constrained channels as result of increasing organic sedimentation on, and progressively within, these floodplain deposits as the nature and pattern of wetland vegetation simultaneously evolved. As described by Styan (1981) the peat successional sequence begins in freshwater, sedge-grass marsh environments with formation of dark mucky gyttja (sapropel) and/or muddy sedge-clay peats, incorporating sedge stems, roots and accumulated wood and bark fragments deposited with clay-rich flood sediments.

As sedge-grass marshes evolve and/or supply of mineral sediments is gradually reduced, resulting sedge-grass peats become more fibrous.

Ultimately, depending on site-specific geomorphology and depositional setting, continued organic accumulation and/or further reduction in clasitic sedimentation favours gradual succession to sedge-sphagnum and sphagnum peats. However, the precedent at DhRp-52, together with the natural range of wapato habitat (Spurgeon, 2001), suggests that the stratigraphic context of interest is associated with early-stage gyttja, sedge-clay and sedge-grass peats.

Thus, midway through the Holocene, sea level is gradually stabilizing following more than 2000 years of relatively rapid marine transgression. Across the Lower Fraser floodplain, including Pitt delta, the rate of sedimentation is declining and the pattern and composition of wetland vegetation is becoming established within a wide range of evolving depositional environments. The appearance is that by 3800 BP, local inhabitants are gathering and potentially managing a wide range of aquatic and terrestrial plant resources, including wapato, at sites throughout the Pitt River wetlands. In particular, findings at DhRp-52 suggest that wapato was being harvested from shallow-water, marsh-like environments where decaying plant remains were simultaneously accumulating, together with flood-deposited inorganic sediments, to form early-stage peat deposits.

Although neither the present investigation nor related archaeological testing yielded any direct evidence to suggest that foregoing resource exploitation and management activities were occurring in proximity of ILM tower sites, the presence of potentially significant peat deposits remains uncertain.

In particular, as regards the mapping of lowland peat deposits in Figure 47, description of associated soil unit SAb notes that these deposits are “in part overlying Fb” (later Holocene overbank deposits) and this appears to be the case at tower site 5065 on the basis of auger testing. In effect, the implication is that the identified peat deposit surrounding tower site 5065 (Figure 47) amounts to surface organics-rich layers (Units 1 and 2 – Figure 28). Notably, However, these surface units were also encountered and are generally more substantial at tower site 5066, well beyond the mapped deposit.

It is also notable that the identified SAb deposit in proximity of tower site 5065, as well as others north and south of the project site, were added subsequent to an earlier version of the map (Armstrong and Brown, 1957). Unfortunately, the basis upon which SAb deposits were added is not described, nor is there any indication of the extent of variability within a given deposit.

As a former delta/floodplain, the polder is generally characterized by low relief. However, a wide range of active and relict fluvial landforms have and continue to be subject to periodic or sustained flooding by surface water, groundwater and/or rainfall. As described by Styan (1981), it is within these depressed topographic features that peat deposits accumulate and, consequently, the occurrence, nature and extent of peat deposits should presumably be well correlated with the scale and morphology of these features. Moreover, to the extent that the aim is detect and identify archaeological sites in association with peat deposits, related geomorphic features are in large part or entirely submerged in sediments, both organic and inorganic.

Consequently, although the presence of significant subsurface peat accumulations has not been directly established or confirmed, it may be possible to infer potential deposits by identifying associated stratigraphic structures, and results at tower site 5065 suggest a plausible example.

In particular, combined assessment of radar scan GPR-1 (Figures 17 and 43), together with constraints provided by auger investigations at adjacent site GPR-1-AH1, suggests that the prominent band of reflectivity observed at the northern end of the transect is likely associated with the upper section of stratified overbank deposits (Units 7/8). Moreover, as previously noted, anomalous reflectivity may be due in part to substantial organic content within these sediments. Irrespective of the origin of observed reflectivity, however, there is evident indication of a broad pre-existing depression north of 20N that has apparently been leveled via subsequent accumulation of sediments. There is also limited suggestion of a similar feature beyond the eastern end of radar scan GPR-2.[21]

Radiocarbon dating in Table 6 suggests that substantial organic content within the upper section of Units 7/8 at auger site GPR-1-AH1 and GPR-2-AH2 is potentially consistent with sea level stabilization and onset of organic sedimentation around 5000 – 4500 BP (Styan, 1981; Clague et al., 1983). Interestingly, however, the later transition (~3000 BP) from laminated silty sands / clayey silts (Units 7/8) to largely uniform clayey silts / silty clays (Units 4-6), with relatively limited organic content, appears to suggest a more significant shift in the local depositional environment.

Unfortunately, it was not possible to extend auger investigations north of GPR-1-AH1 due to potential environmental impacts. However, shovel testing (to a minimum depth of 0.5 m) was carried out at four sites indicated in Figure 43 and

[21] Note also that the nature of soil/sediments associated with similar banded reflectivity at the south end of radar scan GPR-1 was not investigated as part of auger testing as the site is located outside the ILM impact area. Although a shovel test located at 16S gave no indication of unusual conditions, it is uncertain whether the depth of investigation was sufficient to assess the origin of identified reflectivity.

with no significant or unusual conditions noted (Tyler Hicks, 2013, personal communication). Unfortunately, soils/stratigraphic information was not recorded and, consequently, there is no basis for comparison/correlation with results of subsequent auger investigations.

As regards the longer-range continuity of stratigraphy and soil/sediment units identified at tower site 5065, it is noted that shovel tests at tower sites 5060, 5062 and 5064 (Wilkerson, 2012) consistently identified “mottled orange/gray sandy/silty clay” immediately below grade and overlying “grey-blue silty clay”. Perhaps more significantly, the foregoing units were found at all locations to overly a thin (< 0.2 m) “peat-like” stratum, comprising a “dark brown peaty loam”, at approximately 0.3 m below grade. Underlying “gray brown silty clay” was observed to a maximum depth of 1.0 m, with “plant material” noted near base of excavations at all sites.

Accepting subjective variability in the qualitative description of soil/sediment attributes, it is possible that the upper section of the foregoing described sequence correlates with the transition from Unit 6 to Units 7 at tower site 5065, and with the “peat-like” stratum associated with the upper organics-rich section of Unit 7 at auger sites including GPR-1-AH1 and GPR-2-AH1.[22] It is more difficult, however to reconcile the underlying “gray brown silty clay” stratum with extended sequences of variably-textured and interbedded sediments (Units 7/8) identified at tower site 5065. Although it is beyond the scope of the present project, a review of geotechnical logs recorded by Golder Associates at all sites may provide a consistent basis for assessing site-wide near-surface stratigraphic correlation.[23]

6.0 CONCLUSIONS AND RECOMENDATIONS

Although archaeological sampling, including shovel testing and auger investigations, yielded no direct evidence of cultural activity, foregoing described ground radar reconnaissance was generally inconclusive in regard to the identification of potential cultural deposits at planned ILM tower sites 5060, 5062, 5064, 5065 and 5066.

[22] Notably, this interpretation suggests that overlying soil units observed at tower site 5065, comprising roughly 0.25 – 0.5 m, were potentially removed and/or redistributed at tower sites 5060, 5062 and 5064 during clearance and/or regrading of agricultural fields. This interpretation may also be consistent with anomalous antenna-ground coupling characteristics observed at these sites. Note that center elevations at tower sites 5060, 5062 and 5064 are 1.446 m, 1.222 m and 1.286, respectively.

[23] For complete analysis and reporting of site-wide auger investigations and associated radiocarbon dating see Locher (2014).

In contrast with preliminary radar scans adjacent to the Pitt River dyke, the quality and interpretability of data acquired at tower sites 5060, 5062 and 5064 (within developed agricultural fields) was degraded and compromised by system noise associated with antenna-ground coupling and uncertainty regarding the extent of ground disturbance associated with agriculture development. A thick and irregular cover of sphagnum mosses, together with localized standing water, imposed similar restrictions at tower site 5066.

Only at tower site 5065 were acquired radar scans considered interpretable with a sufficient degree of confidence to identify features of potential significance. In particular a prominent reflectivity feature was delineated at the northern end of transect GPR-1, with a similar pattern of reflectivity noted at the southern end of the same transect and at the eastern end of transect GPR-2. Although subsequent shovel testing indicated an absence of cultural materials, the depth of investigation was largely insufficient to sample the identified feature and auger investigations were limited by environmental impact considerations. Consequently, the origin of observed reflectivity and potential archaeological significance remain uncertain.

As much as ground radar investigations were inconclusive in respect of primary reconnaissance aims, however, results are simultaneously encouraging and represent significant initial progress in developing the potential of GPR for non-invasive archaeological reconnaissance within the wetlands context. In particular, integrated analysis of radar scans at tower site 5065, together with coincident auger investigations and associated laboratory measurements, has established a preliminary soil/sediment sequence and confirmed direct correlation between key stratigraphic contacts and associated radar reflectivity.

Significantly, a limited range of representative soil horizons (units), established largely on qualitative field evaluation of observable characteristics, proved to be well differentiated on the basis of associated electrical properties. Although significant limitations were noted, the extent to which preliminary soil units formed an adequate basis for predicting observed radar reflectivity was unexpected and bodes well for GPR's ultimate potential as a reconnaissance tool in the polder context. Further work, however, is required to establish the fuller extent of stratigraphic variability and to appropriately augment and refine the range and characteristics of representative soil/sediment units.

For example, it is notable that the substantial extent of organic content within stratified sediments comprising the upper section of Units 7/8 (at tower site 5065) was not apparent in the field and recognized only under subsequent laboratory examination. Thus, although Unit 7 is here designated (separate of Unit 8) primarily on the basis of significant orange mottling, it is evident in hindsight that Unit 7 is more significantly distinguishable on the basis of organic content that in some instances extends beyond observed mottling. Moreover, there may be sufficient basis for subdividing Unit 7 to distinguish a relatively limited upper section that is apparently less strongly stratified or laminated than the underlying section.

Foregoing suggested adjustments should be given further consideration in relation to the reported stratigraphic sequence encountered by shovel testing at tower sites 5060, 5062 and 5054 (Wilkerson, 2012), together with reassessment of acquired radar scans and a review of associated auger logs (and corresponding core images) recorded by Golder Associates.

Beyond the present project site, and to further establish a quantitative connection between results reported herein and previous experience at DhRp-52, it would be of significant interest to obtain one or more samples of the peat deposits identified at DhRp-52. Assuming intact portions of these deposits remain accessible, sufficient samples could be recovered by hand auger and subsequently analyzed in accordance with methods described in Section 3.1 to characterize associated electrical properties. Moreover, to the extent that sufficient sample is available, consideration should be given to paleobotanical assessment of the organic fraction from the upper section of Unit 7 at tower site 5065, as well as to related radiocarbon dating.

More generally, it is recommended that consideration be given to further integrated investigations within the Pitt Polder, combining ground radar and auger sampling to further calibrate and develop the potential of GPR for more confident identification of potential peat deposits as indicators of wet-site potential. In particular, it is suggested that investigations could focus on previously investigated sites where peat deposits have already been confirmed by excavation, or at other sites where surficial peat deposits have been previously mapped (e.g. within the Pitt Polder Wildlife Management Area - Armstrong and Hicock, 1980).

Finally for optimum results, ground radar investigations within the polder should be carried out during summer months or early autumn to avoid high groundwater levels and saturated surface conditions.

We trust that the foregoing report satisfies your current requirements. Should you require addition information or clarification, please contact the undersigned.

Yours truly,
Terrascan Geophysics

Guy Cross, Ph.D.

REFERENCES

Ashley, G. M., 1977, Sedimentology of a freshwater tidal system, Pitt River – Pitt Lake, British Columbia, Unpublished Ph.D. dissertation, Department of Geological Sciences, University of British Columbia, Vancouver, Canada.

Armstrong, J. E. and Hicock, S. R., 1980, Surficial geology, New Westminster, west of sixth meridian, British Columbia, Geological Survey of Canada, Map 1484A, Scale 1:50,000, Ottawa, Canada.

Clague, J. J., Luternauer, J. L., and Hebda, R. J., 1983, Sedimentary environments and postglacial history of the Fraser Delta and lower Fraser Valley, British Columbia, Canadian Journal of Earth Science, 20, 1314 – 1326.

Clague, J., Harper, J. R., Hebda, R. J., and Howes, D. E., 1981, Late Quaternary sea levels and crustal movements, coastal British Columbia, Canadian Journal of Earth Science, 19, 597 – 618.

Connaughton, S. P., and Diaz, A., 2010, Radiocarbon chronology, Section 5 in Archaeological Excavations at DhRp-52 Heritage Investigation Permit #2007-097, Volume 1 – Final Permit Report, T. Hoffmann, Editor.

Cross, G., 2000, Soil properties and GPR detection of landmines: a basis for forecasting and evaluation of GPR performance, Contract Report DRES CR 2000 - 091, Defence Research and Development Canada.

Cross, G., 2007, Katzie wet site (DhRp-52) – ground radar investigation, Report on file, Katzie Development Corporation, Pitt Meadows, BC.

Crowe-Swords, D. B., 1974, The Carruthers site: a late prehistoric site in the Lower Fraser Valley, Unpublished M.A. dissertation, Department of Archaeology, Simon Fraser University, Burnaby.

Diaz, A., and Hoffmann, T., 2010, Geology and geomorphological setting, Section 3 in Archaeological Excavations at DhRp-52 Heritage Investigation Permit #2007-097, Volume 1 – Final Permit Report, T. Hoffmann, Editor.

Hoffmann, T., and Huddlestan, S., 2010, Chaper discussion and conclusions, Section 11 in Archaeological Excavations at DhRp-52 Heritage Investigation Permit #2007-097, Volume 1 – Final Permit Report, T. Hoffmann, Editor.

Hoffmann, T., Wilkerson, E. and Nord, C., 2010, Natural and cultural context, Section 2 in Archaeological Excavations at DhRp-52 Heritage Investigation Permit #2007-097, Volume 1 – Final Permit Report, T. Hoffmann, Editor.

Locher, P., 2014, Sonic sediment assessment for Interior to Lower Mainland transmission line project (ILM), Pitt Polder, District of Pitt Meadows, Report on file, Katzie Development Corporation, Pitt Meadows, BC.

Locher, P., and Clague, J., 2007, Investigation of sediment cores from Katzie Slough, Pitt Meadows / Maple Ridge, British Columbia, Report on file, BC Archaeology Branch, Victoria.

Mathews, W. H., Fyles, J. G. and Nasmith, H. W., 1970, Postglacial crustal movements in southwestern British Columbia and adjacent Washington state, Canadian Journal of Earth Sciences, 7, 690 – 702.

Spurgeon, T., 2001, Wapato (Sagittaria latifolia) in Katzie traditional territory, Pitt Meadows, British Columbia, Unpublished M.A. dissertation, Simon Fraser University, Burnaby.

Styan, W. B., 1981, The sedimentology, petrography and geochemistry of some Fraser Delta peat deposits, Unpublished M.Sc. dissertation, Department of Geological Sciences, University of British Columbia, Vancouver.

Wilkerson, E., 2012, ILM Pitt Polder AIA preliminary results for towers 5060, 5062 and 5064, Internal Report, KDC Archaeology, Pitt Meadows, BC.

Zohdy, A. A. R., 1989, A new method for automated interpretation of Schlumberger and Wenner sounding curves, *Geophysics,* 54, 2, 245-253.

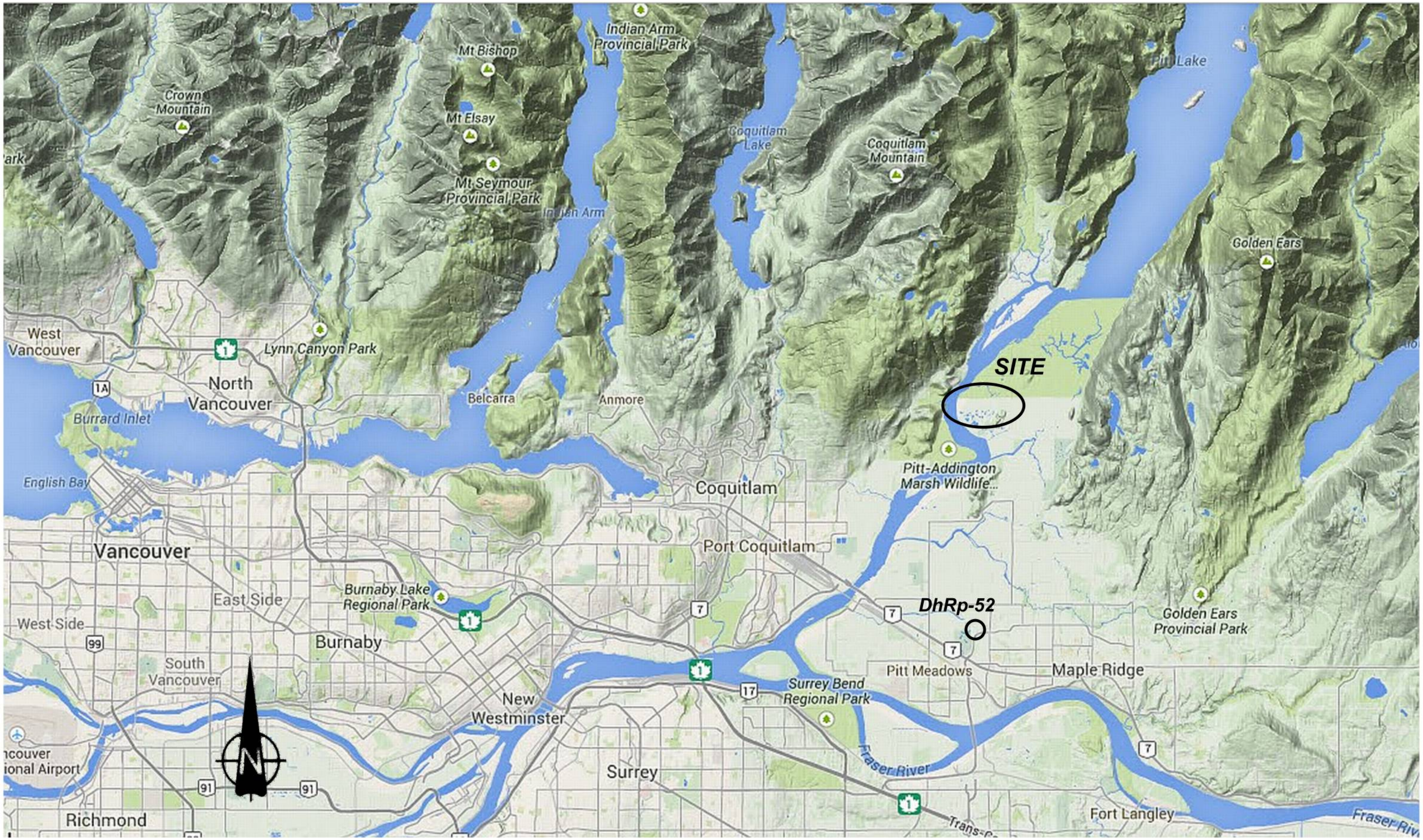

Terrascan Geophysics	**PROJECT SITE LOCATION**		FIGURE: **1**
	PROJECT: *KDC – Pitt Polder*	DRAWN BY: *GMC*	DATE: *20 January, 2013*

Terrascan Geophysics

PHASE 1 INVESTIGATION SITES

PROJECT:	DRAWN BY:	DATE:	FIGURE:
KDC – Pitt Polder	*GMC*	*20 January, 2013*	*2*

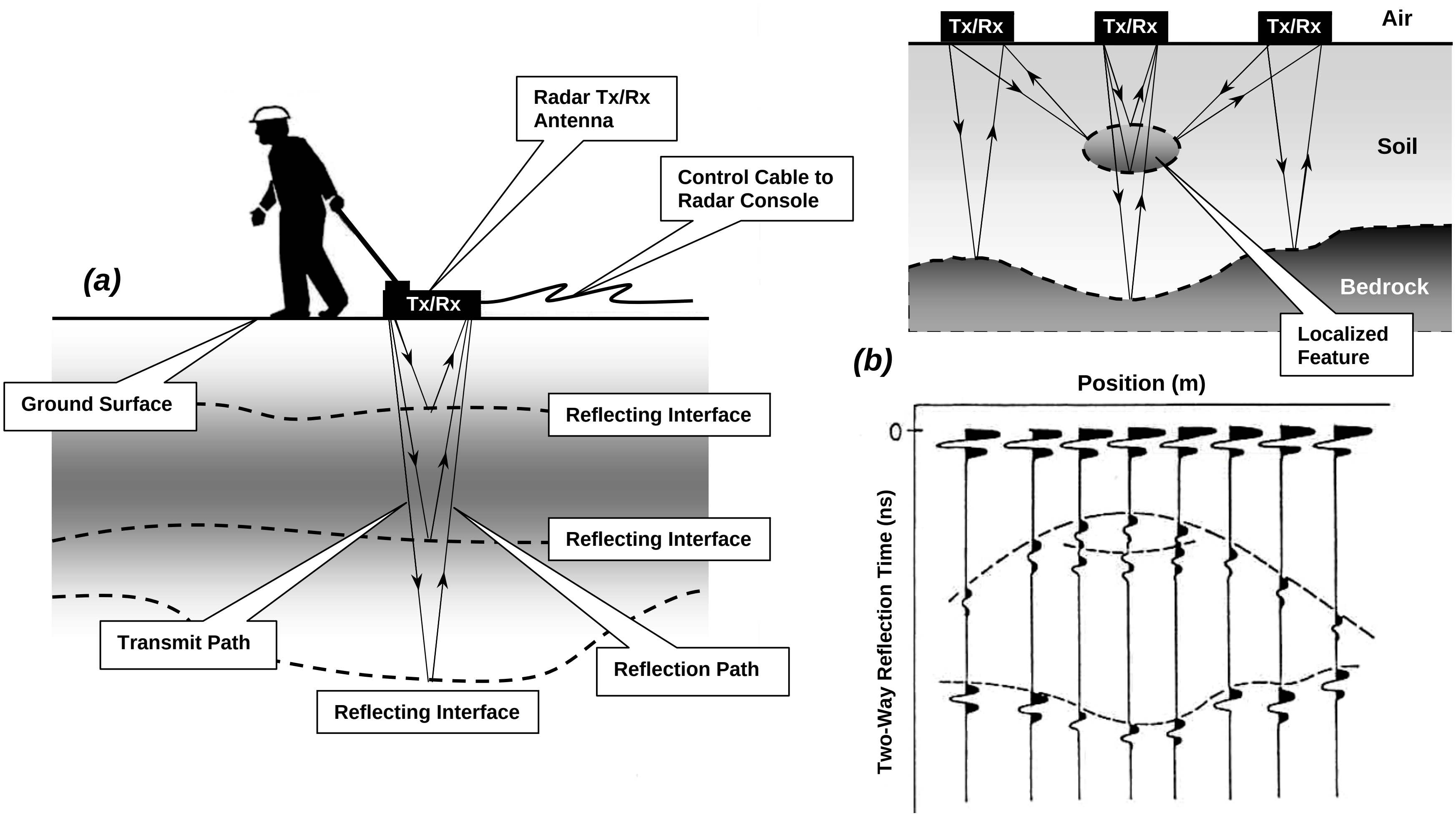

Terrascan Geophysics	GROUND PENETRATING RADAR		FIGURE: 3
	PROJECT: *KDC – Pitt Polder*	DRAWN BY: *GMC*	DATE: *20 January, 2013*

NOTE: Electrical resistivity measurement involves incnjection of a controlled test curernt I by application of high voltage across electrodes C_1 and C_2 and measurement of resulting potential differnce ΔV between electrodes V_1 and V_2 .

The corresponding effective resistance is given by Ohm's law $R=\Delta V/I$.

The effective resistance is scaled by a geometrical constant γ for specific electrode configuration to yied apparent resistivity $\rho_a=\gamma R$.

For the Wenner configuration as depicted $\gamma=2\pi a$, yielding $\rho_a=\gamma R=2\pi aR$.

For the case of a uniform soil, the apparent resistivity is equivalent to the actual intrinsic resistivity $\rho_a=\rho$.

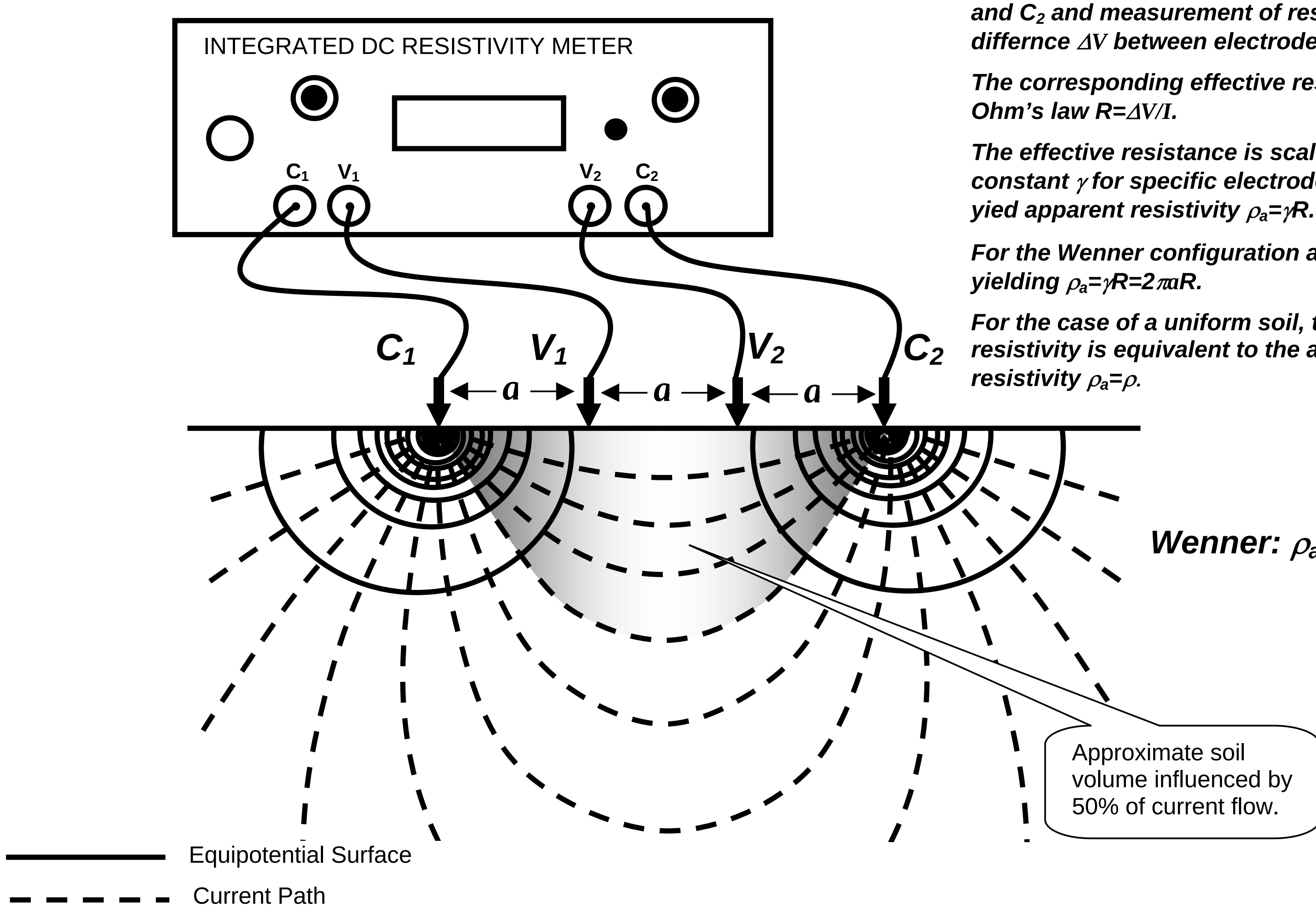

Terrascan Geophysics	***ELECTRICAL RESISTIVITY***			FIGURE: **4**
	PROJECT: ***KDC – Pitt Polder***	DRAWN BY: ***GMC***	DATE: ***20 January, 2013***	

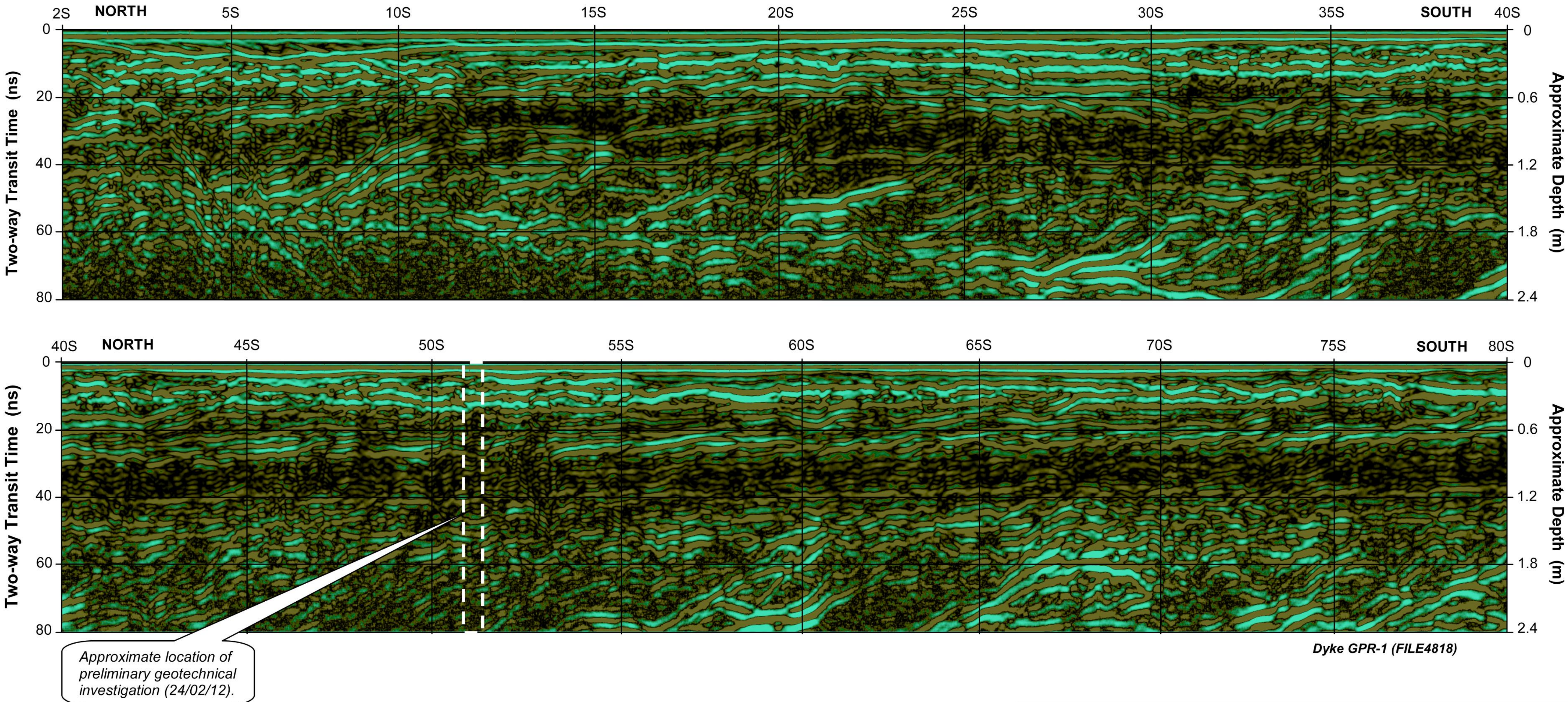

Dyke GPR-1 (FILE4818)

NOTE: Approximate depth scale based on estimated average radar velocity v=0.06 m/ns.

Radar velocity varies with soil composition, texture and moisture content. Indicated depth scale is provided for approximate reference only. Fundamental reference is two-way transit time in nanoseconds (ns).

GROUND PENETRATING RADAR
DYKE ROAD – GPR-1 – 400 MHz – 80 ns

PITT POLDER – KDC/BC HYDRO ILM

Terrascan Geophysics

PROJECT: *KDC Pitt Polder*	
DRAWN BY: *GMC*	FIGURE: **5**
DATE: *15 January, 2013*	

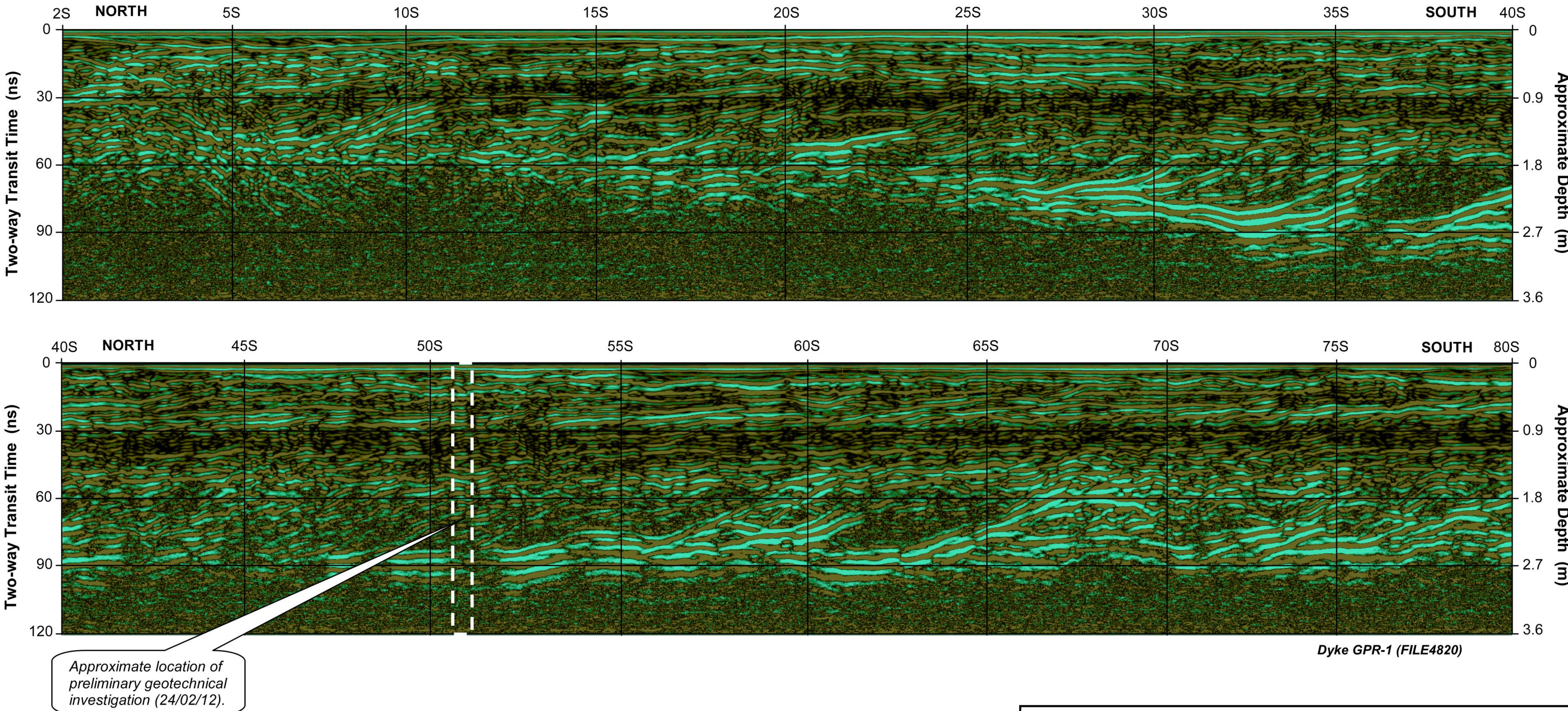

Dyke GPR-1 (FILE4820)

***NOTE:** Approximate depth scale based on estimated average radar velocity v=0.06 m/ns.*

Radar velocity varies with soil composition, texture and moisture content. Indicated depth scale is provided for approximate reference only. Fundamental reference is two-way transit time in nanoseconds (ns).

GROUND PENETRATING RADAR **DYKE ROAD – GPR-1 – 400 MHz – 120 ns**		
PITT POLDER – KDC/BC HYDRO ILM		
Terrascan Geophysics	PROJECT: *KDC Pitt Polder*	
	DRAWN BY: *GMC*	FIGURE: **6**
	DATE: *15 January, 2013*	

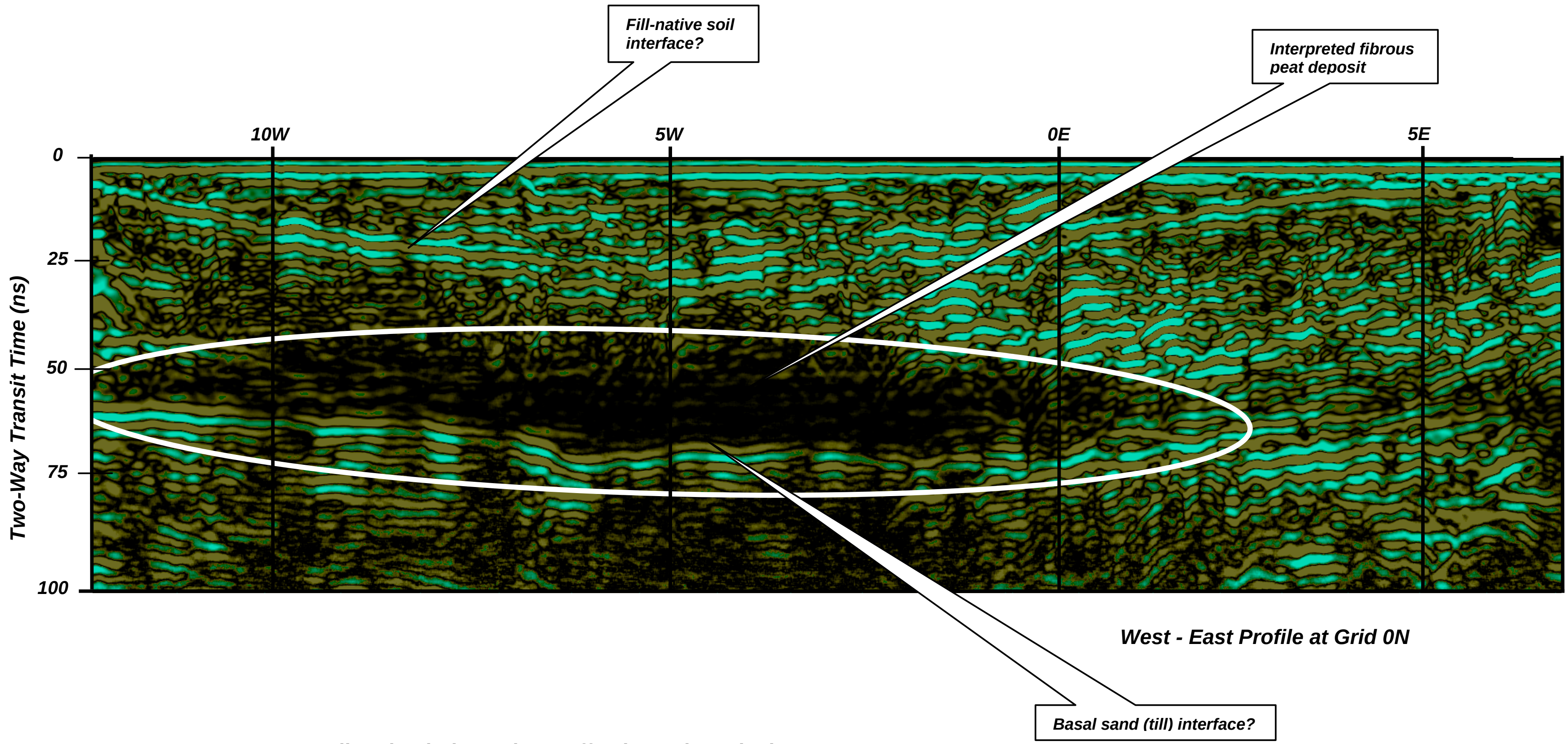

NOTE: Corresponding depth depends on effective radar velocity.
Estimated radar velocity varies with soil composition
and ranges from approximately v=0.04 – 0.05 m/ns in peat
to roughly v=0.05 – 0.06 m/ns in sands (till). In general,
low velocities are attributed to saturated conditions.

SOURCE: Cross (2007) - revised

Terrascan Geophysics	KATZIE WET SITE (DhRp-52) - GROUND RADAR INTERPRETED WEST – EAST BASELINE PROFILE		FIGURE: 7
	PROJECT: Katzie Wet Site	DRAWN BY: GMC	DATE: 18 November, 2007

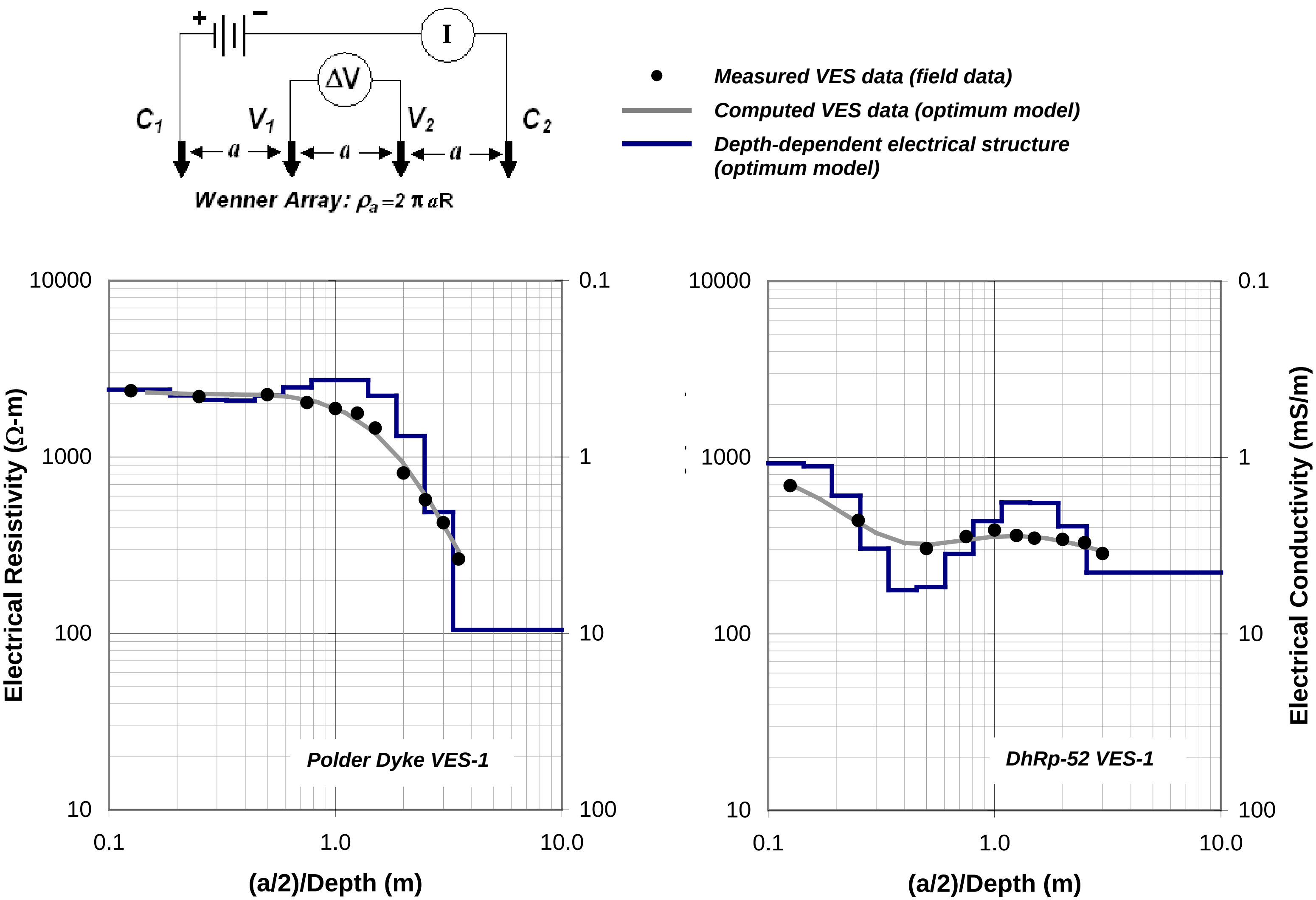

Terrascan Geophysics	***VERTICAL ELECTRICAL SOUNDINGS*** ***PITT RIVER DYKE – DhRp-52***	FIGURE: **8**
	PROJECT: *KDC – Pitt Polder* · DRAWN BY: *GMC* · DATE: *20 January, 2013*	

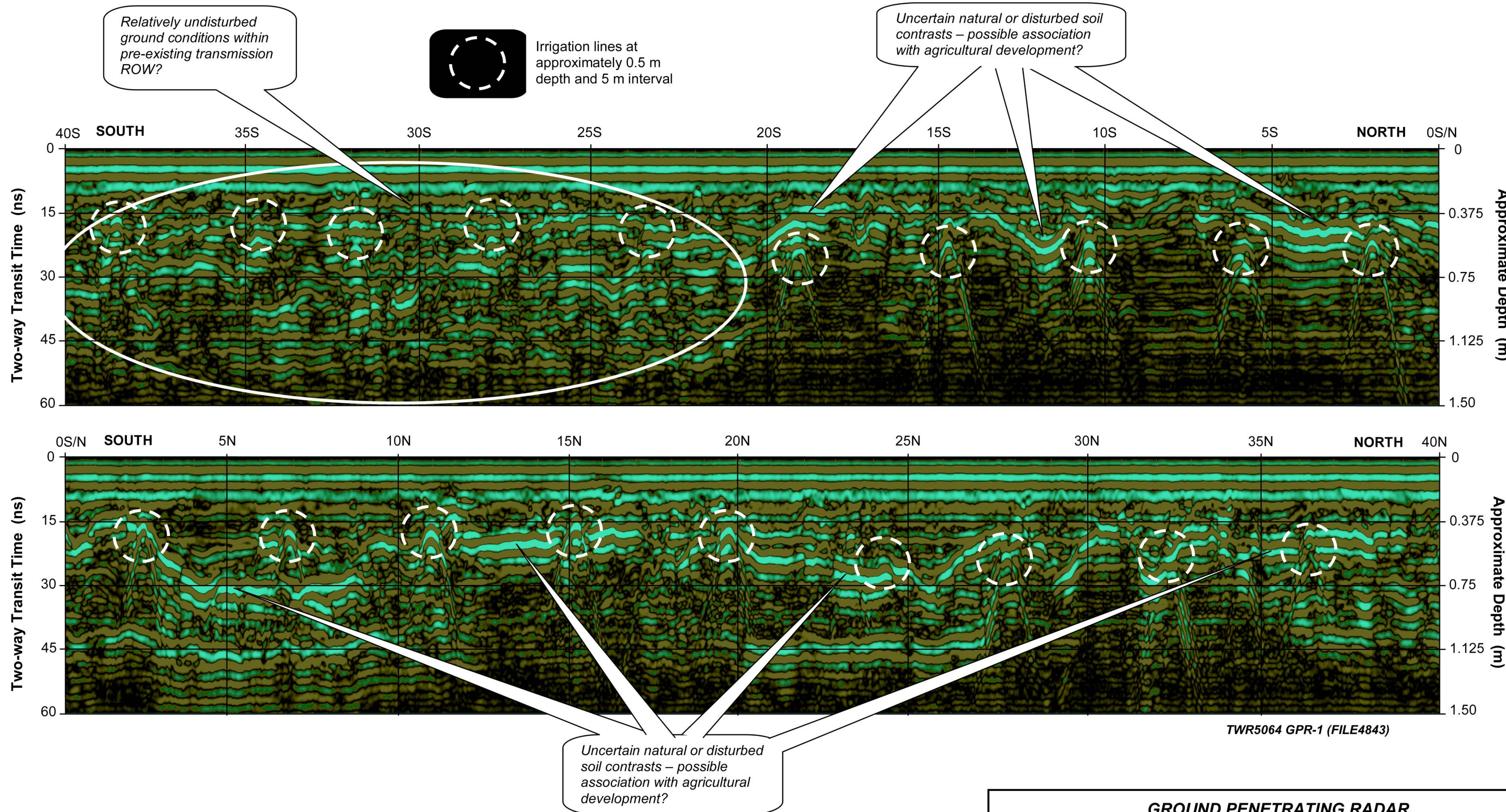

NOTE: Approximate depth scale based on estimated average radar velocity v=0.05 m/ns.

Radar velocity varies with soil composition, texture and moisture content. Indicated depth scale is provided for approximate reference only. Fundamental reference is two-way transit time in nanoseconds (ns).

GROUND PENETRATING RADAR Tower Site 5064 – GPR1 – 400 MHz – 60 ns	
PITT POLDER – KDC/BC HYDRO ILM	
Terrascan Geophysics	PROJECT: KDC Pitt Polder
	DRAWN BY: GMC
	DATE: 15 January, 2013
	FIGURE: 9

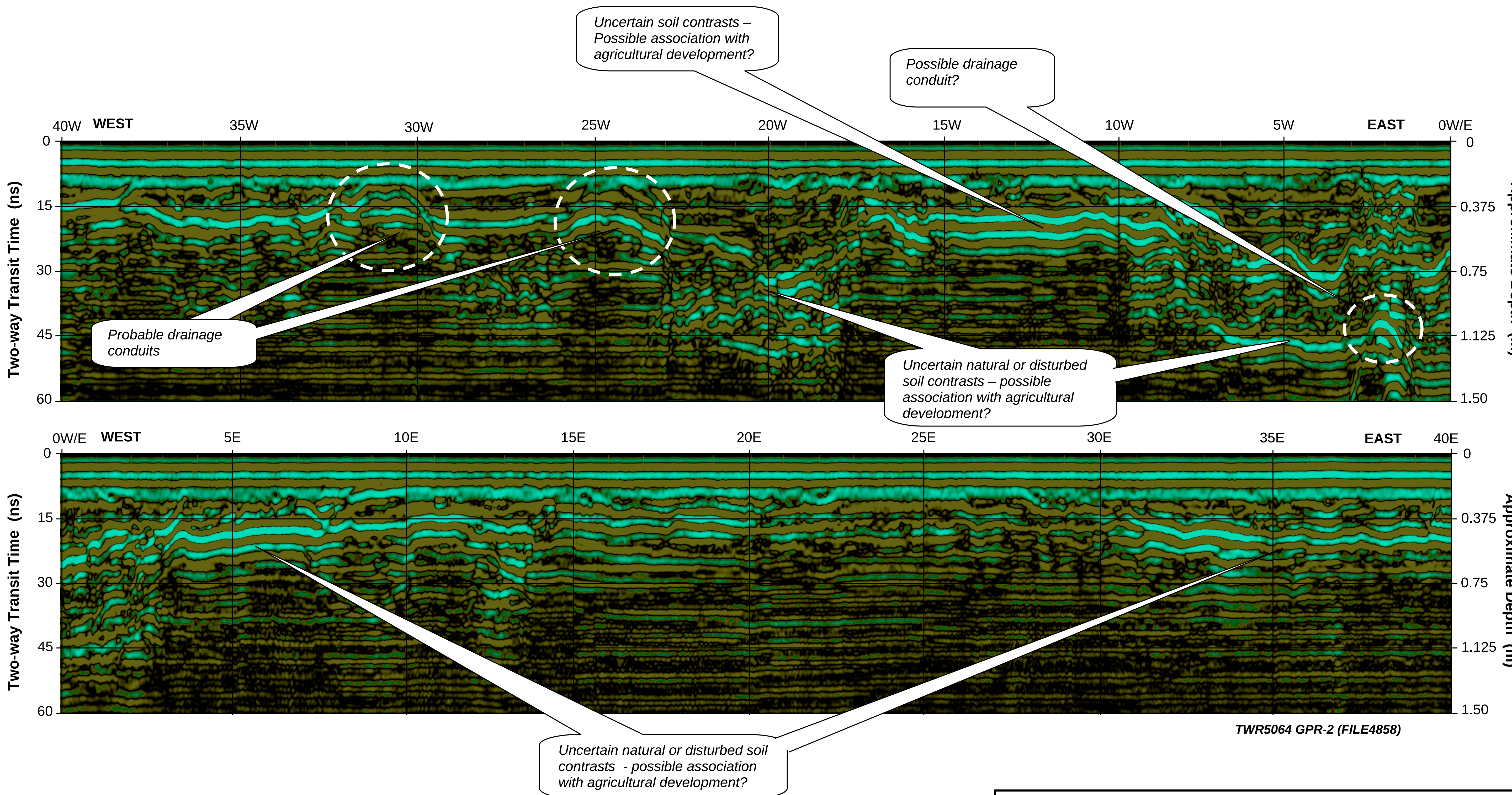

TWR5064 GPR-2 (FILE4858)

NOTE: Approximate depth scale based on estimated average radar velocity v=0.05 m/ns.

Radar velocity varies with soil composition, texture and moisture content. Indicated depth scale is provided for approximate reference only. Fundamental reference is two-way transit time in nanoseconds (ns).

GROUND PENETRATING RADAR ***Tower Site 5064 – GPR2 – 400 MHz – 60 ns***	
PITT POLDER – KDC/BC HYDRO ILM	
Terrascan Geophysics	PROJECT: *KDC Pitt Polder*
	DRAWN BY: *GMC*
	FIGURE: ***10***
	DATE: *15 January, 2013*

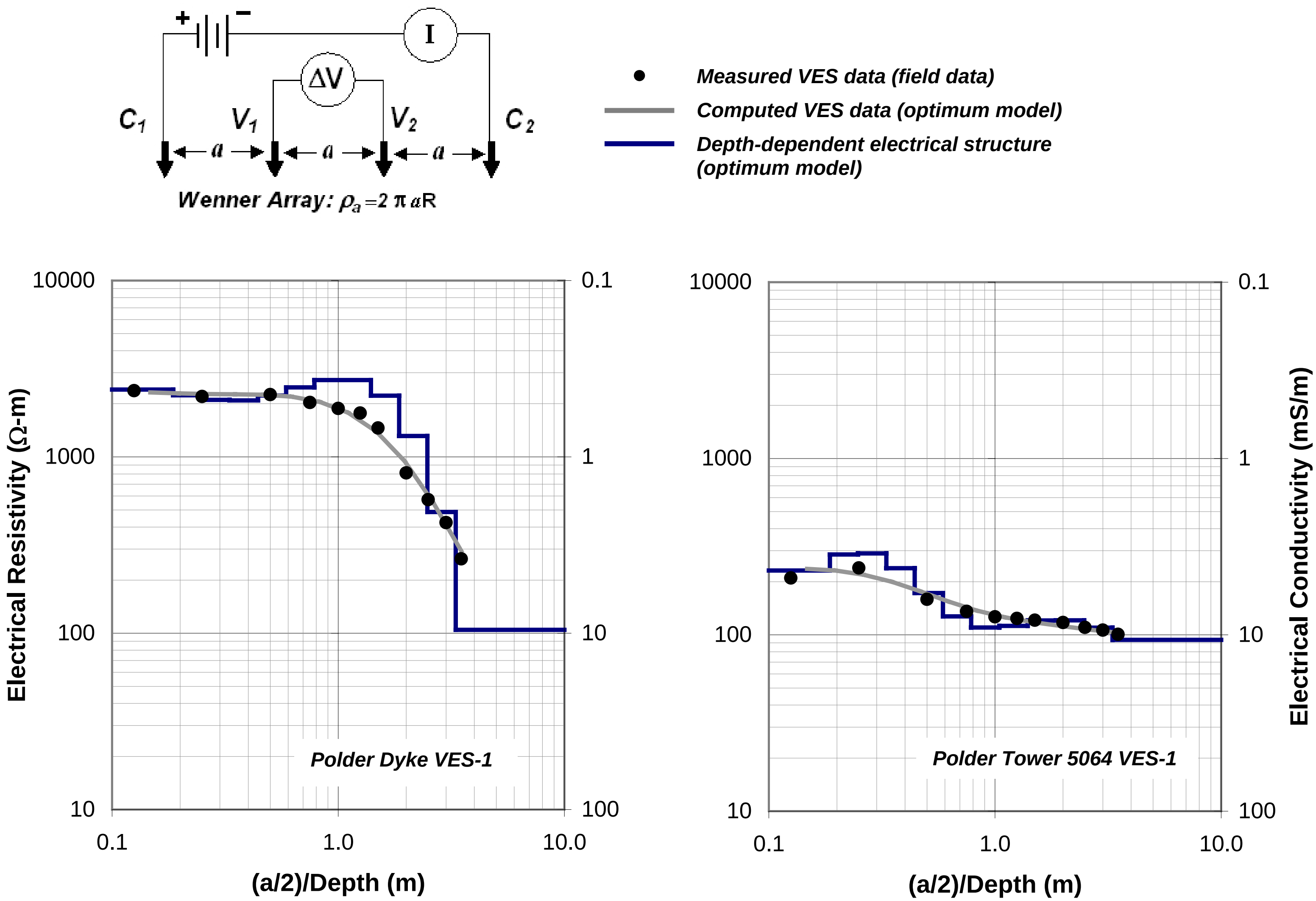

Terrascan Geophysics	**VERTICAL ELECTRICAL SOUNDINGS** **PITT RIVER DYKE – TOWER SITE 5064**			FIGURE: **11**
	PROJECT: *KDC – Pitt Polder*	DRAWN BY: *GMC*	DATE: *20 January, 2013*	

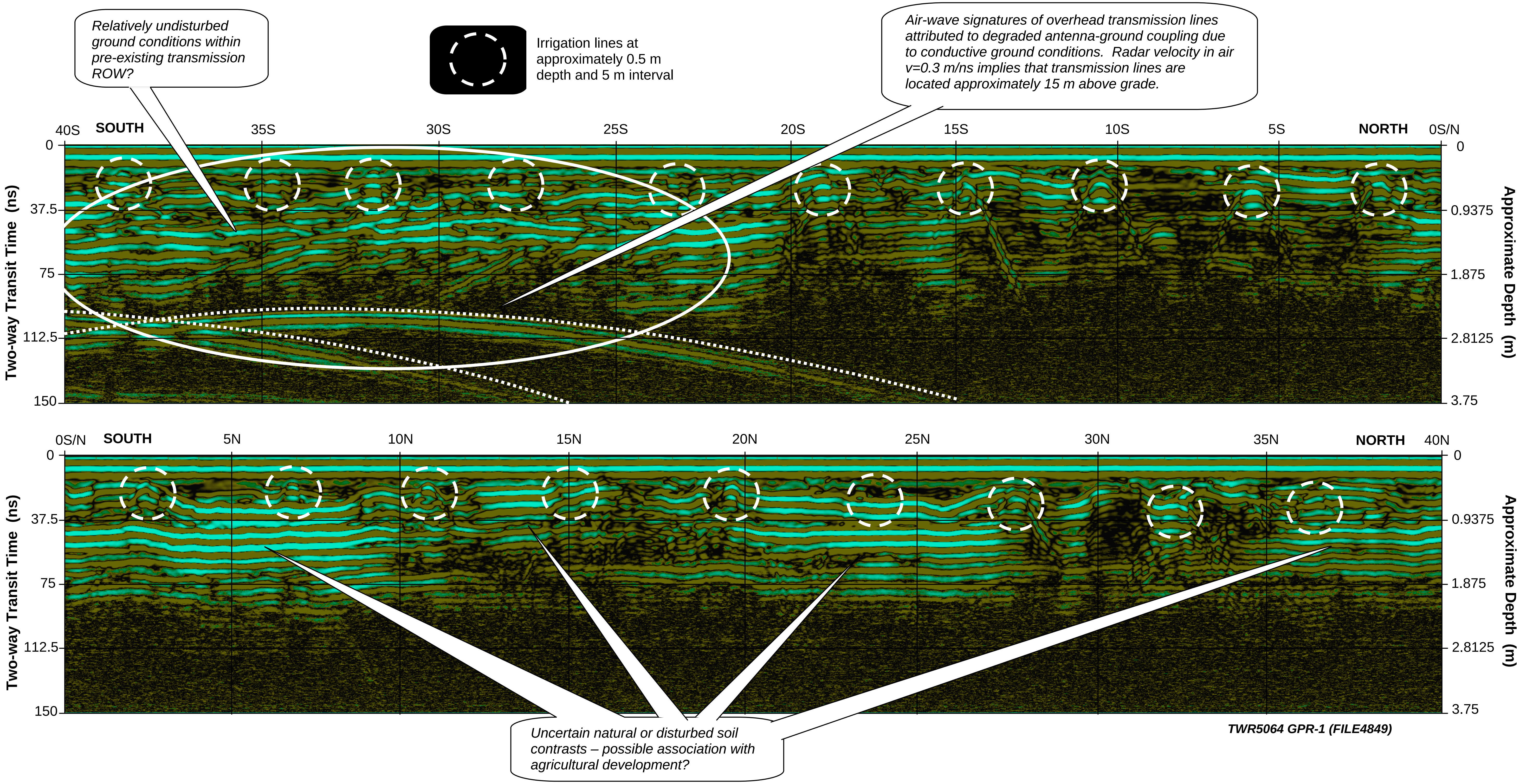

NOTE: Approximate depth scale based on estimated average radar velocity v=0.05 m/ns.

Radar velocity varies with soil composition, texture and moisture content. Indicated depth scale is provided for approximate reference only. Fundamental reference is two-way transit time in nanoseconds (ns).

GROUND PENETRATING RADAR
Tower Site 5064 – GPR-1 – 200 MHz – 150 ns

PITT POLDER – KDC/BC HYDRO ILM

Terrascan Geophysics

PROJECT: *KDC Pitt Polder*	
DRAWN BY: *GMC*	FIGURE:
DATE: *15 January, 2013*	***12***

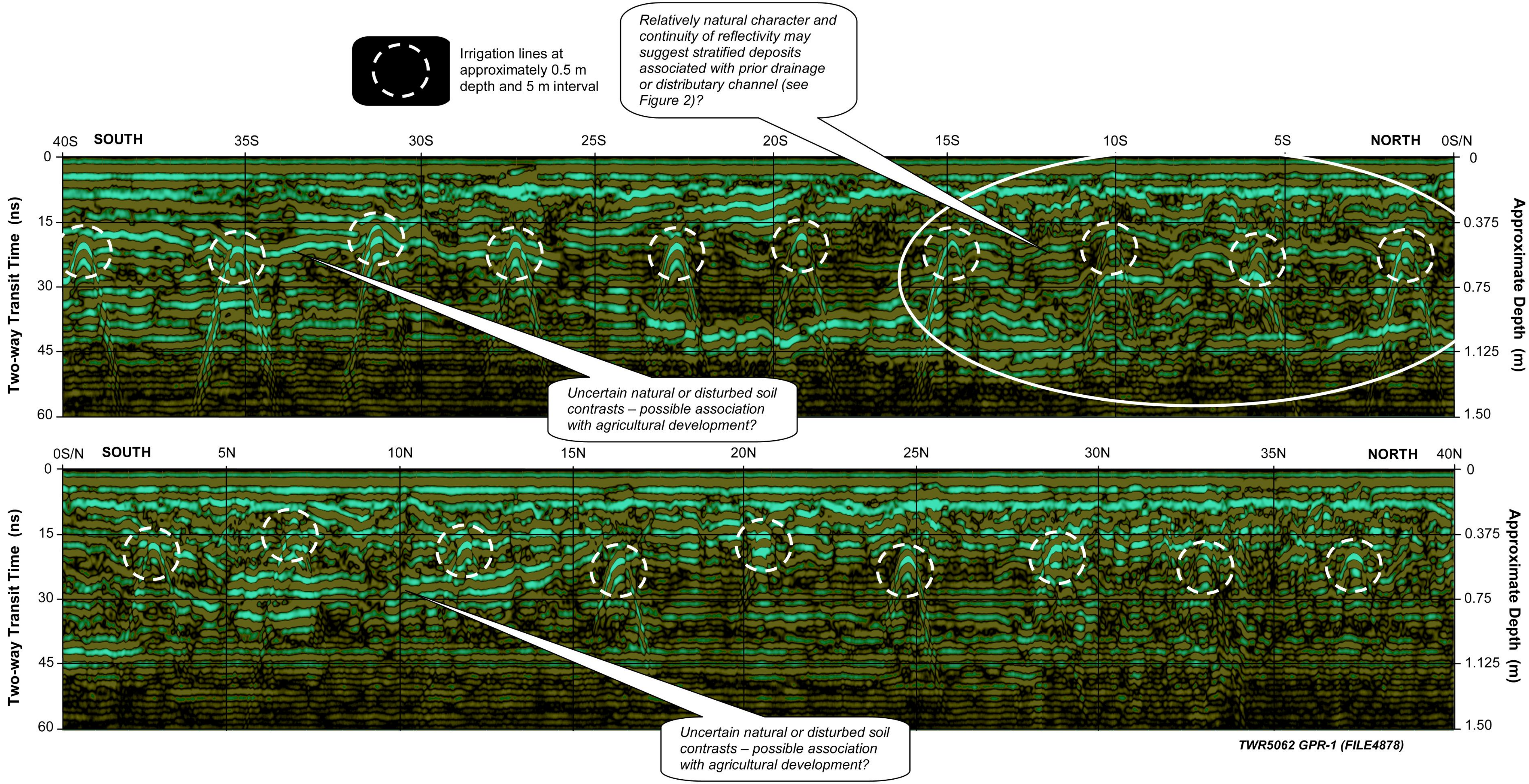

NOTE: Approximate depth scale based on estimated average radar velocity v=0.05 m/ns.

Radar velocity varies with soil composition, texture and moisture content. Indicated depth scale is provided for approximate reference only. Fundamental reference is two-way transit time in nanoseconds (ns).

GROUND PENETRATING RADAR ***Tower Site 5062 – GPR1 – 400 MHz – 60 ns***	
PITT POLDER – KDC/BC HYDRO ILM	
Terrascan Geophysics	PROJECT: *KDC Pitt Polder*
	DRAWN BY: *GMC* — FIGURE: ***13***
	DATE: *15 January, 2013*

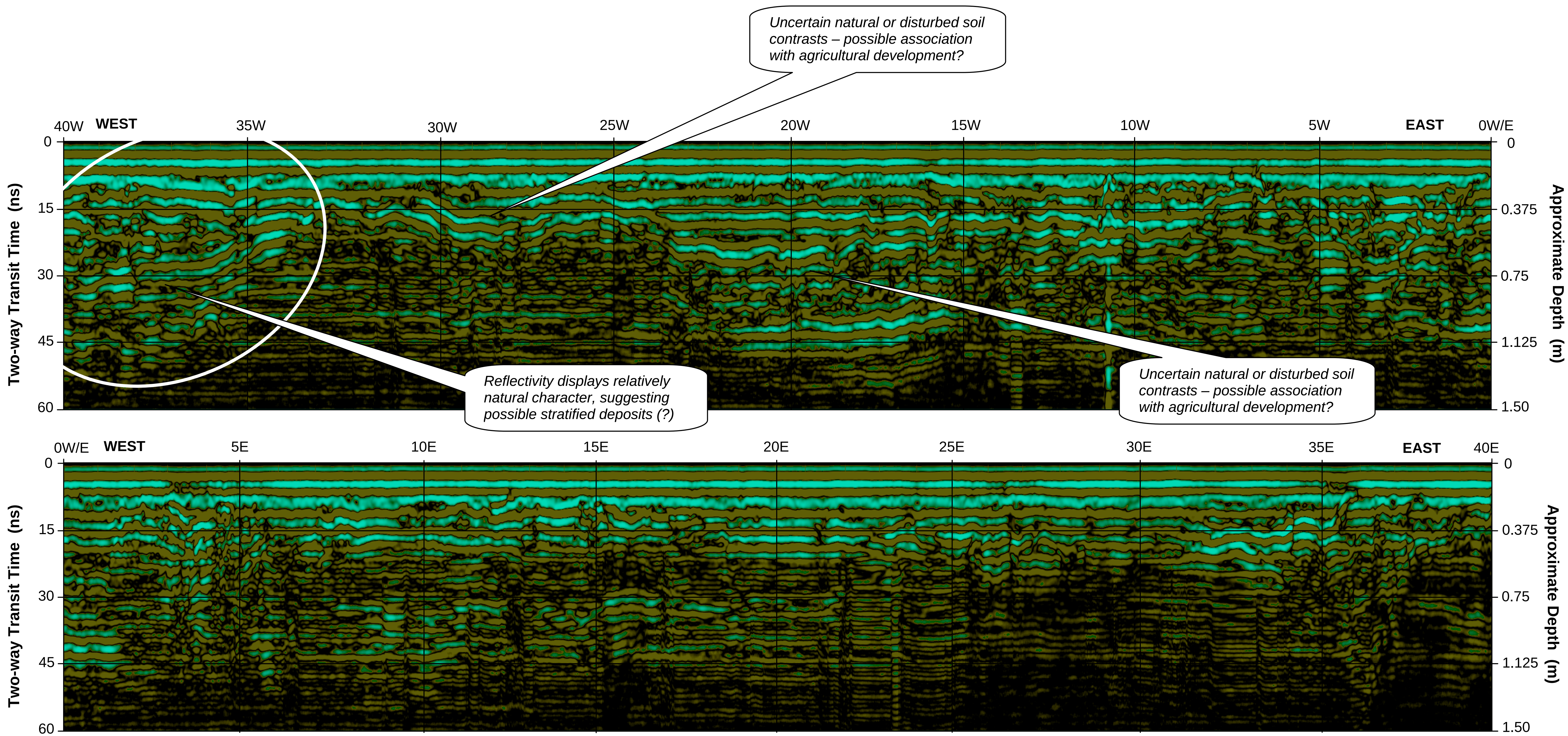

TWR5062 GPR-2 (FILE4863)

NOTE: Approximate depth scale based on estimated average radar velocity v=0.05 m/ns.

Radar velocity varies with soil composition, texture and moisture content. Indicated depth scale is provided for approximate reference only. Fundamental reference is two-way transit time in nanoseconds (ns).

GROUND PENETRATING RADAR ***Tower Site 5062 – GPR2 – 400 MHz – 60 ms***	
PITT POLDER – KDC/BC HYDRO ILM	
Terrascan Geophysics	PROJECT: *KDC Pitt Polder*
DRAWN BY: *GMC*	FIGURE: ***14***
DATE: *15 January, 2013*	

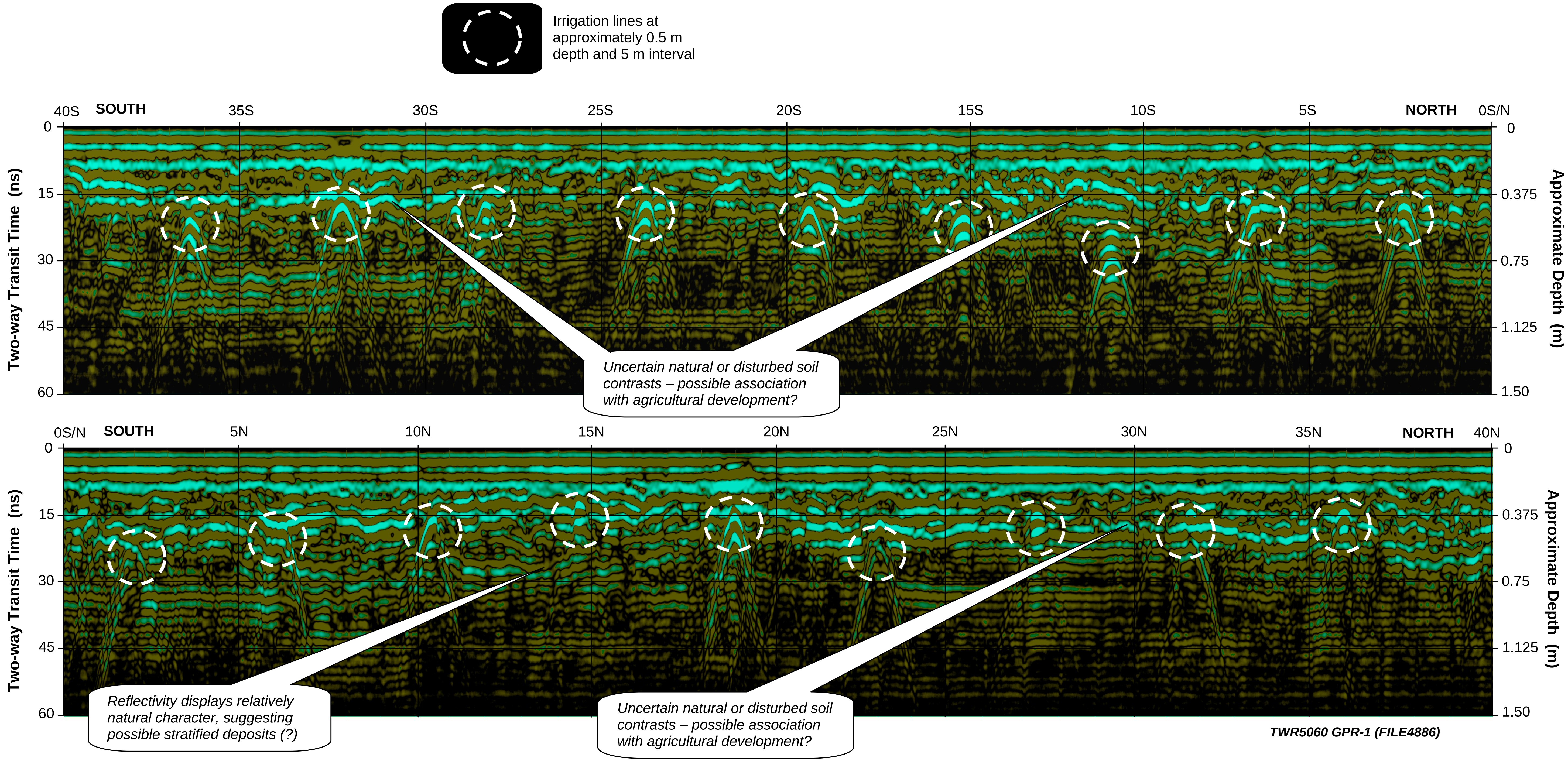

NOTE: Approximate depth scale based on estimated average radar velocity v=0.05 m/ns.

Radar velocity varies with soil composition, texture and moisture content. Indicated depth scale is provided for approximate reference only. Fundamental reference is two-way transit time in nanoseconds (ns).

GROUND PENETRATING RADAR
Tower Site 5060 – GPR1 – 400 MHz – 60 ns

PITT POLDER – KDC/BC HYDRO ILM

Terrascan Geophysics

PROJECT: *KDC Pitt Polder*	
DRAWN BY: *GMC*	FIGURE: ***15***
DATE: *15 January, 2013*	

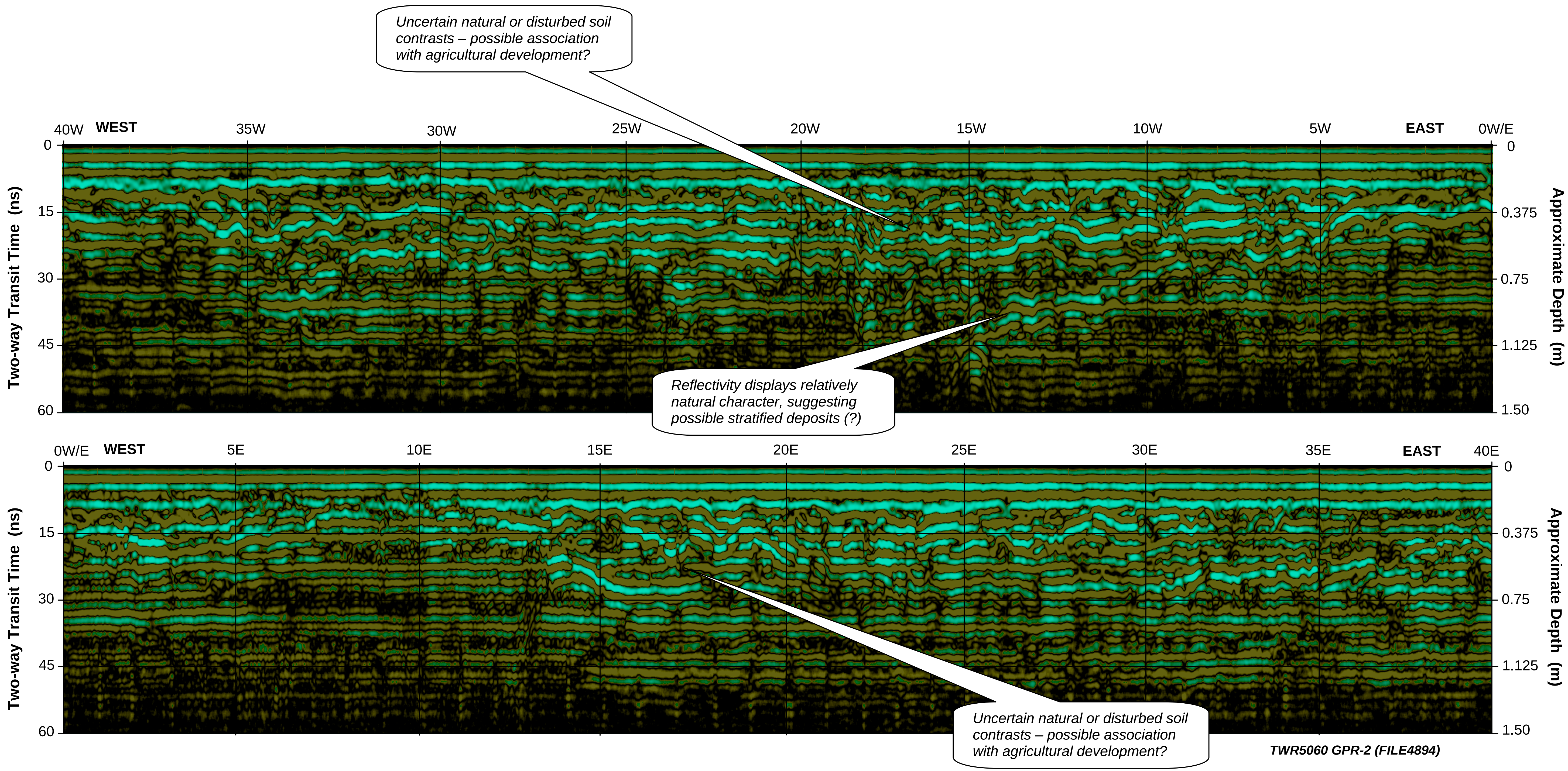

NOTE: Approximate depth scale based on estimated average radar velocity v=0.05 m/ns.

Radar velocity varies with soil composition, texture and moisture content. Indicated depth scale is provided for approximate reference only. Fundamental reference is two-way transit time in nanoseconds (ns).

GROUND PENETRATING RADAR
Tower Site 5060 – GPR2 – 400 MHz – 60 ns

PITT POLDER – KDC/BC HYDRO ILM

Terrascan Geophysics

PROJECT: *KDC Pitt Polder*	
DRAWN BY: *GMC*	FIGURE: ***16***
DATE: *15 January, 2013*	

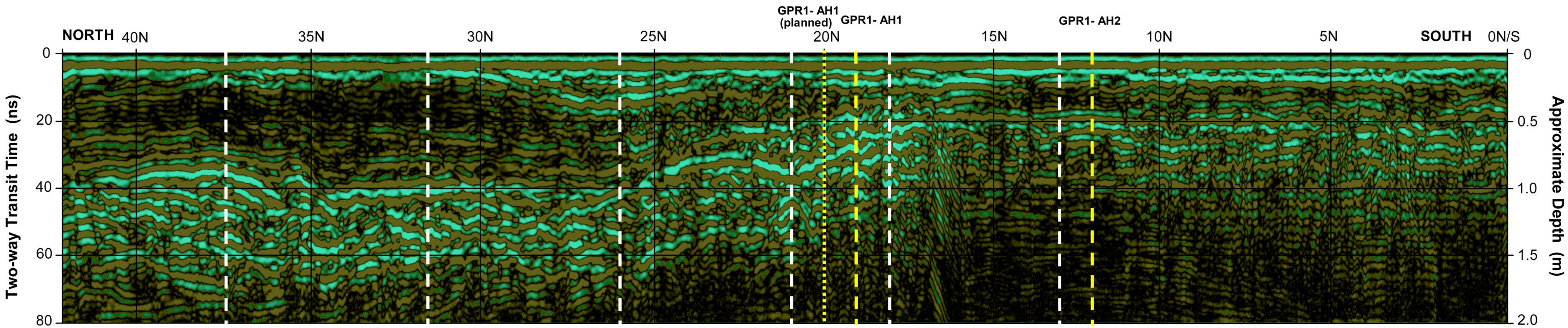

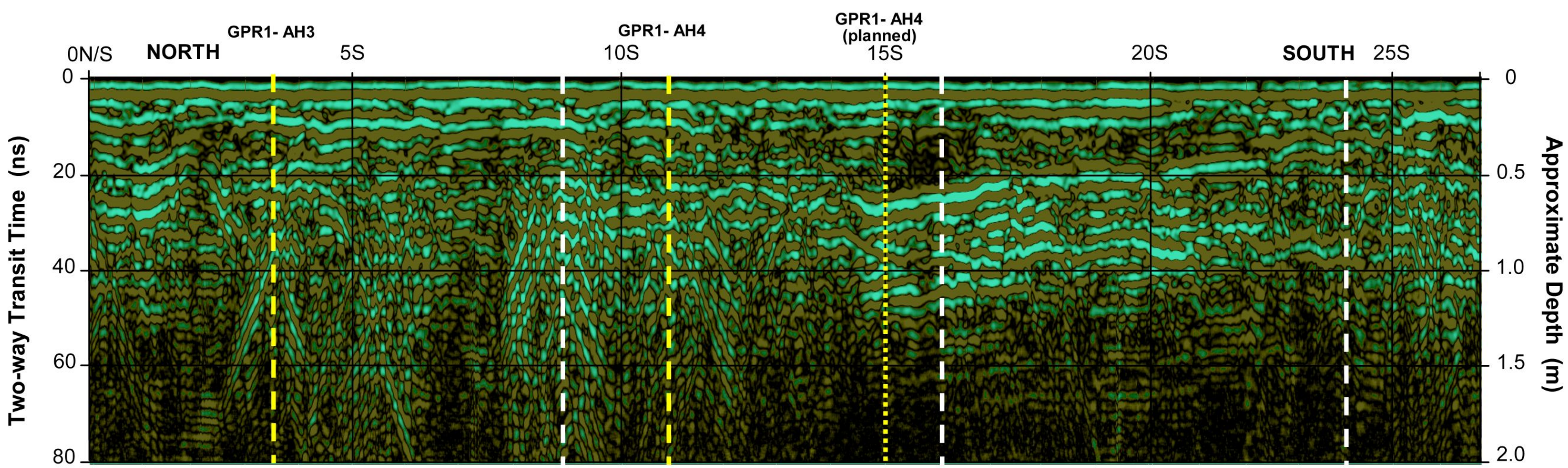

Shovel test location

Auger core location

Auger core location (planned)

Tower 5065 GPR-1 (FILE4900)

***NOTE:** Approximate depth scale based on estimated average radar velocity v=0.05 m/ns.*

Radar velocity varies with soil composition, texture and moisture content. Indicated depth scale is provided for approximate reference only. Fundamental reference is two-way transit time in nanoseconds (ns).

GROUND PENETRATING RADAR
TOWER 5065 – GPR-1 – 400 MHz

PITT POLDER – KDC/BC HYDRO ILM

Terrascan Geophysics

PROJECT: KDC Pitt Polder	
DRAWN BY: GMC	FIGURE: 17
DATE: 11 March, 2013	

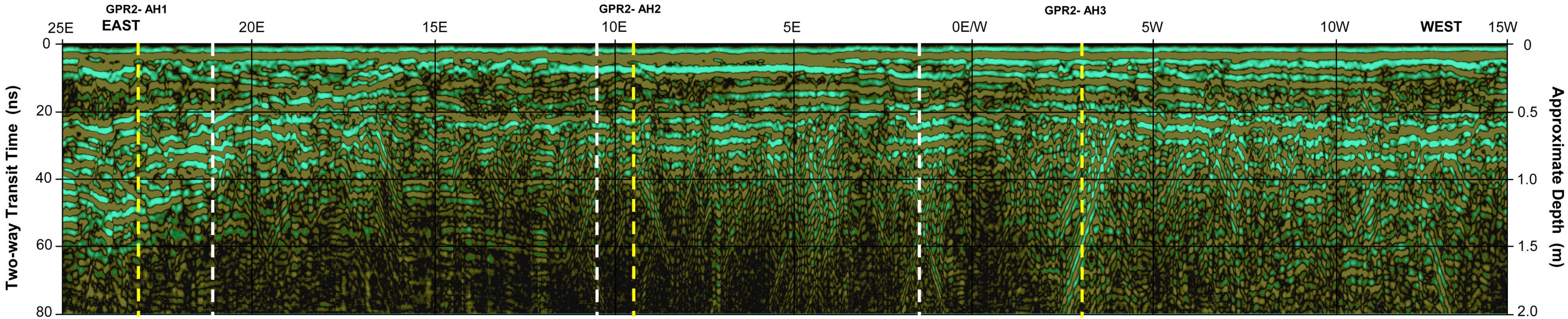

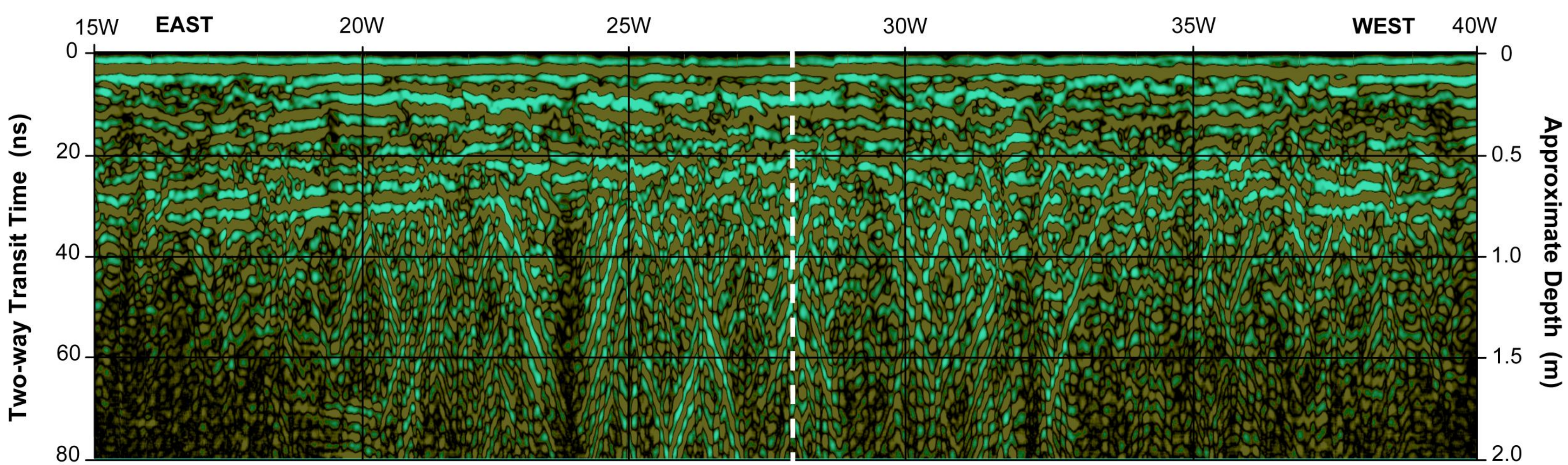

Tower 5065 GPR-2 (FILE4909)

NOTE: Approximate depth scale based on estimated average radar velocity v=0.05 m/ns.

Radar velocity varies with soil composition, texture and moisture content. Indicated depth scale is provided for approximate reference only. Fundamental reference is two-way transit time in nanoseconds (ns).

GROUND PENETRATING RADAR **TOWER 5065 – GPR-2 – 400 MHz**	
PITT POLDER – KDC/BC HYDRO ILM	
Terrascan Geophysics	PROJECT: KDC Pitt Polder
	DRAWN BY: GMC
	DATE: 11 March, 2013
	FIGURE: 18

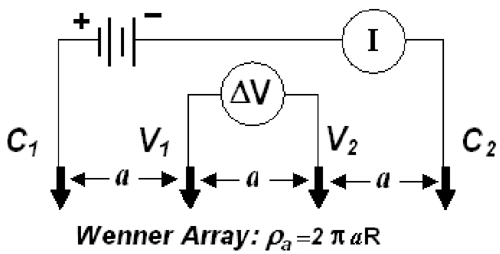

● *Measured VES data (field data)*

Computed VES data (optimum model)

Depth-dependent electrical structure (optimum model)

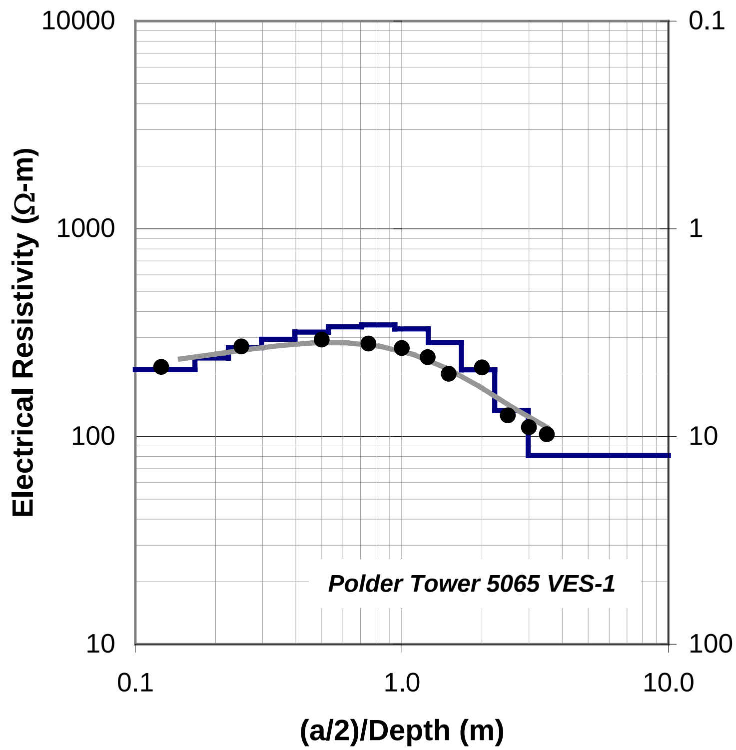

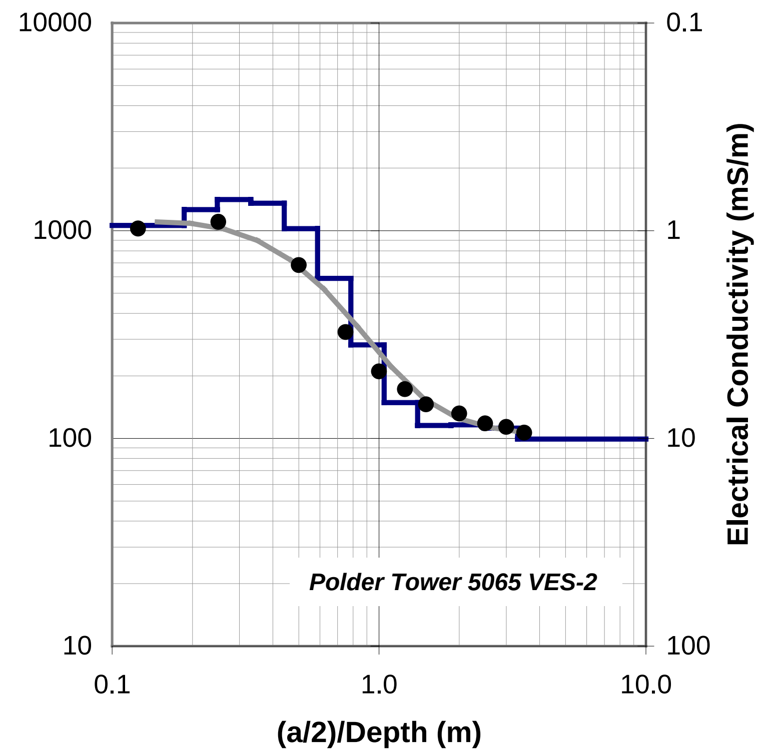

Terrascan Geophysics

VERTICAL ELECTRICAL SOUNDINGS
TOWER SITE 5065

PROJECT:	DRAWN BY:	DATE:	FIGURE:
KDC – Pitt Polder	*GMC*	*20 January, 2014*	*19*

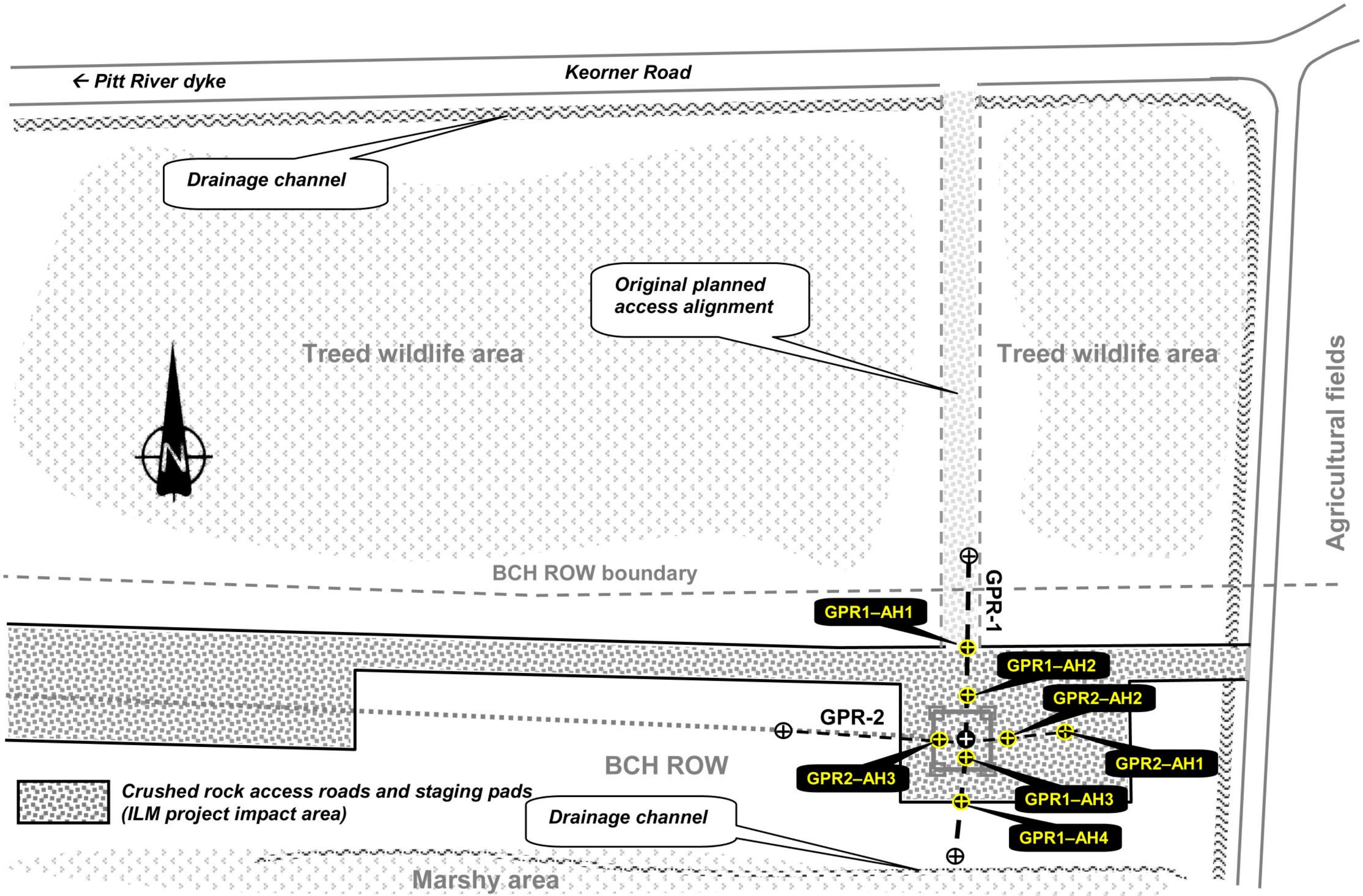

Terrascan Geophysics

PHASE II – TOWER SITE 5065
GPR TRANSECTS & PLANNED AUGER HOLE LOCATIONS

PROJECT:	DRAWN BY:	DATE:	FIGURE:
KDC – Pitt Polder	GMC	20 January, 2014	20

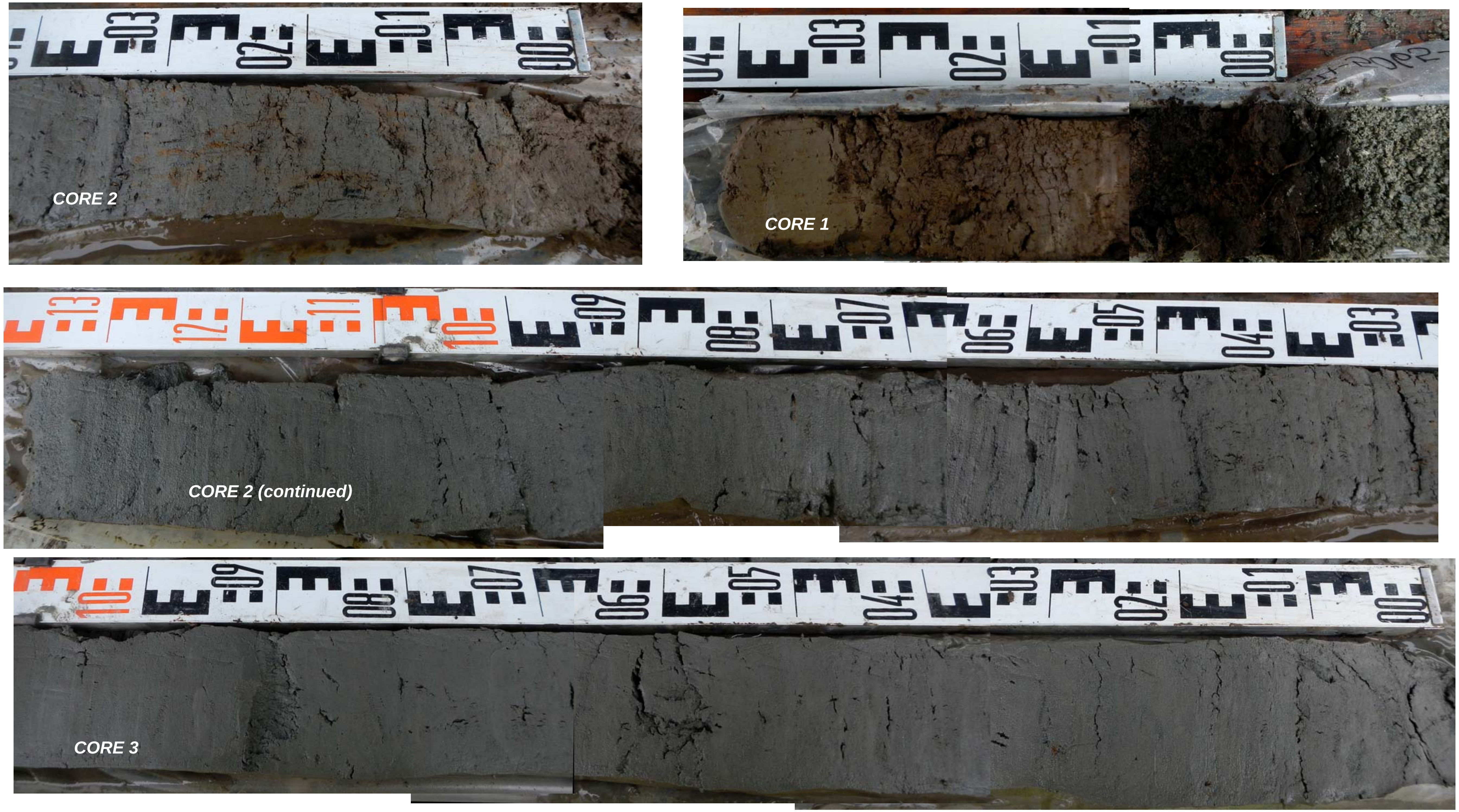

BH13-54-5065 - GPR-1-AH1

CORE1

	Core Depth (m)		Net Depth (m)	Unit
Sample 1	0.00	0.10	0.00	1
	0.10	0.12	0.10	1/2
Sample 2	0.12	0.22	0.12	3
Sample 3	0.22	0.32	0.22	3
Sample 4	0.32	0.40	0.32	4

CORE2

	Core Depth (m)		Net Depth (m)	Unit
	0.00	0.05	0.40	
Sample 5	0.05	0.32	0.46	7
Sample 6	0.32	1.35	0.76	8

CORE3

	Core Depth (m)		Net Depth (m)	Unit
Sample 7	0.00	1.52	1.92	8

AUGER CORES
GPR-1-AH1 BH13-54-5065

PITT POLDER – KDC/BC HYDRO ILM

Terrascan Geophysics

PROJECT: KDC Pitt Polder

DRAWN BY: GMC

DATE: 18 January, 2014

FIGURE: 21

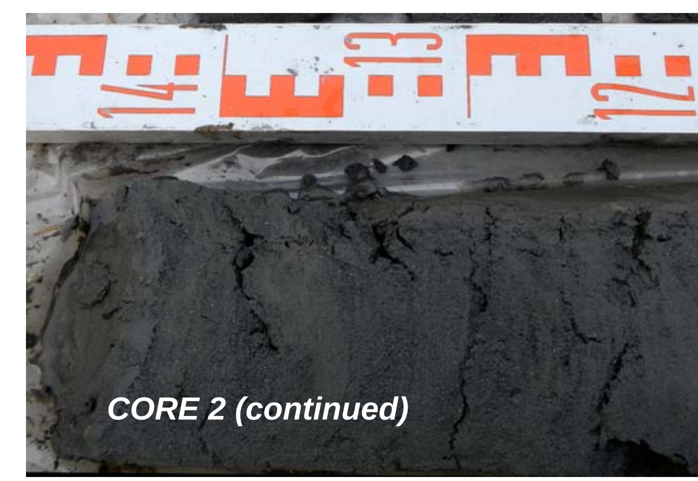

BH13-53-5065 - GPR-1-AH2

CORE1

	Core Depth (m)		Net Depth (m)	Unit
Sample 1	0.00	0.08	0.00	1
Sample 2	0.08	0.19	0.08	2
Sample 3	0.19	0.24	0.19	3
Sample 4	0.24	0.32	0.24	3
Sample 5	0.32	0.37	0.32	4
Sample 6	0.37	0.44	0.37	5
Sample 7	0.44	0.75	0.44	6

CORE2

	Core Depth (m)		Net Depth (m)	Unit
Sample 8	0.00	0.11	0.75	
Sample 9	0.11	0.90	0.87	7
Sample 10	0.90	1.44	1.70	8

CORE3

	Core Depth (m)		Net Depth (m)	Unit
Sample 11	0.00	1.40	2.27	8

AUGER CORES
GPR-1-AH2 BH13-53-5065

PITT POLDER – KDC/BC HYDRO ILM

Terrascan Geophysics

PROJECT: *KDC Pitt Polder*

DRAWN BY: *GMC*

FIGURE: *22*

DATE: *18 January, 2014*

CORE 1

CORE 2

CORE 3

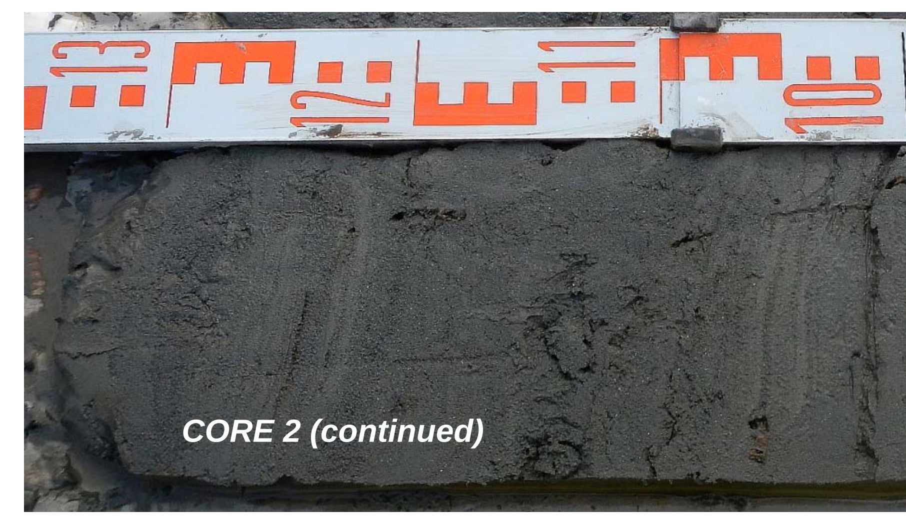

CORE 2 (continued)

BH13-48-5065 - GPR-1-AH3

CORE1

Core Depth (m)	Net Depth (m)	Unit
0.00 0.08	0.00	1
0.08 0.13	0.08	2
0.13 0.22	0.13	3
0.22 0.25	0.22	3
0.25 0.55	0.25	6

CORE2

Core Depth (m)	Net Depth (m)	Unit
0.00 0.30	0.55	6/7
0.30 1.00	0.90	8
1.00 1.32	1.70	9

CORE3

Core Depth (m)	Net Depth (m)	Unit
0.00 1.45	2.07	9

AUGER CORES
GPR-1-AH3 BH13-48-5065

PITT POLDER – KDC/BC HYDRO ILM

Terrascan Geophysics

PROJECT: *KDC Pitt Polder*

DRAWN BY: *GMC*

DATE: *18 January, 2014*

FIGURE: *23*

BH13-49-5065 - GPR-1-AH4

CORE1

Core Depth (m)	Net Depth (m)	Unit
0.00 0.09	0.00	1
0.09 0.14	0.09	2
0.14 0.25	0.14	3
0.25 0.40	0.20	4
0.40 0.65	0.40	6
0.65 0.71	0.65	7

CORE2

Core Depth (m)	Net Depth (m)	Unit
0.00 0.60	0.71	8
0.60 1.10	1.36	9
1.10 1.40	1.90	8

CORE3

Core Depth (m)	Net Depth (m)	Unit
0.00 1.40	2.23	8

AUGER CORES
GPR-1-AH4 BH13-49-5065

PITT POLDER – KDC/BC HYDRO ILM

Terrascan Geophysics

PROJECT: *KDC Pitt Polder*	
DRAWN BY: *GMC*	FIGURE: *24*
DATE: *18 January, 2014*	

BH13-46-5065 - GPR-2-AH1

CORE1

	Core Depth (m)		Net Depth (m)	Unit
Sample 1	0.00	0.10	0.00	1
Sample 2	0.10	0.23	0.10	3
Sample 3	0.23	0.30	0.23	2
Sample 4	0.30	0.47	0.30	3
Sample 5	0.47	0.50	0.47	3
Sample 6	0.50	0.65	0.50	4

CORE2

	Core Depth (m)		Net Depth (m)	Unit
	0.00	0.21	0.65	
Sample 7	0.21	0.45	0.88	7
Sample 8	0.45	0.63	1.14	8
Sample 9	0.63	1.40	1.33	9

CORE3

	Core Depth (m)		Net Depth (m)	Unit
	0.00	0.30	2.17	
Sample 10	0.30	1.30	2.48	8

AUGER CORES
GPR-2-AH1 BH13-46-5065

PITT POLDER – KDC/BC HYDRO ILM

Terrascan Geophysics

PROJECT: *KDC Pitt Polder*

DRAWN BY: *GMC*

DATE: *18 January, 2014*

FIGURE: ***25***

BH13-47-5065-SW - GPR-2-AH2

CORE1

	Core Depth (m)		Net Depth (m)	Unit
Sample 1	0.00	0.05	0.00	1
Sample 2	0.05	0.13	0.05	3
Sample 3	0.13	0.28	0.13	4
Sample 4	0.28	0.34	0.28	5
Sample 5	0.34	0.52	0.34	6

CORE2

	Core Depth (m)		Net Depth (m)	Unit
	0.00	0.05	0.52	
Sample 6	0.05	0.40	0.57	7
Sample 7	0.40	1.45	0.94	9

CORE3

	Core Depth (m)		Net Depth (m)	Unit
	0.00	0.50	2.04	
Sample 8	0.50	0.90	2.62	8

AUGER CORES
GPR-2-AH2 BH13-47-5065

PITT POLDER – KDC/BC HYDRO ILM

Terrascan Geophysics

PROJECT: *KDC Pitt Polder*

DRAWN BY: *GMC*

DATE: *18 January, 2014*

FIGURE: *26*

BH13-50-5065 - GPR-2-AH3

CORE1

Core Depth (m)	Net Depth (m)	Unit
0.00 0.06	0.00	1/3
0.06 0.40	0.06	6

CORE2

Core Depth (m)	Net Depth (m)	Unit
0.00 0.10	0.40	6/7
0.10 0.37	0.50	7
0.37 1.10	0.79	8
1.10 1.45	1.55	9

CORE3

Core Depth (m)	Net Depth (m)	Unit
0.00 1.44	1.92	8

AUGER CORES
GPR-2-AH3 BH13-50-5065

PITT POLDER – KDC/BC HYDRO ILM

Terrascan Geophysics

PROJECT: *KDC Pitt Polder*

DRAWN BY: *GMC*

DATE: *18 January, 2014*

FIGURE: *27*

Pitt Polder Tower 5065

Representative Soil/Sediment Units

1. Dark (very dark brown – black) **organic silt** – non-cohesive – including fibrous organic content (decomposed sphagnum mosses, other ground cover (heath) and forest litter, root mass).

2. Dark (dark/very dark brown – reddish/yellowish hues) **silt loam** (clayey silt) – cohesive – granular/massive – variable humic/organic content

3. Medium (gray-brown - light brown – reddish/yellowish hues) **silt loam** (clayey silt) – cohesive – granular/massive – trace organic content

4. Light (brown – reddish/yellowish hues) **silt loam** (clayey silt) – cohesive – granular/massive – trace organic content

5. Medium (orange-brown – reddish hue) **silty clay loam** (silty clay/clayey silt) – cohesive – massive – trace organic content

6. Medium (grey-brown – bluish/yellowish hues – orange/brown mottling) **silty clay loam** (silty clay/clayey silt) – cohesive – massive – trace organic content

7. Medium/Dark (grey – variable bluish hue – variable orange/brown mottling) **silt loam** (clayey silt) – cohesive – variably interbedded with fine **sandy loam**/**loam** (silty sand) – (lamination ranges several millimeters to approximately centimeter thickness) – non-cohesive – variable organic content (locally substantial or “peaty” in upper section)

8. Medium/Dark (grey – bluish hue) **silt loam** (clayey silt) – cohesive – variably interbedded with fine **sandy loam**/**loam** (silty sand) – non-cohesive – (lamination ranges several millimeters to approximately centimeter thickness) – variable organic content (locally substantial or “peaty” in upper section)

9. Medium/Dark (grey – bluish hue) **sandy loam/loam** (silty sand) – non-cohesive – variably interbedded with **silt loam** (clayey silt) – cohesive – (lamination ranges several millimeters to approximately centimeter thickness) – variable organic content.

PITT POLDER – BC HYDRO ILM
REPRESENTATIVE SOIL/SEDIMENT UNITS – TOWER SITE 5065

Terrascan Geophysics	PROJECT: *KDC Pitt Polder*	FIGURE:
	DRAWN BY: *GMC* / DATE: *20 January, 2014*	***28***

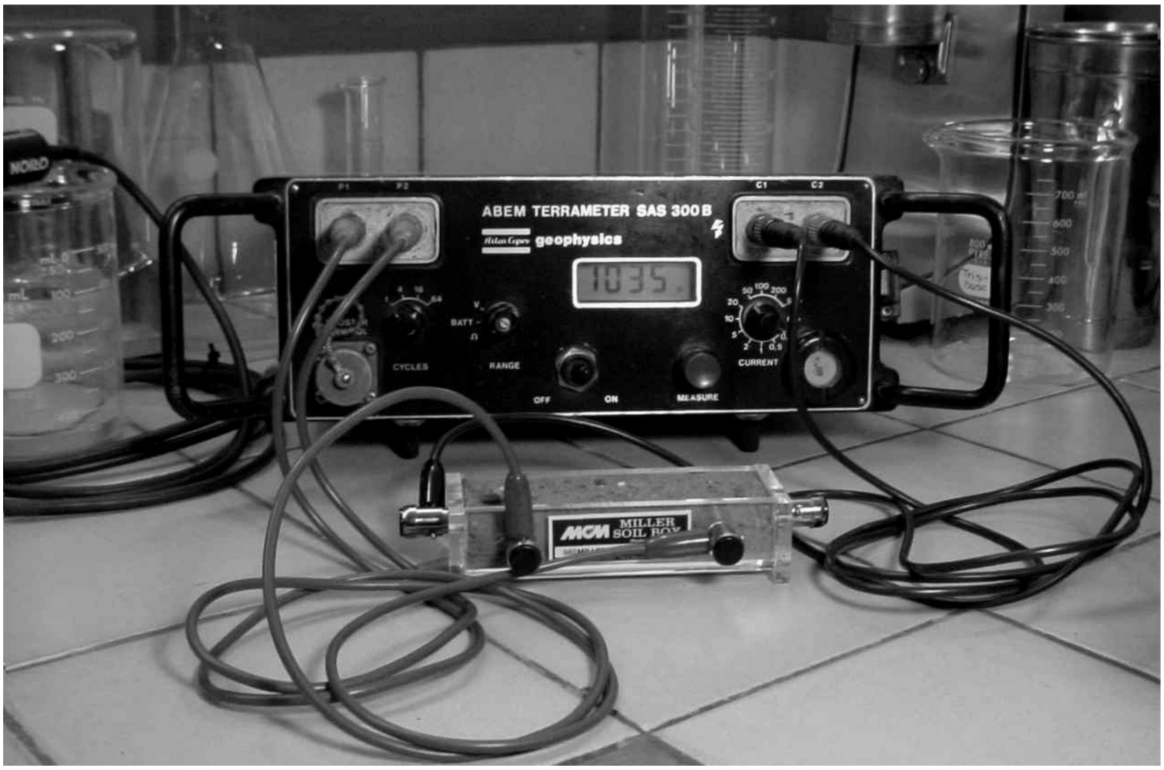

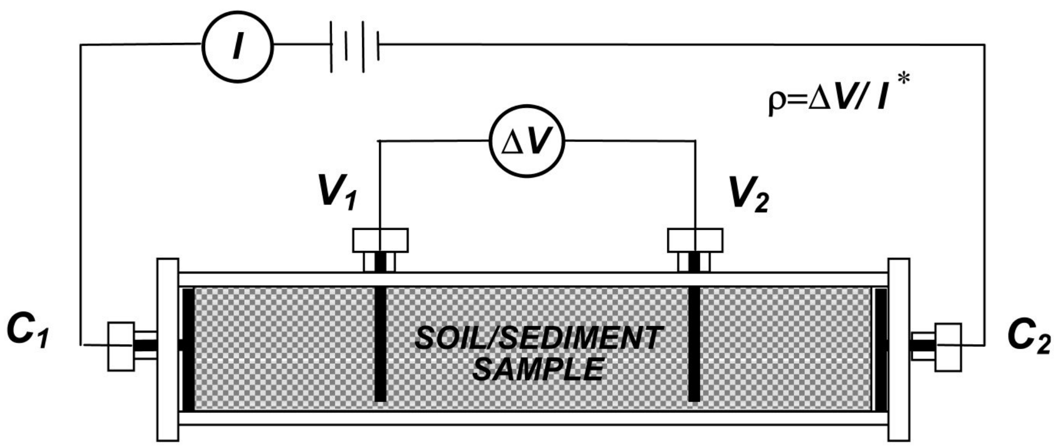

* *Note: valid for calibrated soil box fixture.*

ELECTRICAL RESISTIVITY MEASUREMENT
ABEM SAS-300C TRANSCEIVER / SOIL BOX SAMPLE FIXTURE

Terrascan Geophysics	PROJECT: *KDC – Pitt Polder*	FIGURE: **29**
	DRAWN BY: *GMC* DATE: *10 May, 2014*	

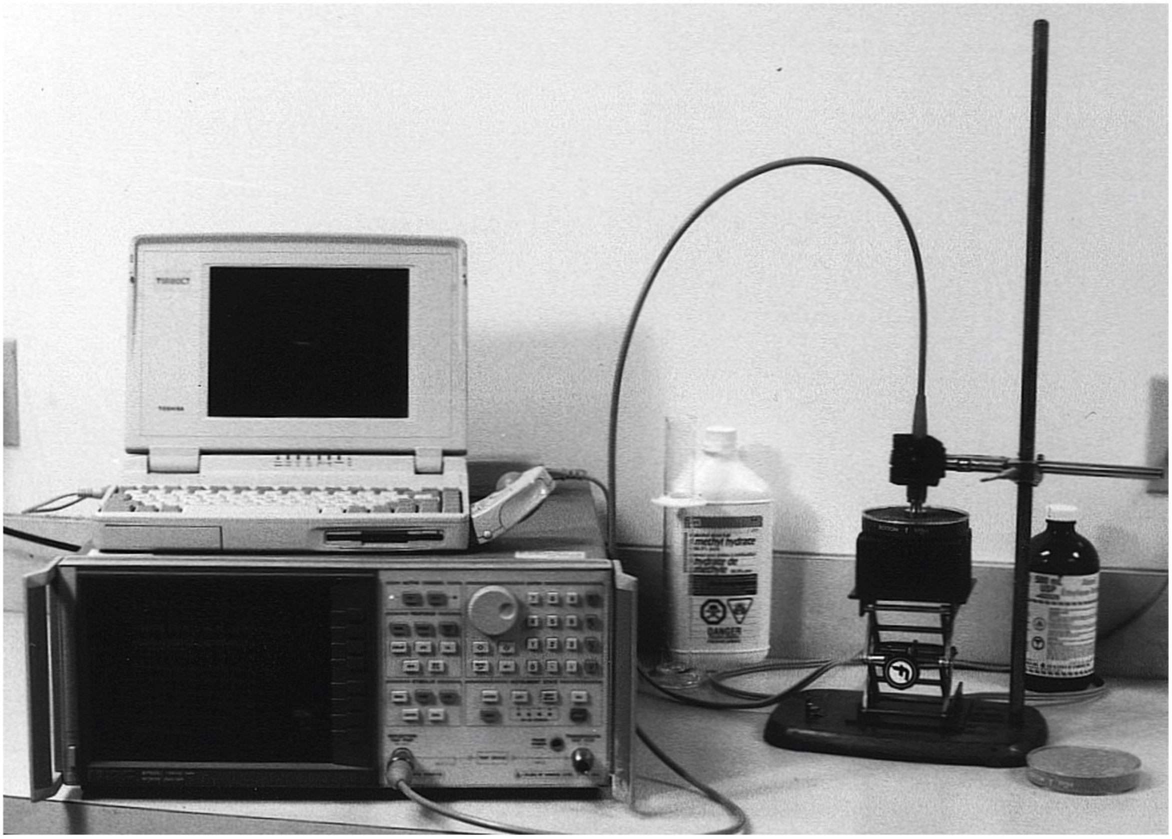

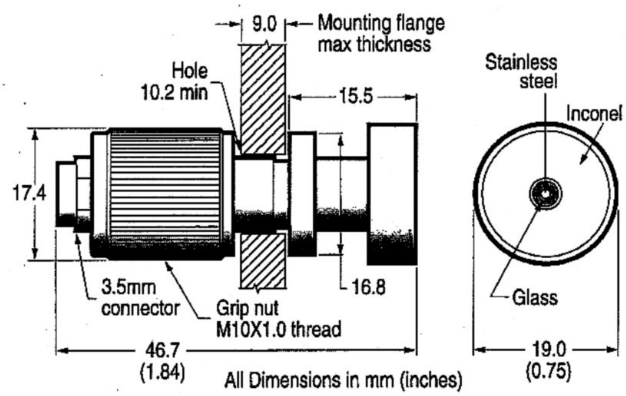

ELECTRICAL PERMITTIVITY MEASUREMENT
HP 85070M DIELECTRIC PROBE SYSTEM

Terrascan Geophysics	PROJECT: *KDC – Pitt Polder*	FIGURE:
	DRAWN BY: *GMC* DATE: *10 May, 2014*	*30*

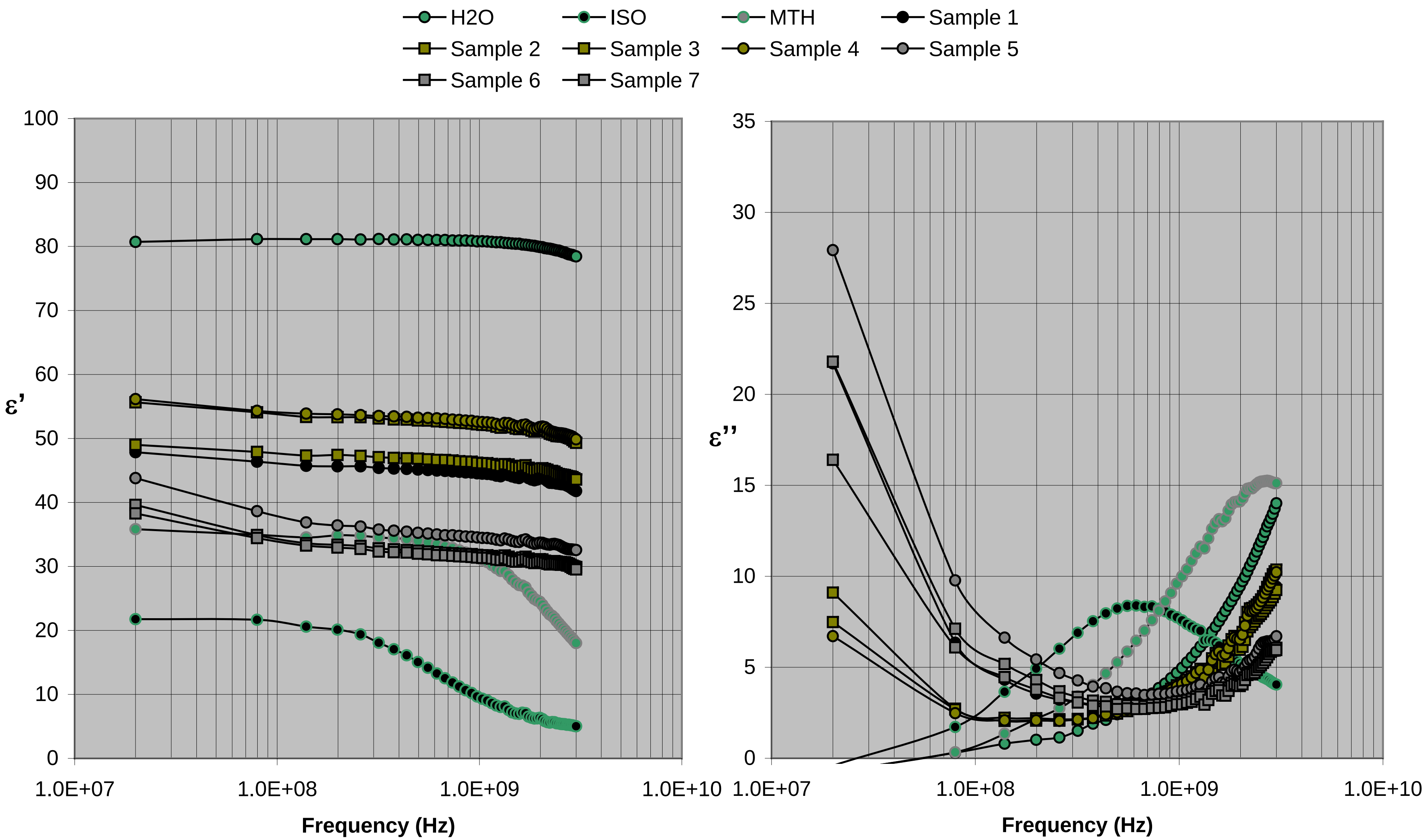

Terrascan Geophysics

DIELECTRIC SPECTRA GPR-1-AH1 – BH13-54-5065			FIGURE: 31
PROJECT: KDC – Pitt Polder	DRAWN BY: GMC	DATE: 10 May, 2014	

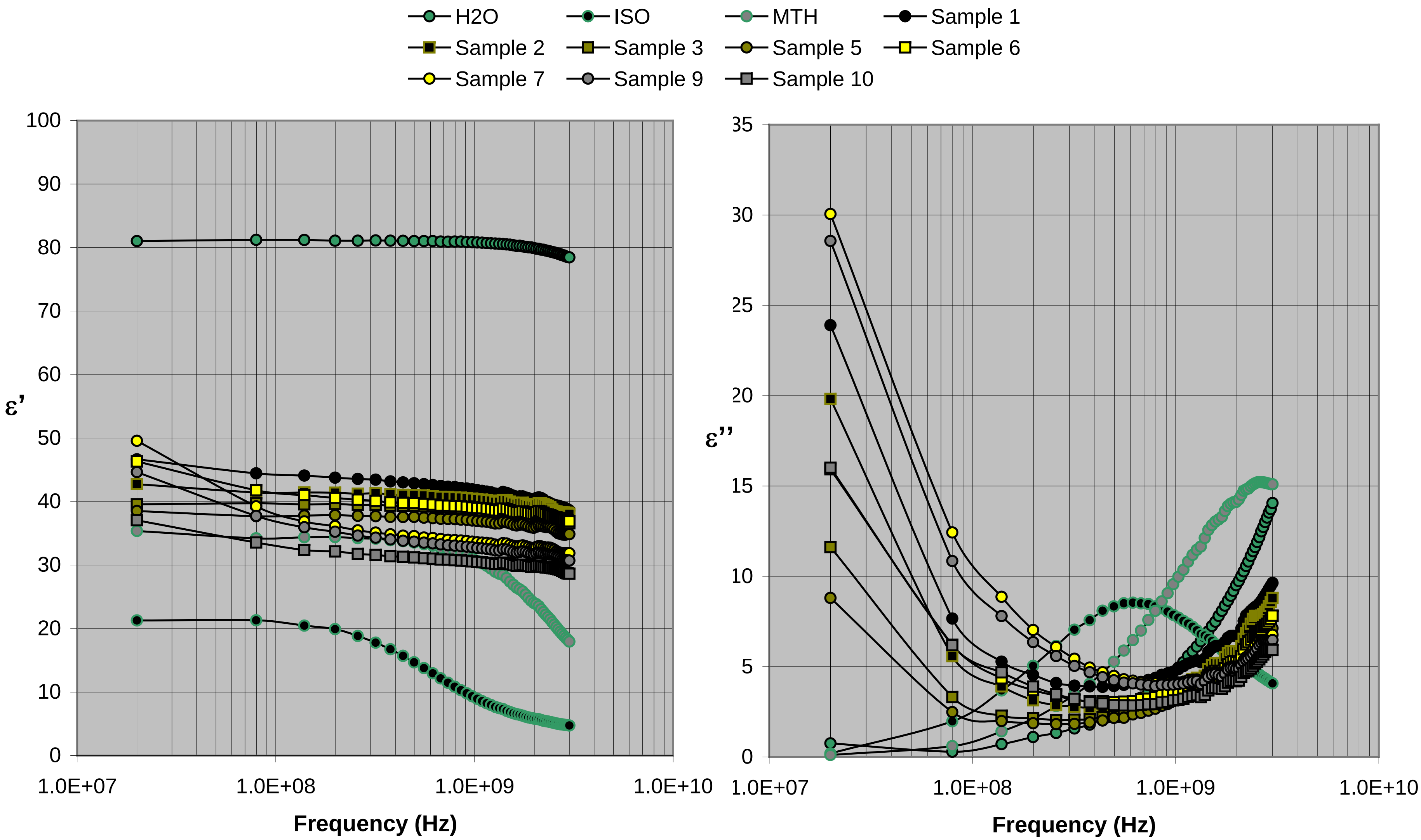

Terrascan Geophysics

DIELECTRIC SPECTRA
GPR-1-AH2 – BH13-53-5065

PROJECT: *KDC – Pitt Polder*	DRAWN BY: *GMC*	DATE: *10 May, 2014*	FIGURE: **32**

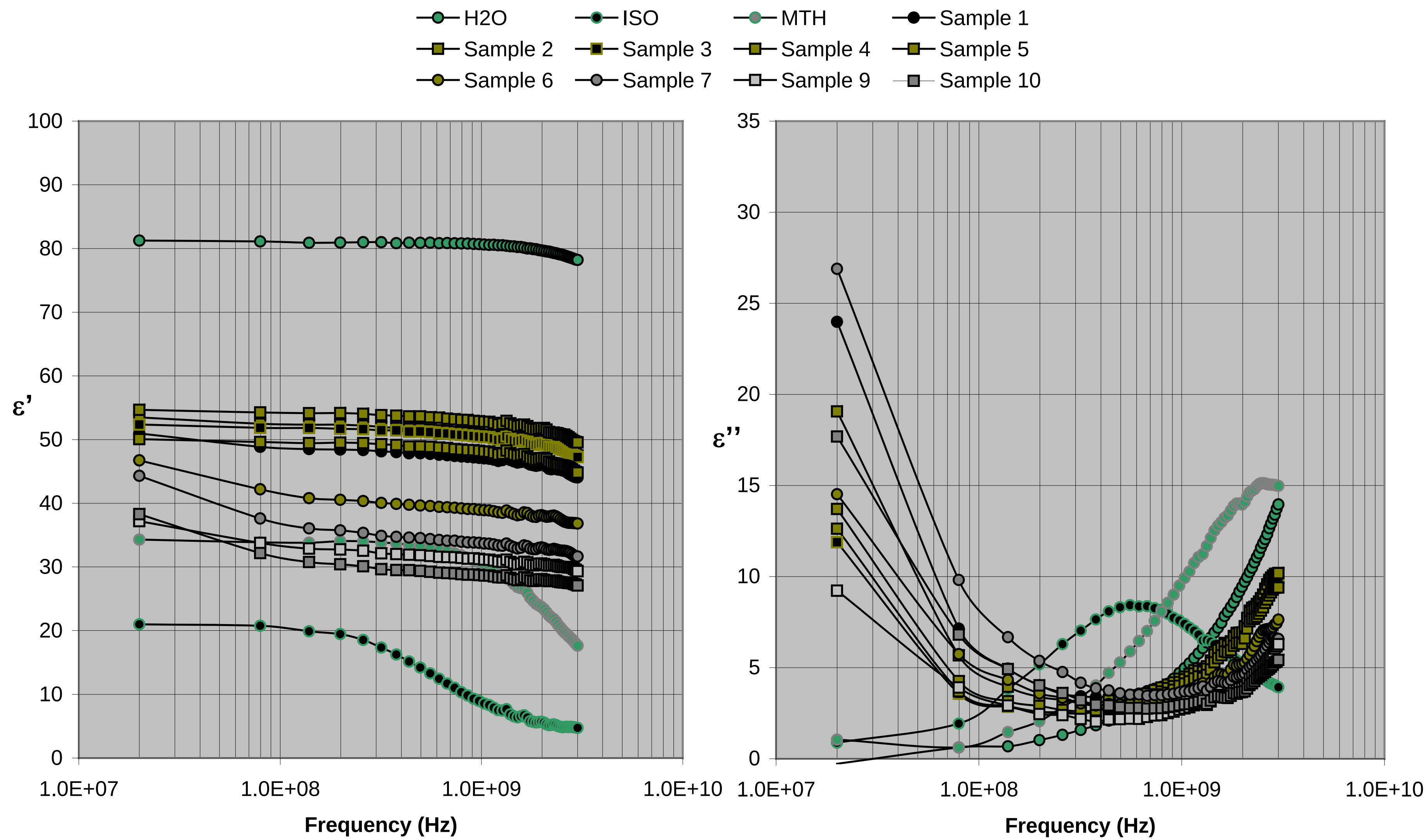

Terrascan Geophysics

DIELECTRIC SPECTRA ***GPR-2-AH1 - BH13-46-5065***			FIGURE: **33**
PROJECT: *KDC – Pitt Polder*	DRAWN BY: *GMC*	DATE: *10 May, 2014*	

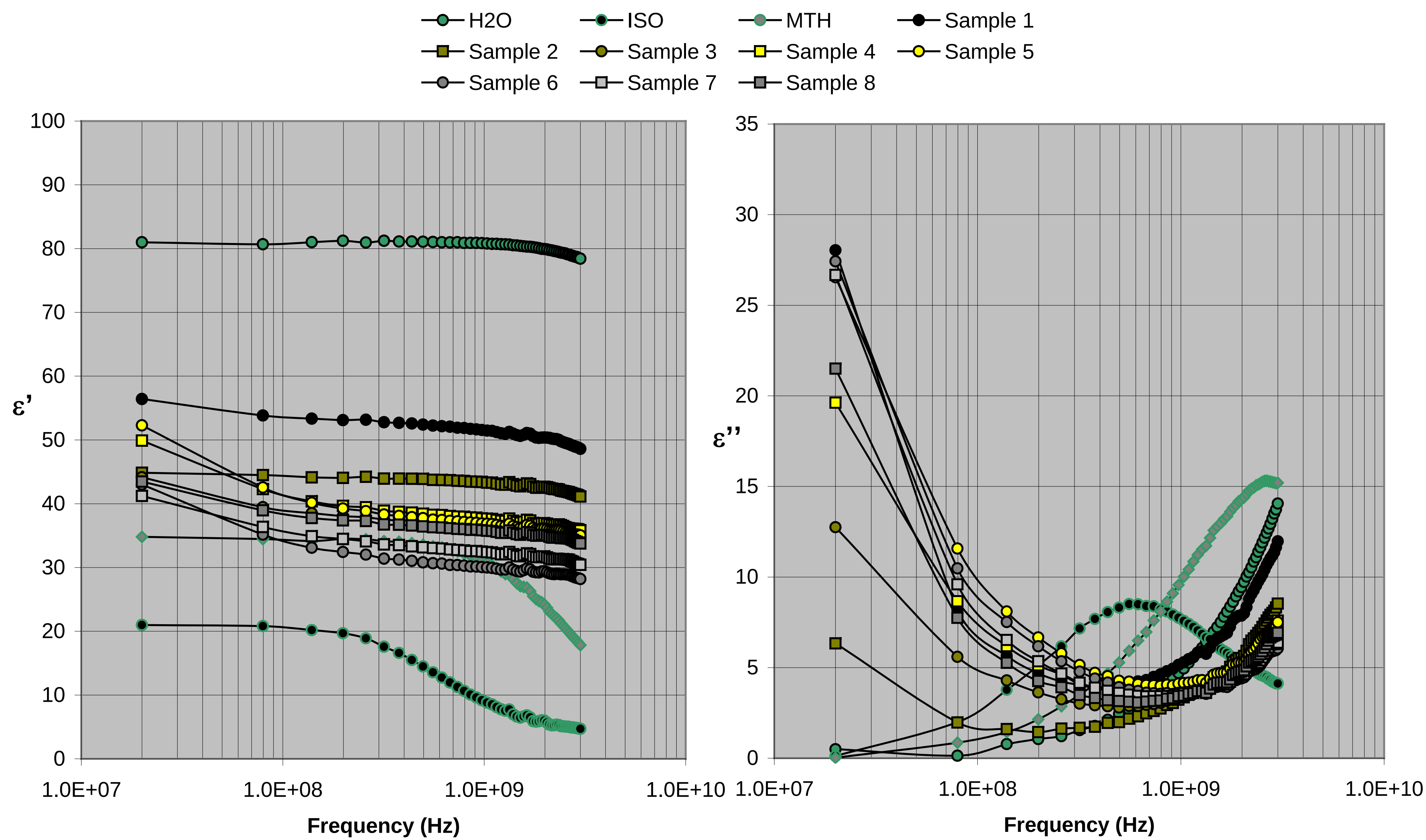

Terrascan Geophysics

DIELECTRIC SPECTRA
GPR-2-AH2 – BH13-47-5065

PROJECT: *KDC – Pitt Polder*	DRAWN BY: *GMC*	DATE: *10 May, 2014*	FIGURE: ***34***

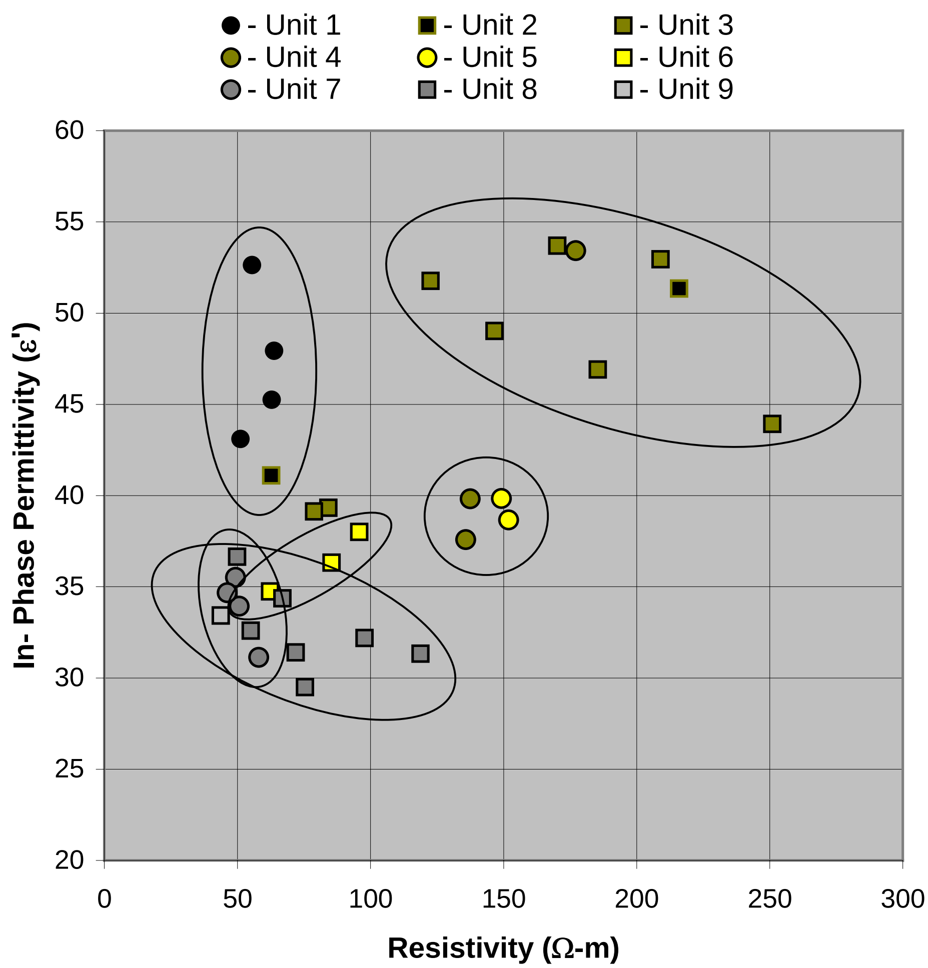

Note: Soil units identified on basis of visual assessment of solid-fraction composition, structure, texture, and colour.

REPRESENTATIVE SOIL UNITS
IN-PHASE PERMITTIVITY / STATIC RESISTIVITY

Terrascan Geophysics	PROJECT: *KDC Pitt Polder*	FIGURE: **35**
	DRAWN BY: *GMC* / DATE: *10 May, 2014*	

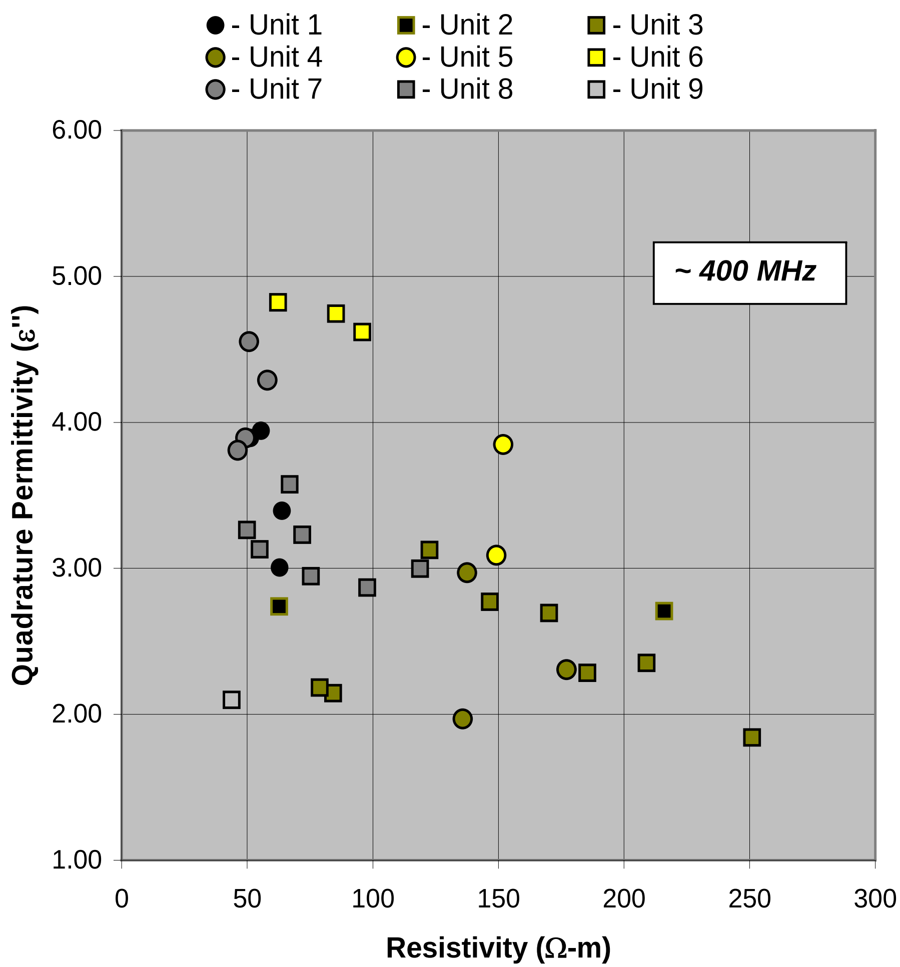

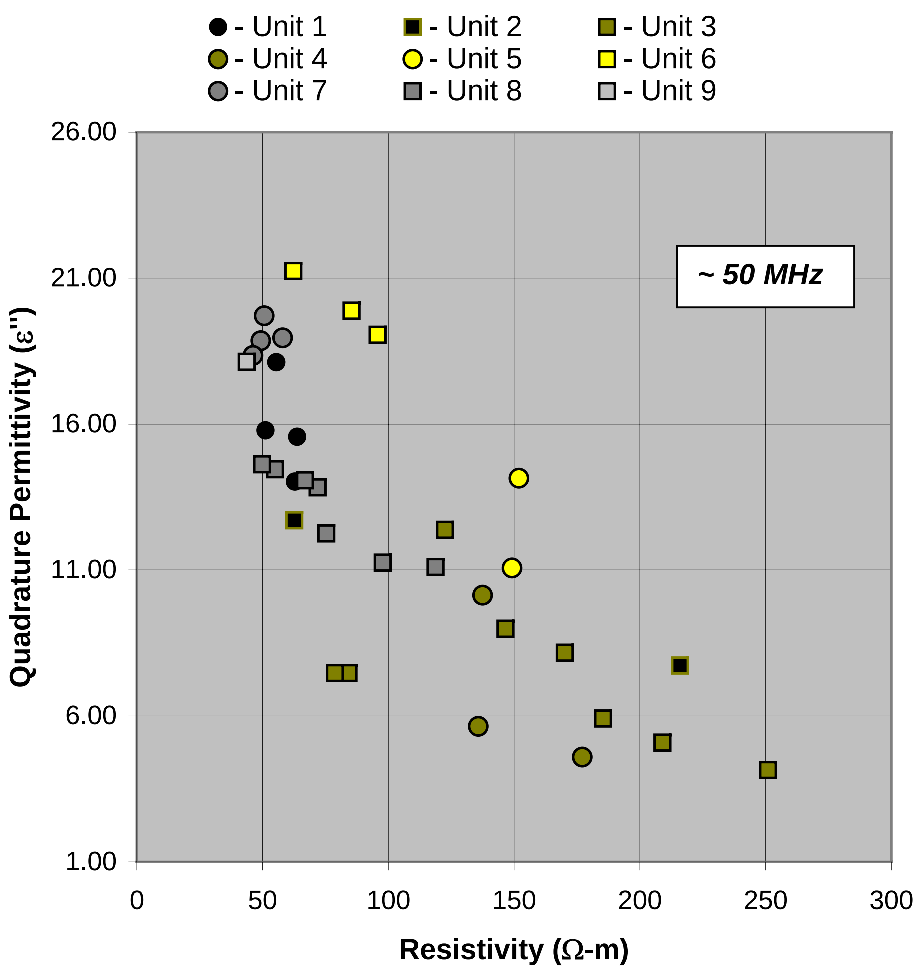

Note: Soil units identified on basis of visual assessment of solid-fraction composition, structure, texture, and colour.

Terrascan Geophysics

REPRESENTATIVE SOIL UNITS
QUADRATURE PERMITTIVITY / STATIC RESISTIVITY

PROJECT:	DRAWN BY:	DATE:	FIGURE:
KDC – Pitt Polder	*GMC*	*10 May, 2014*	*36*

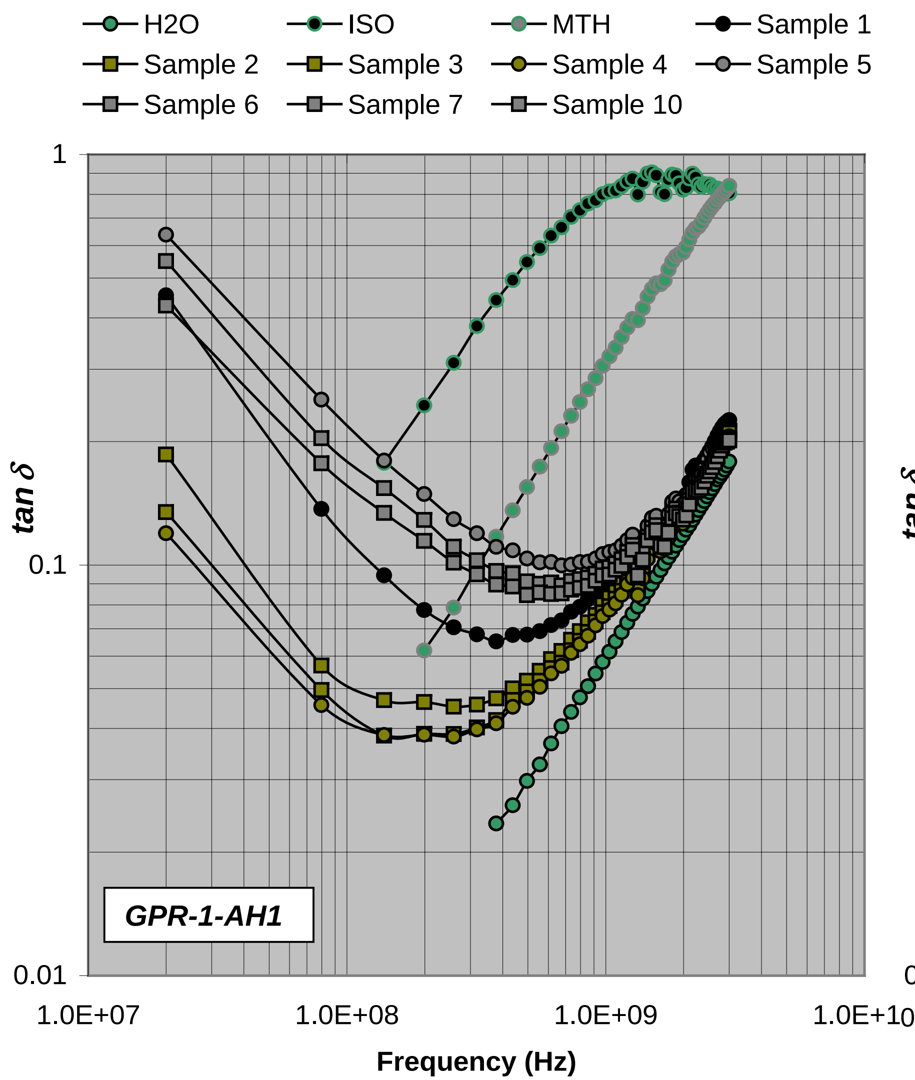

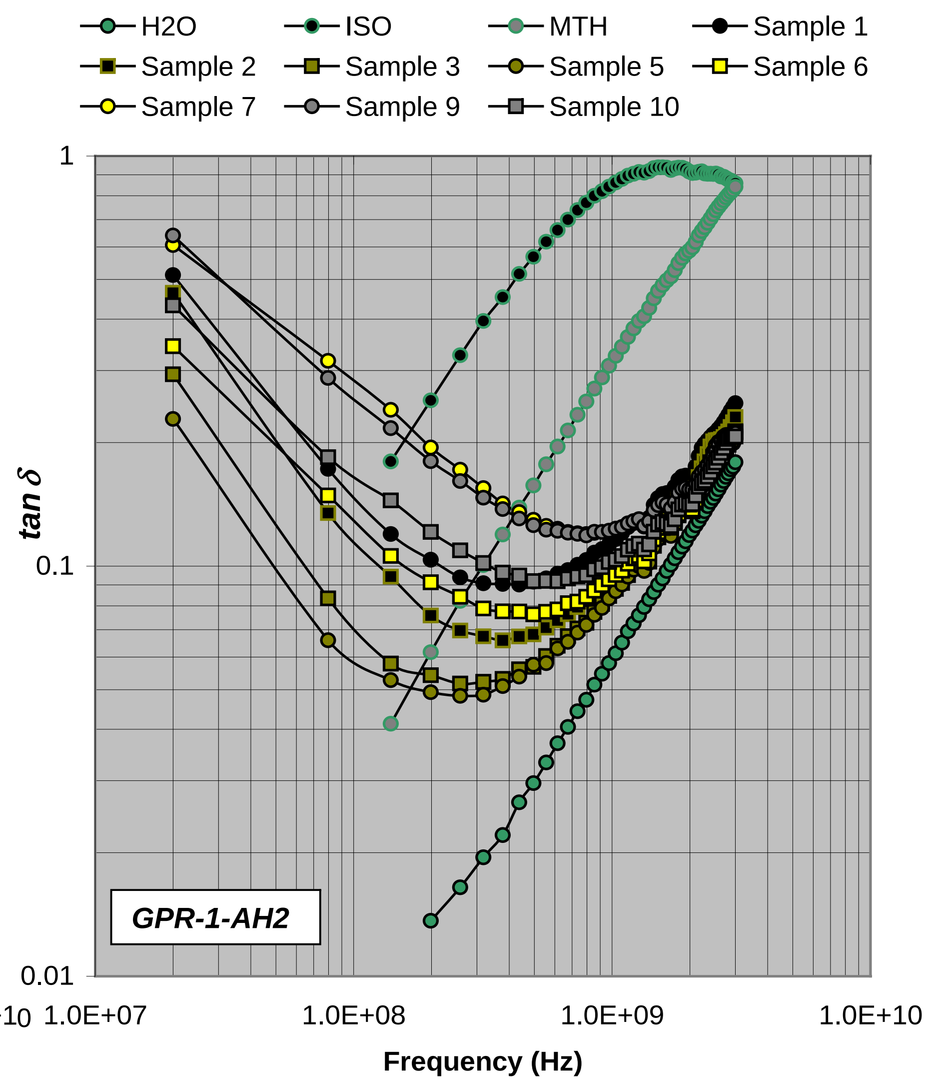

Terrascan Geophysics

LOSS TANGENT SPECTRA
GPR-1-AH1 – BH13-54-5065 / GPR-1-AH2 – BH13-53-5065

PROJECT:	DRAWN BY:	DATE:	FIGURE:
KDC – Pitt Polder	*GMC*	*10 May, 2014*	*37*

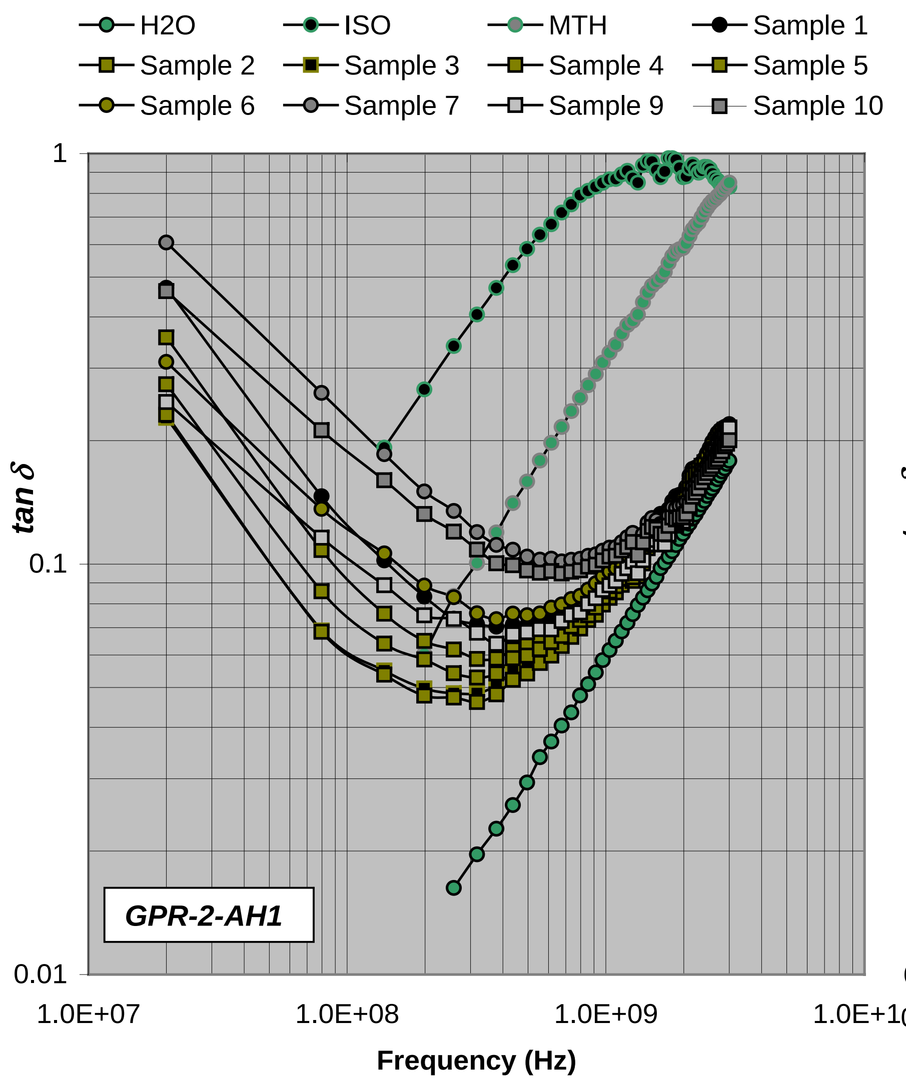

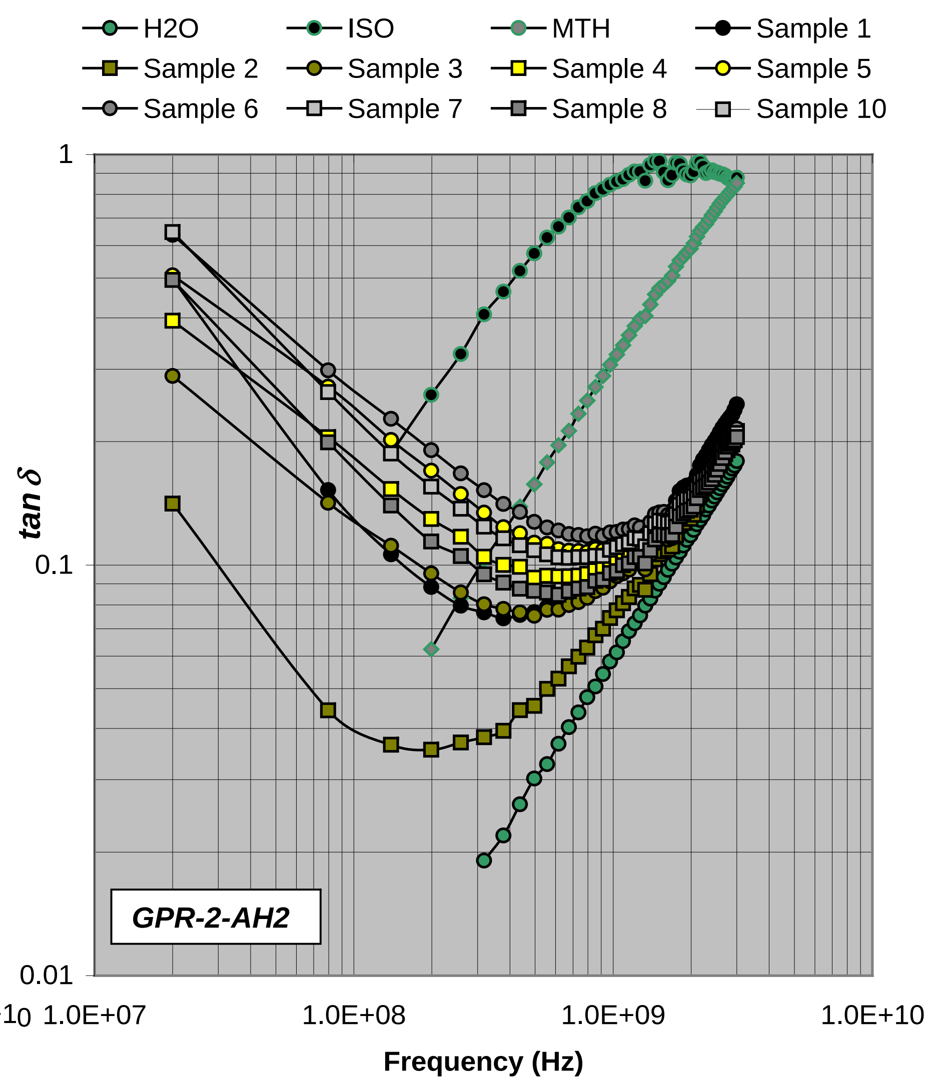

Terrascan Geophysics

LOSS TANGENT SPECTRA
GPR-2-AH1 – BH13-46-5065 / GPR-2-AH2 – BH13-47-5065

PROJECT: *KDC – Pitt Polder*	DRAWN BY: *GMC*	DATE: *10 May, 2014*	FIGURE: **38**

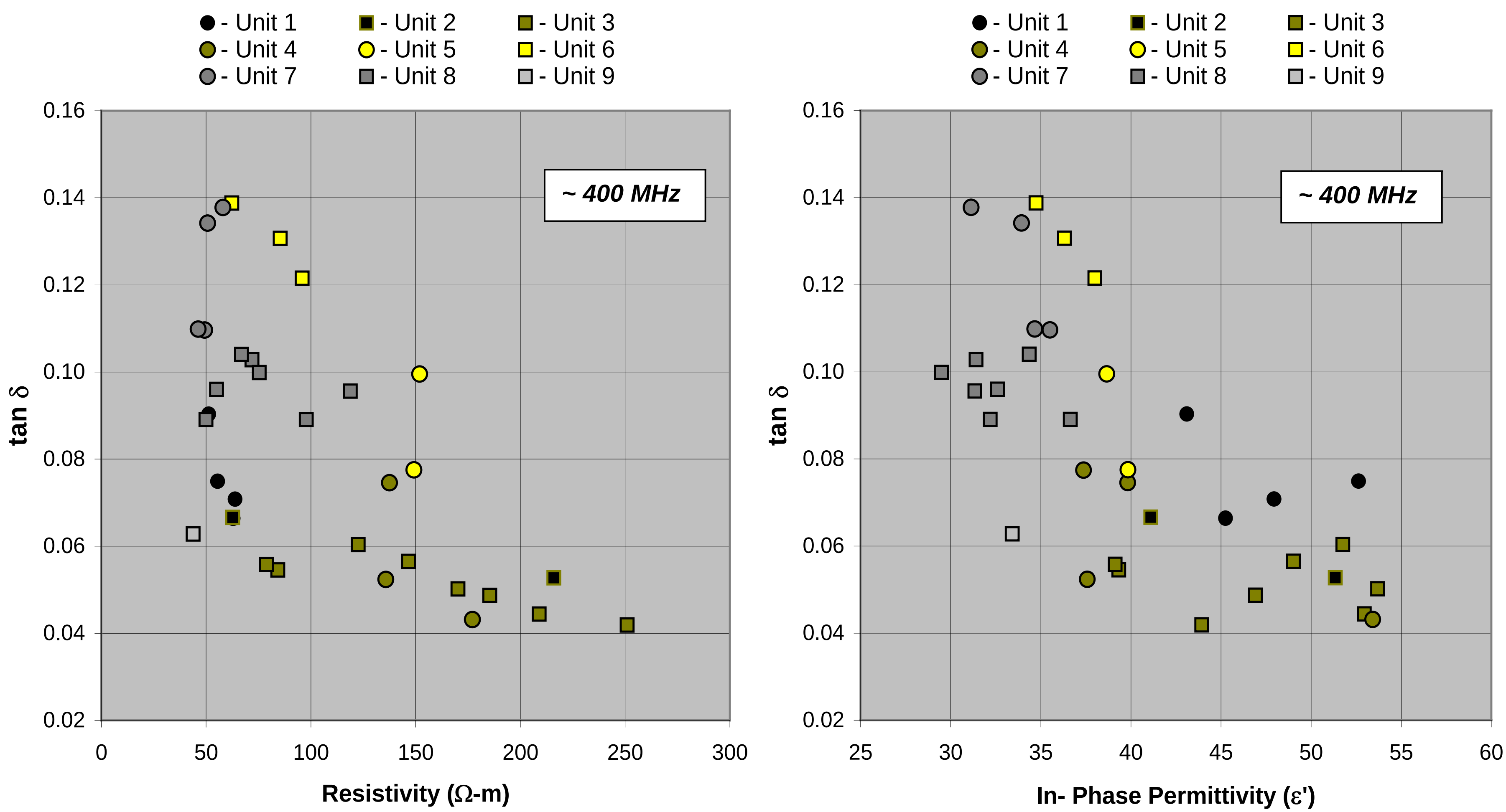

Note: Soil units identified on basis of visual assessment of solid-fraction composition, structure, texture, and colour.

Terrascan Geophysics

REPRESENTATIVE SOIL UNITS
LOSS TANGENT / STATIC RESISTIVITY - PERMITTIVITY

PROJECT: *KDC – Pitt Polder*	DRAWN BY: *GMC*	DATE: *10 May, 2014*	FIGURE: ***39***

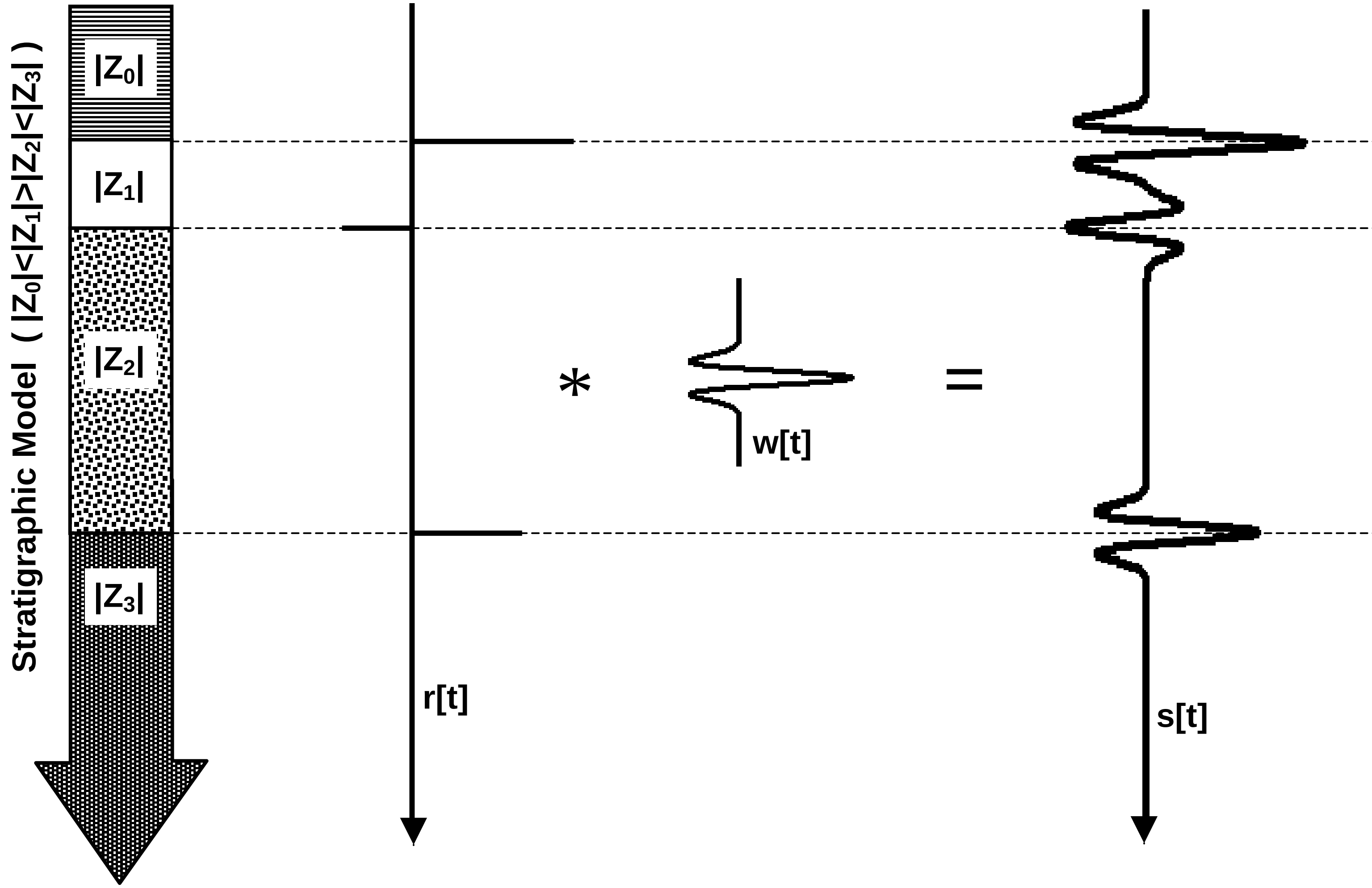

Note: ***$|Z_i|$ represents the magnitude of the intrinsic electromagnetic impedance of the i-th stratigraphic unit, r[t] denotes the corresponding time-sampled reflectivity series (assuming an average or interval-variable radar velocity, w[t] denotes a representative, time-sampled radar wavelet series and s[t]=w[t] $*$ r[t] denotes the resulting radar signal, where $*$ signifies the discrete convolution operation.***

Terrascan Geophysics

CONVOLUTIONAL MODEL OF THE RADAR SIGNAL			FIGURE: ***40***
PROJECT: ***KDC – Pitt Polder***	DRAWN BY: ***GMC***	DATE: ***20 July, 2014***	

Note: synthetic radar scans as indicated are approximate only and based purely on calculated reflection coefficients (via complex permittivity measurements at 400 MHz). The depth-scale assumes a uniform radar velocity and no account has been taken of progressive attenuation or associated dispersion.

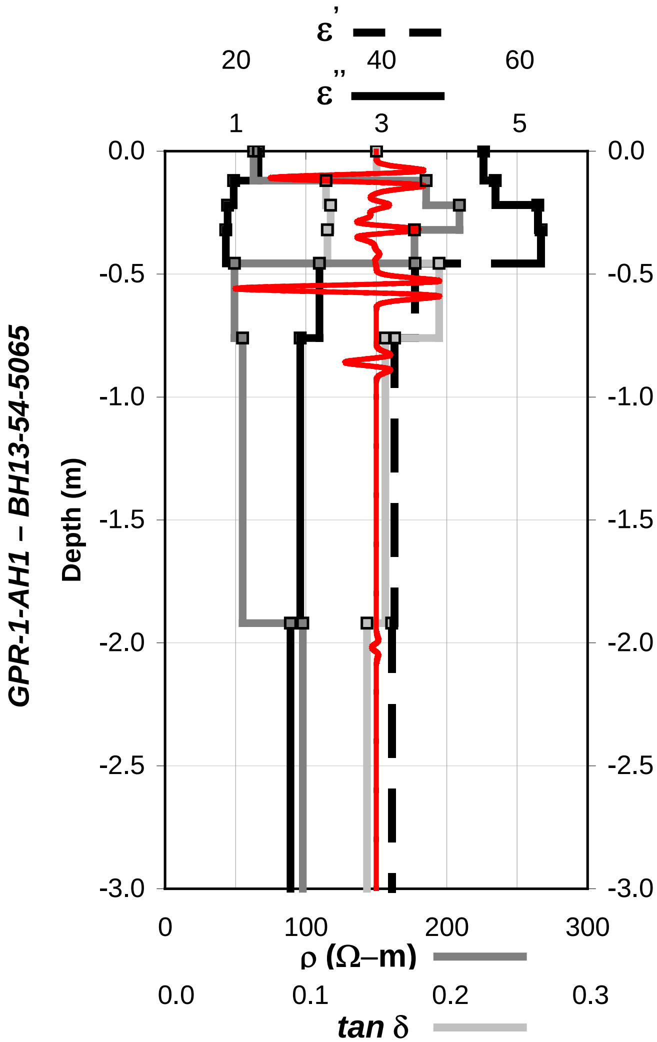

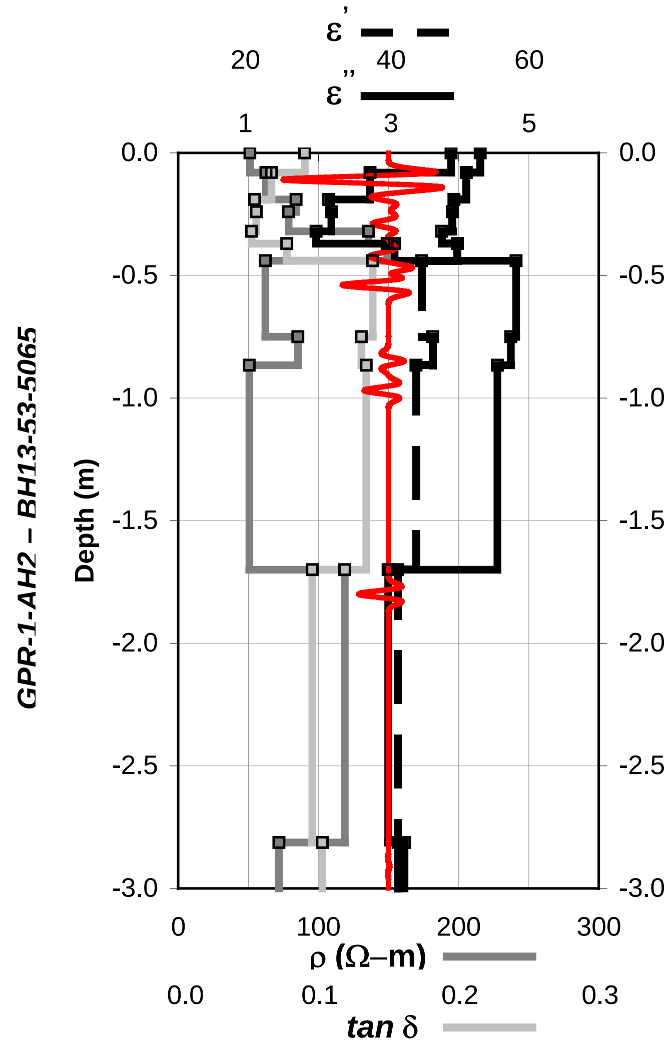

Terrascan Geophysics

LAB-MEASURED ELECTRICAL PROPERTIES
TOWER 5065 – GPR–1 – AUGER CORES

PROJECT: KDC – Pitt Polder	DRAWN BY: GMC	DATE: 20 July, 2014	FIGURE: 41

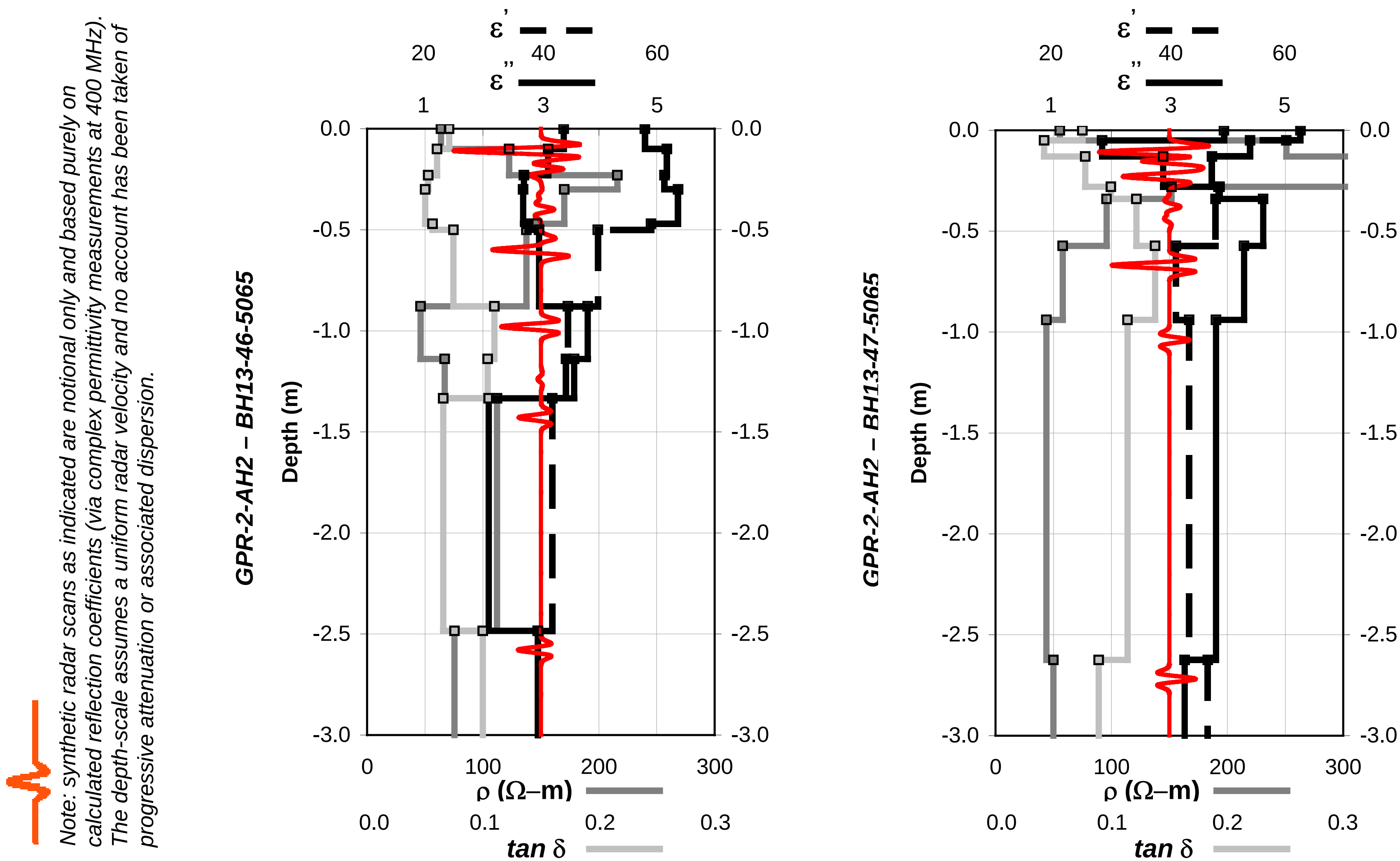

Terrascan Geophysics

LAB-MEASURED ELECTRICAL PROPERTIES
TOWER 5065 – GPR–2 – AUGER CORES

PROJECT: *KDC – Pitt Polder*	DRAWN BY: *GMC*	DATE: *20 July, 2014*	FIGURE: **42**

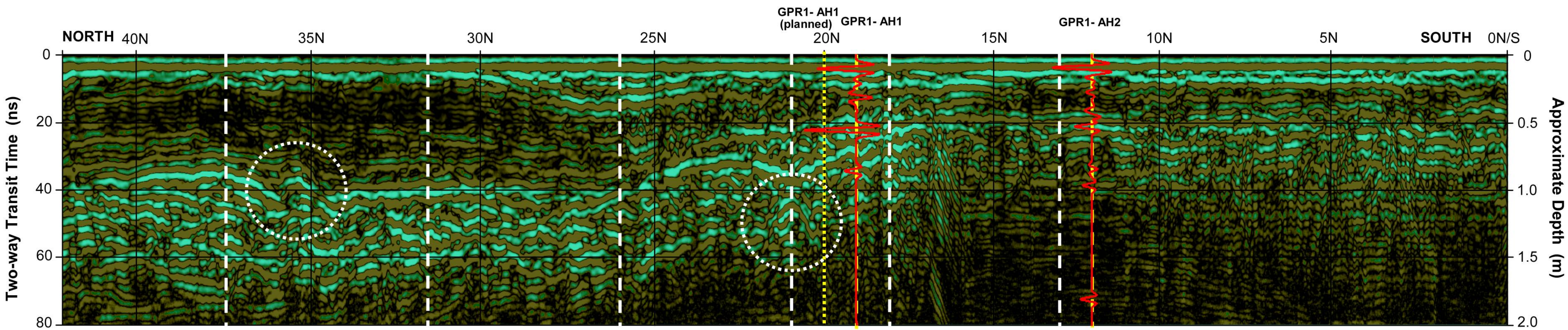

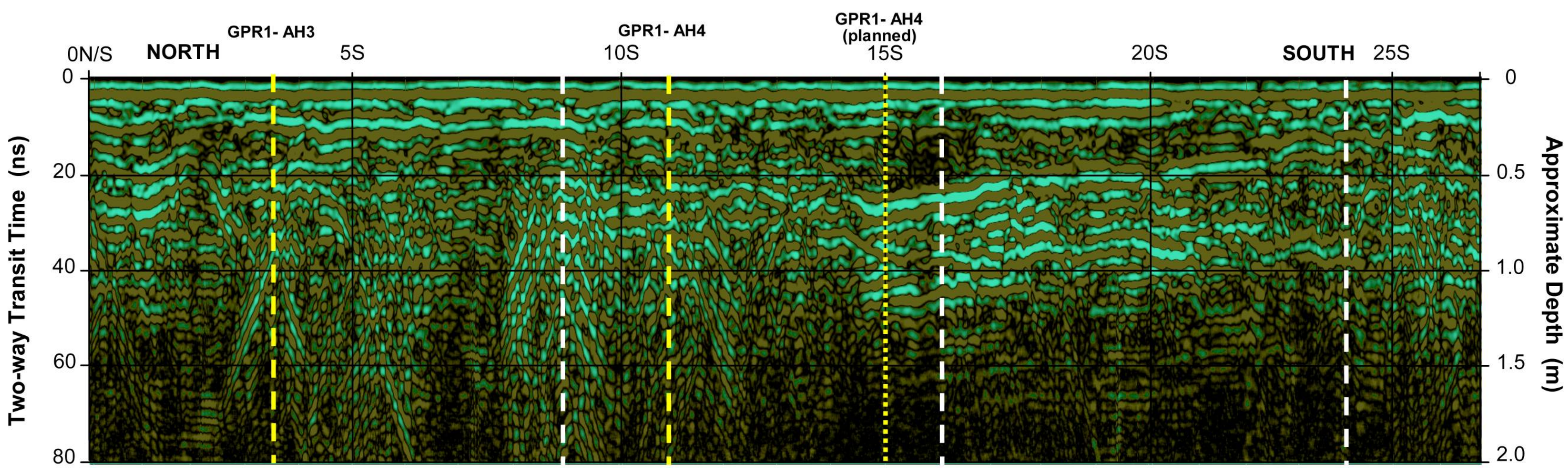

Shovel test location

Auger core location

Auger core location (planned)

Synthetic radar signal

Tower 5065 GPR-1 (FILE4900)

***NOTE:** Approximate depth scale based on estimated average radar velocity v=0.05 m/ns.*

Radar velocity varies with soil composition, texture and moisture content. Indicated depth scale is provided for approximate reference only. Fundamental reference is two-way transit time in nanoseconds (ns).

GROUND PENETRATING RADAR
TOWER 5065 – GPR-1 – 400 MHz

PITT POLDER – KDC/BC HYDRO ILM

Terrascan Geophysics

PROJECT: *KDC Pitt Polder*	
DRAWN BY: *GMC*	FIGURE: *43*
DATE: *20 July, 2014*	

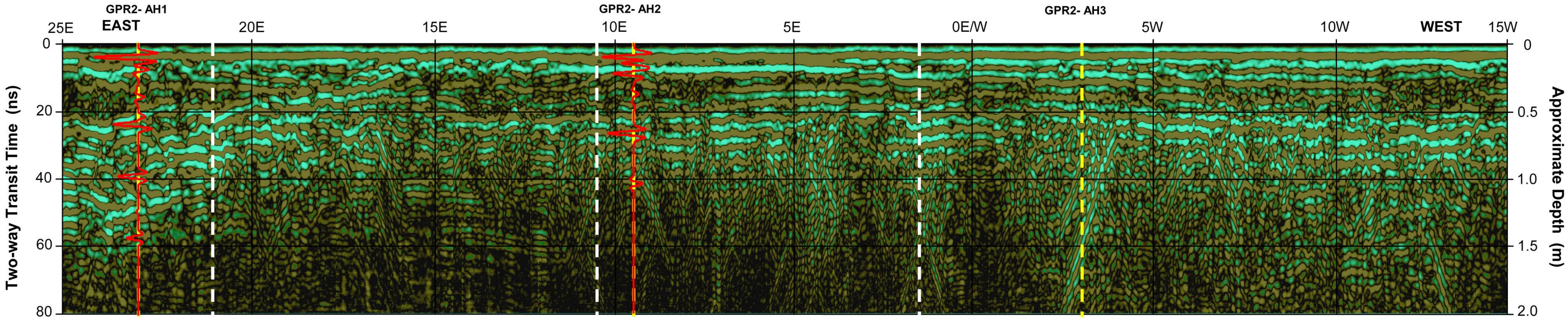

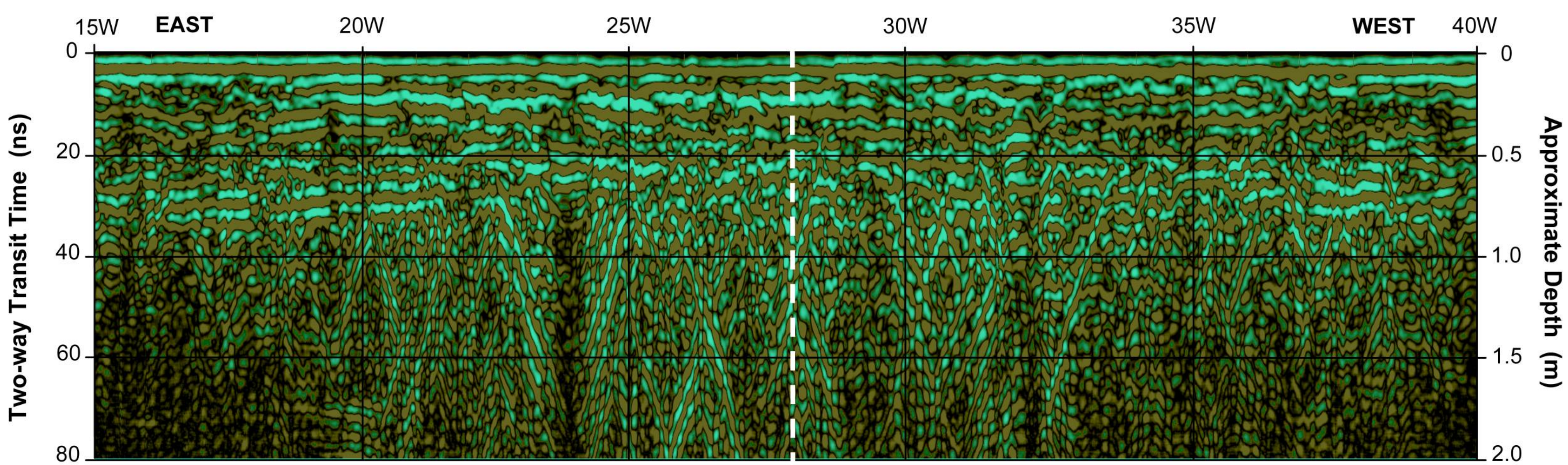

Shovel test location

Auger core location

Synthetic radar signal

Tower 5065 GPR-1 (FILE4909)

***NOTE:** Approximate depth scale based on estimated average radar velocity v=0.05 m/ns.*

Radar velocity varies with soil composition, texture and moisture content. Indicated depth scale is provided for approximate reference only. Fundamental reference is two-way transit time in nanoseconds (ns).

GROUND PENETRATING RADAR
TOWER 5065 – GPR-2 – 400 MHz

PITT POLDER – KDC/BC HYDRO ILM

Terrascan Geophysics

PROJECT: KDC Pitt Polder	
DRAWN BY: GMC	FIGURE: 44
DATE: 20 July, 2014	

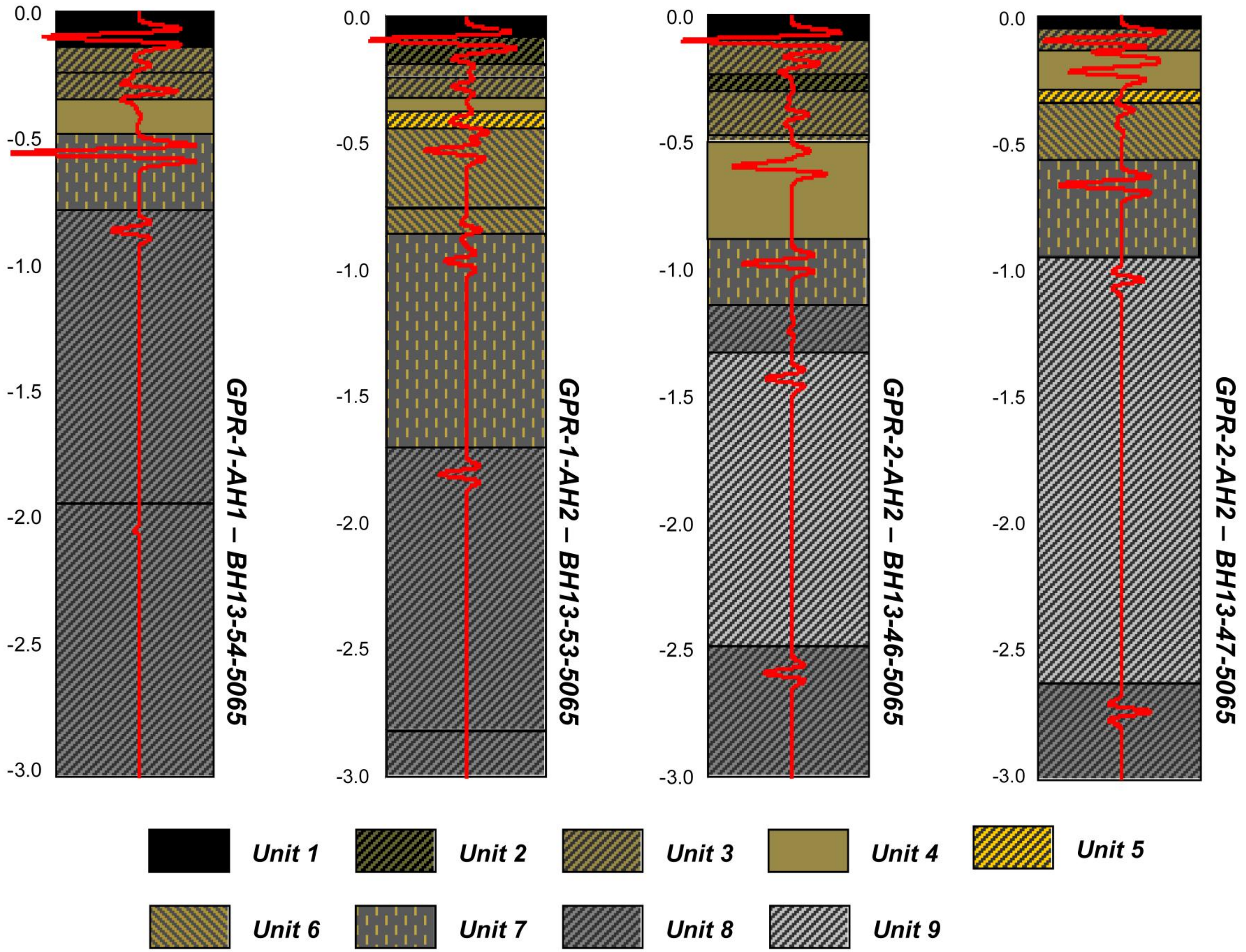

NOTE: see Figure 28 for soil/sediment unit descriptions

Terrascan Geophysics

TOWER SITE 5065 – FIELD-IDENTIFIED SOIL/SEDIMENT SECTIONS
SYNTHETIC RADAR SIGNALS

FIGURE: 45

PROJECT: KDC – Pitt Polder

DRAWN BY: GMC

DATE: 20 July, 2014

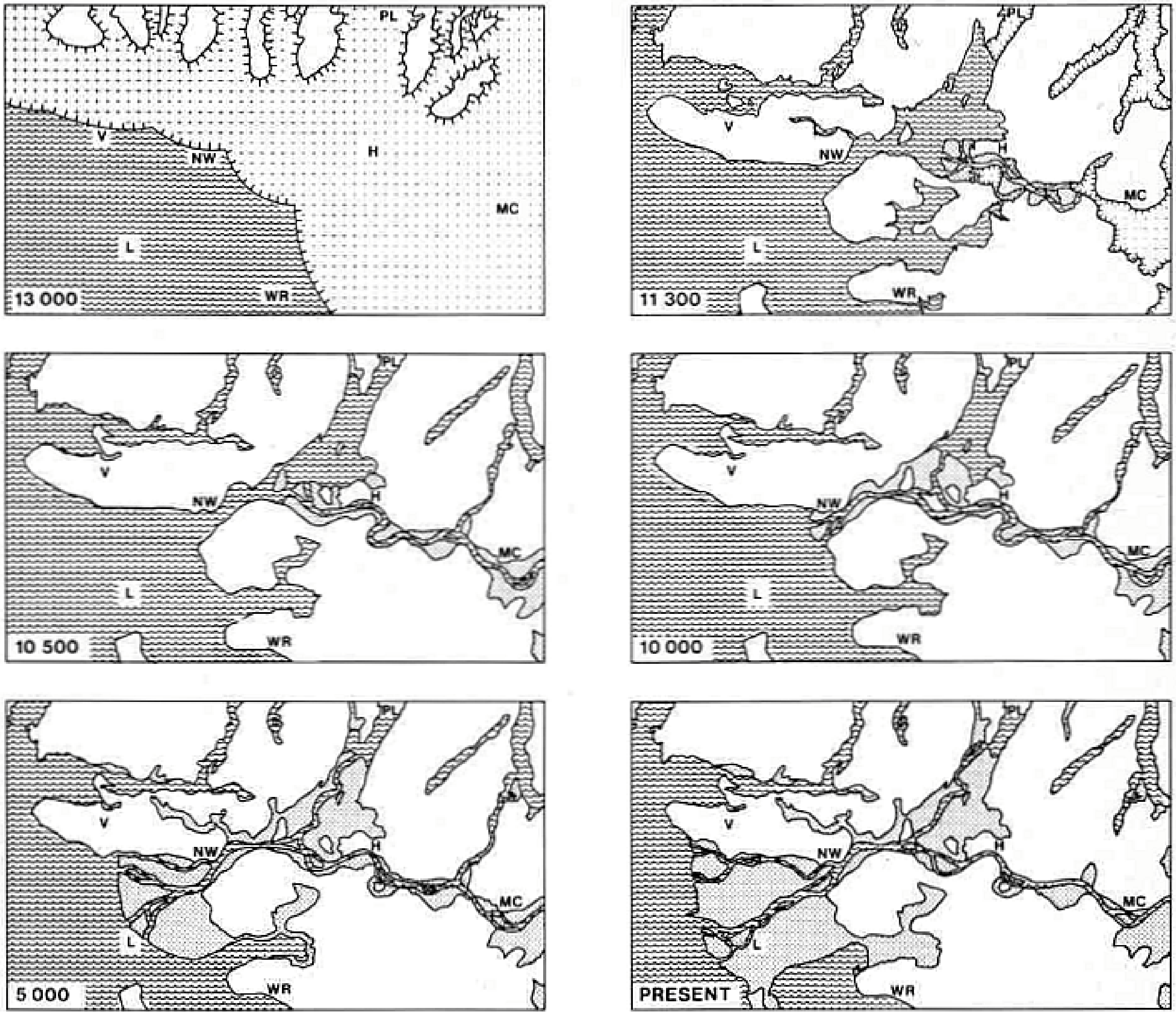

SOURCE: Clague et al. (1983)

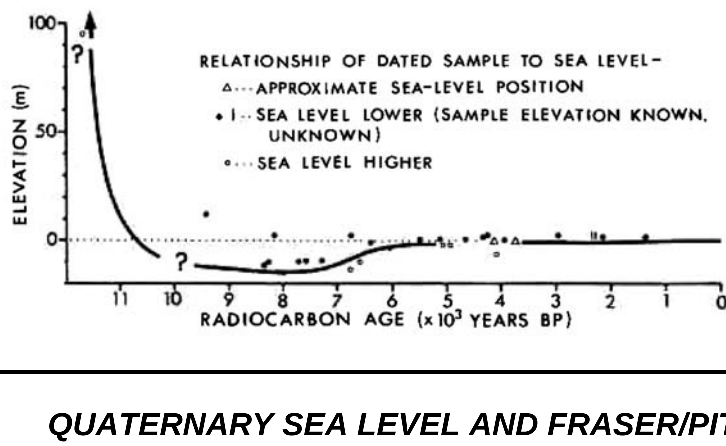

SOURCE: Clague et al, (1982)

QUATERNARY SEA LEVEL AND FRASER/PITT RIVER SEDIMENTATION
LOWER MAINLAND, BC

Terrascan Geophysics

PROJECT: KDC Pitt Polder		FIGURE: 46
DRAWN BY: GMC	DATE: 25 August, 2014	

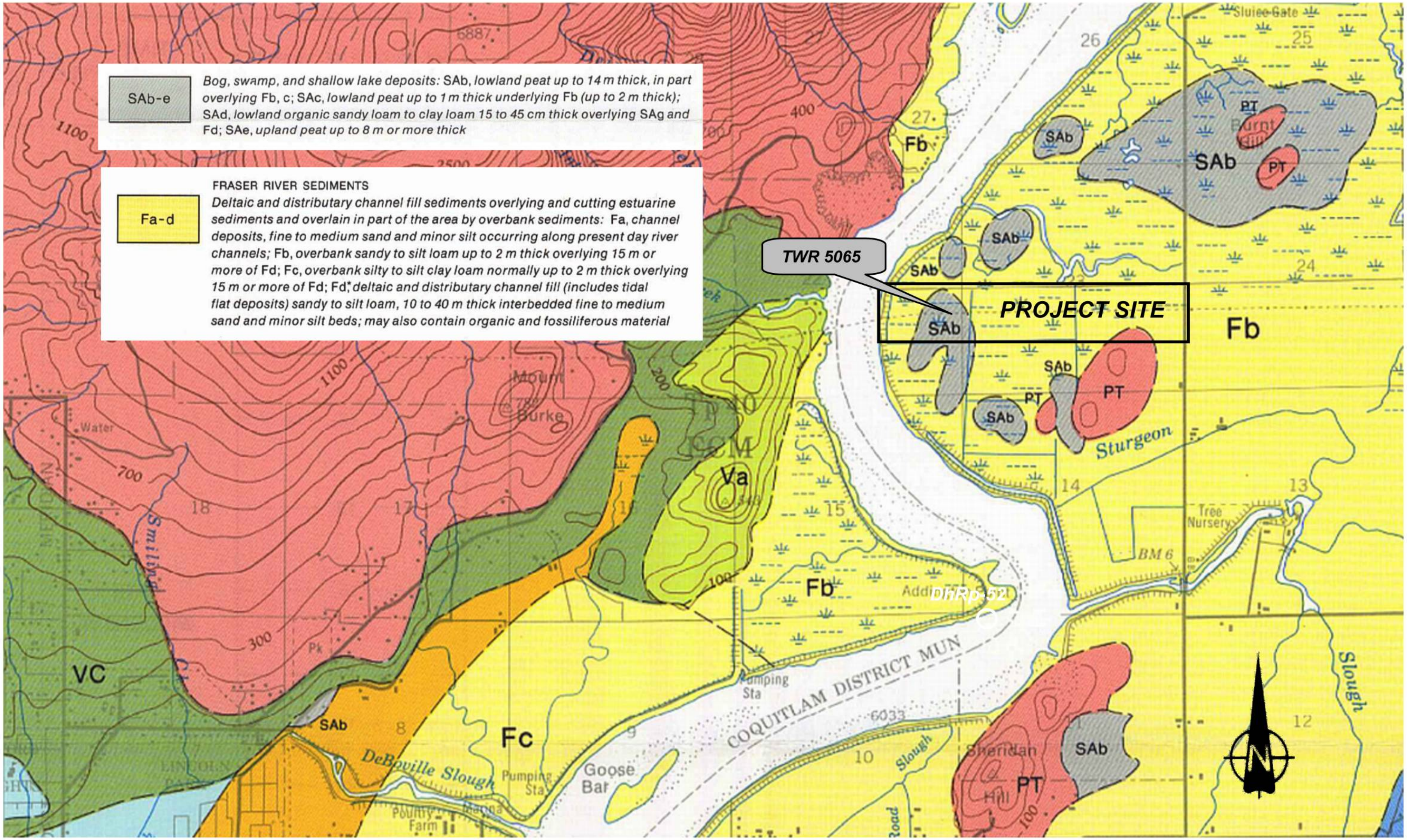

SOURCE: Armstrong and Hicock (1980)

Terrascan Geophysics	**PROJECT SITE – SURFICIAL GEOLOGY**		FIGURE: **47**
	PROJECT: **KDC – Pitt Polder**	DRAWN BY: **GMC**	DATE: **25 August, 2014**

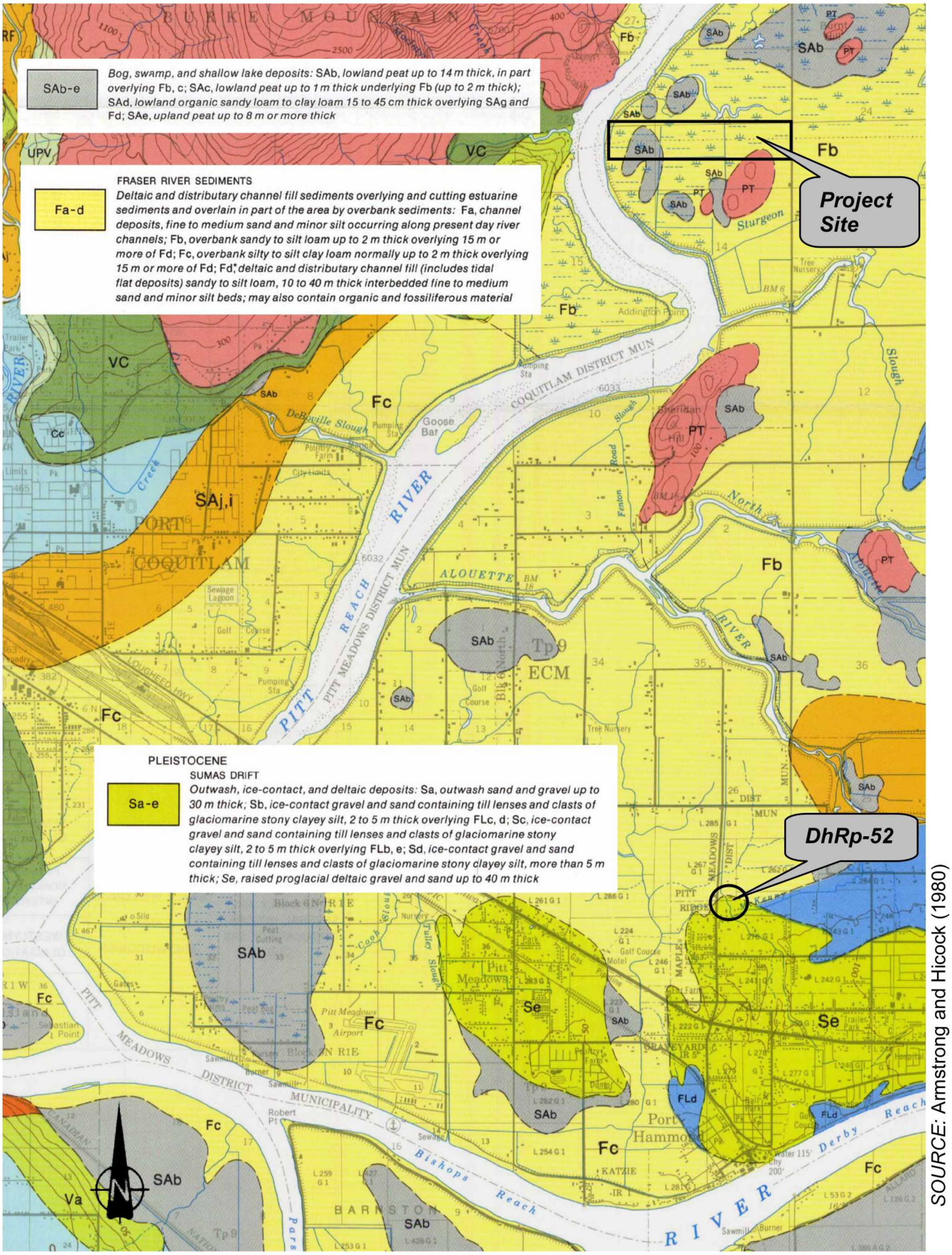

PITT POLDER – SURFICIAL GEOLOGY

Terrascan Geophysics	PROJECT: KDC Pitt Polder	FIGURE: 48
	DRAWN BY: GMC — DATE: 25 August, 2014	